

POLYOLEFIN BLEND MISCIBILITY:
QUANTITATIVE INVESTIGATIONS OF DYNAMIC
HETEROGENEITY

By

LANCE GILL

Bachelor of Arts in Chemistry
Southwestern Oklahoma State University
Weatherford, Oklahoma
2006

Submitted to the Faculty of the
Graduate College of the
Oklahoma State University
in partial fulfillment of
the requirements for
the Degree of
DOCTOR OF PHILOSOPHY
December, 2012

POLYOLEFIN BLEND MISCIBILITY:
QUANTITATIVE INVESTIGATIONS OF DYNAMIC
HETEROGENEITY

Dissertation Approved:

Dr. Jeffery White

Dissertation Adviser

Dr. Frank Blum

Dr. Nick Materer

Dr. Kevin Ausman

Dr. Tracy Quan

Outside Committee Member

Dr. Sheryl A. Tucker

Dean of the Graduate College

TABLE OF CONTENTS

| Chapter | Page |
|--|------|
| I. INTRODUCTION | 1 |
| The Glass Transition | 3 |
| Solid State NMR | 5 |
| CODEX – Centerband Only Detected Exchange | 12 |
| Theoretical Calculations of Normalized Exchange Intensity E(T) | 17 |
| Distribution of Correlation Times | 23 |
| II. POLYPROPYLENE AND POLYETHYLENE COPOLYMER BLEND MISCIBILITY: SLOW CHAIN DYNAMICS IN INDIVIDUAL BLEND COMPONENTS NEAR THE GLASS TRANSITION | 27 |
| Introduction | 27 |
| Experimental | 29 |
| Calculations and Theory | 30 |
| Results and Discussion | 31 |
| Candidates for a Miscible aPP/PEB System | 31 |
| Slow Chain Dynamics near T _g in aPP, PEB-66, and aPP/PEB-66 Blend by CODEX NMR | 33 |
| Data Analysis via Correlation Time Distribution and Arrhenius vs. WLF Models | 38 |
| Conclusions | 43 |
| III. POLYOLEFIN BLEND MISCIBILITY: POLARIZATION TRANSFER VERSUS DIRECT EXCITATION EXCHANGE NMR | 48 |
| Introduction | 48 |
| Experimental Section | 49 |
| Results and Discussion | 51 |

| Chapter | Page |
|--|------|
| IV. GLASS TRANSITIONS, SEGMENTAL DYNAMICS, AND FRICTION COEFFICIENTS FOR INDIVIDUAL POLYMERS IN MULTICOMPONENT POLYMER SYSTEMS BY CHAIN-LEVEL EXPERIMENTS..... | 56 |
| Introduction..... | 56 |
| Experimental Section..... | 59 |
| Samples and Data Collection..... | 59 |
| Experimental Verification of Blend Miscibility..... | 60 |
| Calculations and Theory..... | 61 |
| Results and Discussion..... | 62 |
| Exchange Data for Pure PI and PVE..... | 62 |
| Exchange Data for Polymers in the Miscible Blend: Model-Independent Conclusions..... | 65 |
| Quantitative Segmental Dynamics for PI and PVE in the Miscible Blend..... | 68 |
| Comparison with Previously Published Data..... | 73 |
| Comparison of Correlation Time Constants Obtained from CODEX Data Analysis to Discrete Variable Mixing Time Experiments..... | 74 |
| Conclusions..... | 76 |
| V. CONCLUSION..... | 77 |
| REFERENCES..... | 81 |
| APPENDICES..... | 88 |
| A.1 CODEX Pulse Program (Bruker XWINN 2.0)..... | 88 |
| A.2 Example of Mathematica Deconvolution for Exchange Points E(T)..... | 96 |
| A.3 Example of Mathematica Notebook (Arrhenius/log-Gaussian Distribution) | 100 |
| A.4 Applying the Temperature Dependent Weighting Factor [$\sigma(T)$] to the Log- Gaussian Distribution (Mathematica Notebook Example)..... | 114 |
| A.5 Direct Excitation Version of CODEX Pulse Program..... | 117 |

LIST OF TABLES

Chapter III

| Table | Page |
|---|------|
| Table 1. Modified Phase Table for the $\pi/2$ Pulses in the Direct Excitation CODEX Experiment shown in Figure 1 | 50 |

Chapter IV

| Table | Page |
|---|------|
| Table 1. DSC T_g values for the polymers and blends acquired using a $10^\circ\text{K}/\text{min}$ rate, and $T_{1\rho\text{H}}$ measurements obtained at 230 K. The pure polymers have essentially identical $T_{1\rho\text{H}}$ values at 198K | 61 |
| Table 2. Comparison of literature data previously summarized in Reference 108 with experimental results in this contribution for 50/50 PI/PVE blends | 74 |

EQUATIONS

| Equation | Page |
|--|------|
| 1) $\frac{\text{Styrene Butadiene Rubber (SBR)@20k} - \text{SBR@5k}}{\text{SBR@20k}} = \% \text{ rigid SBR}$ | 8 |
| 2) $\frac{\text{normalized area of PS}}{\Sigma \text{PS \& PB}} = \text{mole \% PS}$ | 8 |
| 3) ${}^1\text{H mole \% PDMS} = \frac{\text{integrated area PDMS}}{\text{integrated area PDMS} + \text{integrated area PB}}$ | 9 |
| 4) $\% \text{ PB missing} = \frac{\text{theoretical integrated area PB} - \text{integrated area PB (} {}^1\text{H NMR)}}{\text{theoretical integrated area PB}}$ | 10 |
| 5) $\mathbf{E(T)} = \frac{\mathbf{S_0 - S}}{\mathbf{S_0}} = \frac{\int_0^\infty \{ \text{Re}[\mathbf{G_- (t_z, \tau, T)}] - \text{Re}[\mathbf{G_- (t_m, \tau, T)}] \} \mathbf{g(\tau) d\tau}}{\int_0^\infty \text{Re}[\mathbf{G_- (t_z, \tau, T)}] \mathbf{g(\tau) d\tau}}$ | 18 |
| 6) $\mathbf{G_- (t_x)} = \langle 1 \exp \left[(\tilde{\Pi} - i\tilde{\omega}) \frac{\tau_{\text{CSA}}}{2} \right] \exp [\tilde{\Pi} t_x] \exp \left[(\tilde{\Pi} + i\tilde{\omega}) \frac{\tau_{\text{CSA}}}{2} \right] \tilde{\mathbf{P}}^{\text{eq}} 1 \rangle$ | 18 |
| 7) $\left\langle \mathbf{P_{ij} (t_m) P_j^{\text{eq}}} \cos \left(\frac{\mathbf{N}}{2} \Phi_j - \frac{\mathbf{N}}{2} \Phi_i \right) \right\rangle = \left\langle \left(\mathbf{e^{\tilde{\Pi} t_m}} \right)_{ij} \mathbf{P_j (0)} \cos \left(\frac{\mathbf{N}}{2} \Phi_j - \frac{\mathbf{N}}{2} \Phi_i \right) \right\rangle$ | 19 |

$$8) \quad \frac{N}{2} \Phi(t) = \frac{N}{2} \left(4 \frac{S_1}{\omega_R} \cos(\gamma + \omega_R t) - 4 \frac{C_1}{\omega_R} \sin(\gamma + \omega_R t) \right) \dots\dots\dots 19$$

$$9) \quad \tilde{\Pi} = \begin{bmatrix} \Pi_{1,1} & \Pi_{1,2} & 0 & 0 & 0 & 0 \\ \Pi_{2,1} & \Pi_{2,2} & \Pi_{2,3} & 0 & 0 & 0 \\ 0 & \Pi_{3,2} & \Pi_{3,3} & \ddots & 0 & 0 \\ 0 & 0 & \ddots & \ddots & \Pi_{m-1,m} & 0 \\ 0 & 0 & 0 & \Pi_{m,m-1} & \Pi_{m,m} & \Pi_{m,m+1} \\ 0 & 0 & 0 & 0 & \Pi_{m+1,m} & \Pi_{m+1,m+1} \end{bmatrix} \dots\dots\dots 19$$

$$10) \quad \Pi_{m,m+1} = \frac{1}{6\tau_c \Delta^2} \frac{\sin(m\Delta)}{\sin[(m+1/2)\Delta]}, \quad \Pi_{m+1,m} = \frac{1}{6\tau_c \Delta^2} \frac{\sin(m\Delta)}{\sin[(m-1/2)\Delta]}, \dots\dots\dots 19$$

$$11) \quad \Pi_{m,m} = \frac{-1}{3\tau_c \Delta^2} \cos\left(\frac{\Delta}{2}\right) \dots\dots\dots 20$$

$$12) \quad P_j^{\text{eq}} = \frac{\sin[(j-0.5)\Delta]}{\sum_{i=1}^N \sin[(i-0.5)\Delta]} = \sin[(j-0.5)\Delta] \sin\left(\frac{\Delta}{2}\right) \dots\dots\dots 20$$

$$13) \quad \tilde{P}^{\text{eq}} = \begin{bmatrix} P_1^{\text{eq}} & 0 & 0 & 0 & 0 & 0 & 0 \\ 0 & P_2^{\text{eq}} & 0 & 0 & 0 & 0 & 0 \\ 0 & 0 & P_3^{\text{eq}} & 0 & 0 & 0 & 0 \\ 0 & 0 & 0 & \ddots & 0 & 0 & 0 \\ 0 & 0 & 0 & 0 & P_j^{\text{eq}} & 0 & 0 \\ 0 & 0 & 0 & 0 & 0 & \ddots & 0 \\ 0 & 0 & 0 & 0 & 0 & 0 & P_N^{\text{eq}} \end{bmatrix} \dots\dots\dots 20$$

$$14) \quad \tilde{\omega} = \begin{bmatrix} \omega_1 & 0 & 0 & 0 & 0 & 0 & 0 \\ 0 & \omega_2 & 0 & 0 & 0 & 0 & 0 \\ 0 & 0 & \omega_3 & 0 & 0 & 0 & 0 \\ 0 & 0 & 0 & \ddots & 0 & 0 & 0 \\ 0 & 0 & 0 & 0 & \omega_i & 0 & 0 \\ 0 & 0 & 0 & 0 & 0 & \ddots & 0 \\ 0 & 0 & 0 & 0 & 0 & 0 & \omega_N \end{bmatrix} \dots\dots\dots 20$$

$$15) \quad \omega_i = \omega_L \left[\frac{1}{3} (\delta_{11}^{i, \text{MF}} + \delta_{22}^{i, \text{MF}} + \delta_{33}^{i, \text{MF}}) + C_2^i \cos(2\omega_R t + 2\gamma) + S_2^i \sin(2\omega_R t + 2\gamma) + C_1^i \cos(\omega_R t + \gamma) + S_1^i \sin(\omega_R t + \gamma) \right] \dots\dots\dots 21$$

$$16) \quad \tilde{\delta}^{i, \text{MF}} = \tilde{\mathbf{R}}^{\text{PAS} \rightarrow \text{MF}} (\mathbf{a}^i, \mathbf{b}^i, \mathbf{c}^i) \tilde{\delta}^{\text{PAS}} \tilde{\mathbf{R}}^{\text{PAS} \rightarrow \text{MF}} (\mathbf{a}^i, \mathbf{b}^i, \mathbf{c}^i)^{-1} \dots\dots\dots 21$$

$$17) \quad g(\tau, T) = \frac{1}{\sigma(T)\sqrt{2\pi}} \exp \left[-\frac{(\ln(\tau) - \ln(\tau_c(T)))^2}{2\sigma^2(T)} \right] \dots\dots\dots 23$$

$$18) \quad g(\tau, \mathbf{T})_{\text{KWW}} = -\frac{\tau_c(\mathbf{T})}{\pi\tau^2} \sum_{\mathbf{k}=0}^{\infty} \frac{(-1)^{\mathbf{k}}}{\mathbf{k}!} \sin(\pi\beta\mathbf{k}) \Gamma(\beta\mathbf{k}+1) \left(\frac{\tau}{\tau_c(\mathbf{T})} \right)^{\beta\mathbf{k}+1} \dots\dots\dots 24$$

$$19) \quad \tau_c(\mathbf{T})_{\text{WLF}} = \tau_{\text{Tg}} \quad 10^{\frac{-C_1(\mathbf{T}-\mathbf{Tg})}{C_2+(\mathbf{T}-\mathbf{Tg})}} \dots\dots\dots 25$$

$$20) \quad E(t_m, \tau_c, T) = \frac{S_0 - S}{S_0} = \frac{\int_0^\infty \{ \text{Re}[G_-(t_z, \tau, T)] - \text{Re}[G_-(t_m, \tau, T)] \} g(\tau) d\tau}{\int_0^\infty \text{Re}[G_-(t_z, \tau, T)] g(\tau) d\tau} \dots\dots\dots 31$$

$$21) \text{ Adams-Gibbs } [\tau_{\text{ex}} = \tau_0 \exp(c/TSc)] \dots\dots\dots 46$$

$$22) \text{ Friction Coefficient } [\zeta = \tau_c k_B T / b^2] \dots\dots\dots 71$$

LIST OF FIGURES

Chapter I

| Figure | Page |
|---|------|
| 1 Reaction showing the synthesis of atactic polypropylene (aPP). | 5 |
| 2 Mathematica results showing the factor associated with magic angle spinning in ssNMR. | 6 |
| 3 Normalized ^1H spectra of a PS/PB copolymer (SBR) at two different MAS rates. 8 | |
| 4 | |
| A stack plot of several example SBR's with different PS:PB compositions at different MAS rates..... | 9 |
| 5 CODEX experimental pulse sequence applied under MAS conditions. | 13 |
| 6 This is an example of the reference (So , black line) and CODEX (S , gray line) spectra stacked to show the exchange intensity (E). | 14 |
| 7 The ^{13}C isolated portion of the CODEX pulse sequence. | 15 |
| 8 CODEX mixing time dependence $E(t_m)$ for a 1,2-polybutadiene sample. | 16 |
| 9 Normalized ($t_m=50\text{ms}$) experimental exchange intensity $E(T)$ data. | 17 |
| 10 CP spectra of PVE at different spinning speeds for Herzfeld-Berger analysis and estimation of the CSA tensor. | 22 |
| 11 Plots of mean correlation time for pure hhPP and hhPP in the hhPP/PIB blend as obtained from CODEX NMR and dielectric spectroscopy experiments. | 24 |
| 12 Plots of discrete 17-points KWW distribution $g(\tau)_{\text{KWW}}$ for a) $\beta_{\text{KWW}} = 0.5$ and b) $\beta_{\text{KWW}} = 0.3$ calculated according to Eq. (19) | 25 |

| Figure | Page |
|--|------|
| 13 Relationship between β_{KWW} parameter of KWW distribution and half-height width of log-Gaussian distribution..... | 26 |
| 14 Normalized 50ms exchange intensity E(T) curves for the total aliphatic region integrated intensity. | 26 |

Chapter II

| Figure | Page |
|--|------|
| 1 CODEX experiment pulse sequence applied under conditions of MAS. | 30 |
| 2 ^{129}Xe static NMR results for xenon gas absorbed in..... | 32 |
| 3 a) The mixing time dependence b) The recoupling time dependence..... | 34 |
| 4 Example ^{13}C CODEX spectra for (a) pure PEB66 at 225 K, (b) aPP/PEB66 50/50 wt. % blend at 250 K, and (c) pure aPP at 274 K. | 35 |
| 5 Normalized exchange intensities E(T) for methyl and methylene signals of pure PEB66 and pure aPP. | 36 |
| 6 Normalized exchange intensities E(T) for pure PEB66 (○), PEB66 in the blend (●), pure aPP (□), and aPP in the blend (■). | 37 |
| 7 Discrete version of log-Gaussian correlation time distribution for aPP | 39 |
| 8 Temperature dependence of correlation time distribution widths for pure versus blended aPP and PEB66..... | 40 |
| 9 Comparison of fits to the aPP exchange data obtained using two different | 41 |
| 10 Temperature dependence of correlation times | 42 |
| 11 Correlation time distributions for aPP and PEB66 in the blend | 43 |
| 12 Correlation time distributions for individual polymer components in the miscible hhPP/PIB blend | 44 |

Chapter III

| Figure | Page |
|--|------|
| 1 Pulse sequence diagram for direct excitation ^{13}C CODEX experiment, | 50 |
| 2 ^{13}C NMR MAS spectra of aPP at 274K: | 51 |
| 3 Normalized exchange intensities $E(T)$ for methyl carbon signal of pure aPP obtained by cross-polarization CODEX (□) versus direct excitation CODEX (●). | 53 |

Chapter IV

| Figure | Page |
|---|------|
| 1 CODEX experiment pulse sequence applied under conditions of MAS. | 60 |
| 2 Example ^{13}C CODEX spectra showing only the aliphatic region | 63 |
| 3 Normalized 200-ms exchange intensity $E(T)$ curves for the total aliphatic region integrated intensity versus only the CH_3 intensity for pure PI, and total aliphatic intensity versus backbone-CH only for PVE. | 64 |
| 4 Normalized 200-ms exchange intensity $E(T)$ curves for the pure components and the same components measured independently in the blend. | 66 |
| 5 Temperature dependence of correlation times obtained using Arrhenius (points) and WLF (smooth line) models. | 69 |
| 6 Example results for discrete versions of log-Gaussian correlation time distributions $g(\tau)$ for PVE, | 70 |
| 7 Temperature dependence of correlation time distribution widths σ for pure PI and pure PVE versus the same polymers in the blend..... | 71 |
| 8 Calculated segmental friction coefficients using the central correlation time constants τ_c | 72 |
| 9 Exchange time constants extracted from an exponential fit to the rising exchange intensity curves are indicated on each of the Figures 8a-d | 75 |

Chapter V

| Figure | Page |
|--|------|
| 1 Normalized $E(T)$ curves for a) PI/PVE, b) aPP/PEB-66, and c) hhPP/PIB. | 78 |
| 2 Calculated values of the total configurational entropy ratios in the miscible blend (Sc Blend / Sc Pure). | 79 |

CHAPTER I

INTRODUCTION

Polymers represent one of the most economically important class of materials in our time. Polymers have been integrated into almost every consumable product available. There is a continuous push to replace classical raw materials, such as wood and steel, with this revolutionary chemical technology. There is no doubt we have seen a materials revolution similar to those were experienced by wood and steel in previous centuries. With this great success one might wonder why there is such an abundance of research to develop new products.

The study of these materials dates back almost a century, but only in recent decades have we begun to understand their true nature. What once were thought to be mysteriously non-covalently bonded colloids are now known to be covalently bonded chemical monomers that form macromolecules of high molecular weight. Furthermore, the chemical identity of the monomer (repeat unit) is one of the main factors determining the properties of polymeric systems, which means that understanding microscopic properties is fundamental to understanding the physical behavior of a particular material. Over the past several decades details about the macroscopic and microscopic properties of macromolecules have begun to emerge.

Polymers are particularly challenging materials to study, and require a modified arsenal of chemical and physical ideas and techniques for new insight. Fundamental chemistry and physical properties research continues to aid in the development of new materials that will impact the economy and consumers alike.

In recent years, public health and environmental impact have also driven the search for new polymeric materials. Chemical and Engineering News (C&EN) has published several articles about the health concerns and environmental issues. Since 2007, there have been dozens of articles about the health concerns of the man-made estrogen mimic, Bisphenol A (BPA).¹ Recently, there has been a push to ban BPA in baby bottles and sippy cups from the industry itself.² This has significantly impacted the polycarbonate industry and led to development of acceptable alternatives. The styrene monomer, vinyl benzene, has recently been added to the cancer warning list by the Health and Human Services,³ and phthalates, used to plasticize polyvinyl chloride, are facing a ban in Europe.⁴ Not only is it important to understand the chemical and physical properties of these materials, but the human and environmental impact also create the need for adjustments in current technologies.

Most of the currently deployed polymers were invented between the late 1930's to mid 1960's. These new materials (i.e. nylon, polyester, polyethylene, polypropylene, and polycarbonate) quickly gained popularity with both manufacturers and developed into widely accepted, colorful, and durable consumer products. There are basically two ways to approach the strategy of developing new materials. Some chemists use a classical approach that includes novel chemistry to generate new polymers and then begin a process of sorting out where the new material might be applicable while others make use of the structure/property functionality present in current polymeric materials to envision routes to new ones. Recently, there has been some success achieved using the later method.⁵

Eastman Chemical developed Tritan, a polyester copolymer made from dimethyl terephthalate, 1,4-cyclohexanedimethanol, and 2,2,4,4-tetramethyl-1,3-cyclobutanediol. Tritan™ appears to be an attractive alternative polycarbonate, where BPA is a concern, and has already broken

into the market and successfully replaced polycarbonate in baby bottles and water containers. DSM, with Stanyl® ForTii™, is also seeing success in the automotive component industry with a terephthalic acid and tetramethylene diamine that has high heat resistance and mechanical strength. Stanyl ForTii was an improved version of DSM's Stanyl 4,6 high-heat polyamide, and Stanyl ForTii doesn't absorb as much moisture as its earlier counterpart making it possible to penetrate more markets. DSM and Eastman Chemicals' success stems from extending existing polymer properties by incorporating new raw material into its backbone. These examples are an indication that achieving success in today's market requires an understanding of the material physics associated with existing polymers. Thus, research into polymer blends, copolymers, and other similar variations will continue.

Polymer blends are an attractive economical alternative to new materials⁶, and this contribution will focus on polymer blends and provide insight into the mixing of amorphous macromolecules. More specifically, our interest is in the fundamental understanding of amorphous polymers and their miscible blends. Although amorphous macromolecules can be quite simple based on the chemical structure of their repeat unit (or chemical monomer), they exhibit some complex physical properties that are not well understood. One is the unique phenomenon known as the glass transition⁷, and another is that only a small number of amorphous polymers form miscible blends.⁸ The fact that chemically similar substances don't readily form miscible blends is quite perplexing, given that in basic organic chemistry we are taught a general rule of "like dissolves like". Understanding the complex issues associated with amorphous polymers and blend systems is important in the development of new materials using a blend strategy.

The Glass Transition.

Amorphous (from the Greek, a-without, morphe'-shape) in condensed matter physics is used to describe a solid that lacks long-range order, or, stated differently, no atomic level crystal structure

exists for these materials in the solid state.⁹ This lack of crystal structure in the solid state prevents defining a clear melting point. Instead, amorphous materials exhibit a unique characteristic that gives rise to the glass transition (T_g) phenomenon. The glass transition is different from solidification by crystallization. Crystallization is a phase transition with a well defined thermodynamic transition temperature. The glass transition occurs with the continuous increase in viscosity of a liquid until it becomes a glass.

The study of the glass transition using calorimetry, is often done using a cooling or heating rate in DSC (Differential Scanning Calorimetry), $T = dT/dt$. The glass transition temperature can be characterized by a change in the heat capacity, over a small interval, that corresponds to the solidification or freezing temperature that is defined at a standard viscosity (i.e. $\eta=10^{12.3}$ Pa·s). DSC thermograms for the glass transition usually contain some peculiar characteristics. A cooling curve may look different than a heating curve for a particular sample. An increase in the heat flow rate of one decade may give a glass transition shift of 3 – 20K depending on the homopolymer.⁷ For miscible blends the DSC trace can appear much less defined, but usually give an apparently singular T_g temperature. Immiscible blends will retain their individual T_g 's. In this respect, DSC can yield a good indication of the physical mixing of a particular blend, and the extended criterion to the miscibility of binary blends, i.e., a single glass transition representative of a two component system mixed at the molecular level.

DSC gives qualitative information about the T_g , but is not able to probe macromolecules at the chain or atomic level. In order to get information about the molecular dynamics at the chain level and more accurately define chain motions of homopolymers and their miscible blends, a more sensitive solid-state nuclear magnetic resonance (ssNMR) can be used. An example amorphous polymer is shown in Figure 1. The atactic polypropylene (aPP), synthesized from propene monomers, has a high density of NMR active proton and carbon nuclei. Also, because these

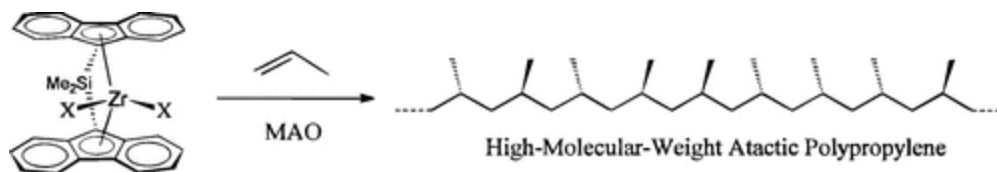


Figure 1. Reaction showing the synthesis of atactic polypropylene (aPP). The reaction scheme shows a typical olefin monomer, propylene, and the polyolefin product aPP using an organometallic catalyst and methylalumoxane.

macromolecules undergo a glass transition and become solid materials, ssNMR is ideal for observing glass transition dynamics of these polymers in their pure unperturbed state. This work, as well as that published by others, has employed temperature controlled ssNMR techniques to observe chain dynamics in polymers at, below, and above T_g 's.

Solid-State NMR

Magic-angle-spinning (MAS) is important for solid phase experiments and was originally proposed by Andrew et al.¹⁰ and by Lowe¹¹ to overcome the large homonuclear dipole-dipole line broadening in solid ^1H spectra. When the solid sample is rotated about an axis making an angle θ with the fixed magnetic field (B_0), the Hamiltonian becomes a sum of constant and time-dependent terms. For dipole-dipole interactions, the time independent spatial component scales with the factor $(3\cos^2\theta - 1)$. Figure 2 shows the Mathematica output of the factor $3\cos^2\theta - 1$, as well a graphical representation for visual reference. When $\theta = 54.7356^\circ = \arccos(1/\sqrt{3})$, the so called “magic angle”, this term disappears and the time-dependent terms are periodic functions of time. This causes the frequency induction decay (FID) to be a train of “rotational echoes” separated by a sample turning period. Fourier transform of the FID yields a spectrum that shows spinning side bands at multiples of the magic-angle spinning speed. A static non-spinning solid sample will give very broad peaks. At low spinning speeds, a high number of spinning side bands will clutter the spectrum. If the spinning speed is much greater than the dipolar linewidth, then dipole-dipole interactions will effectively disappear.

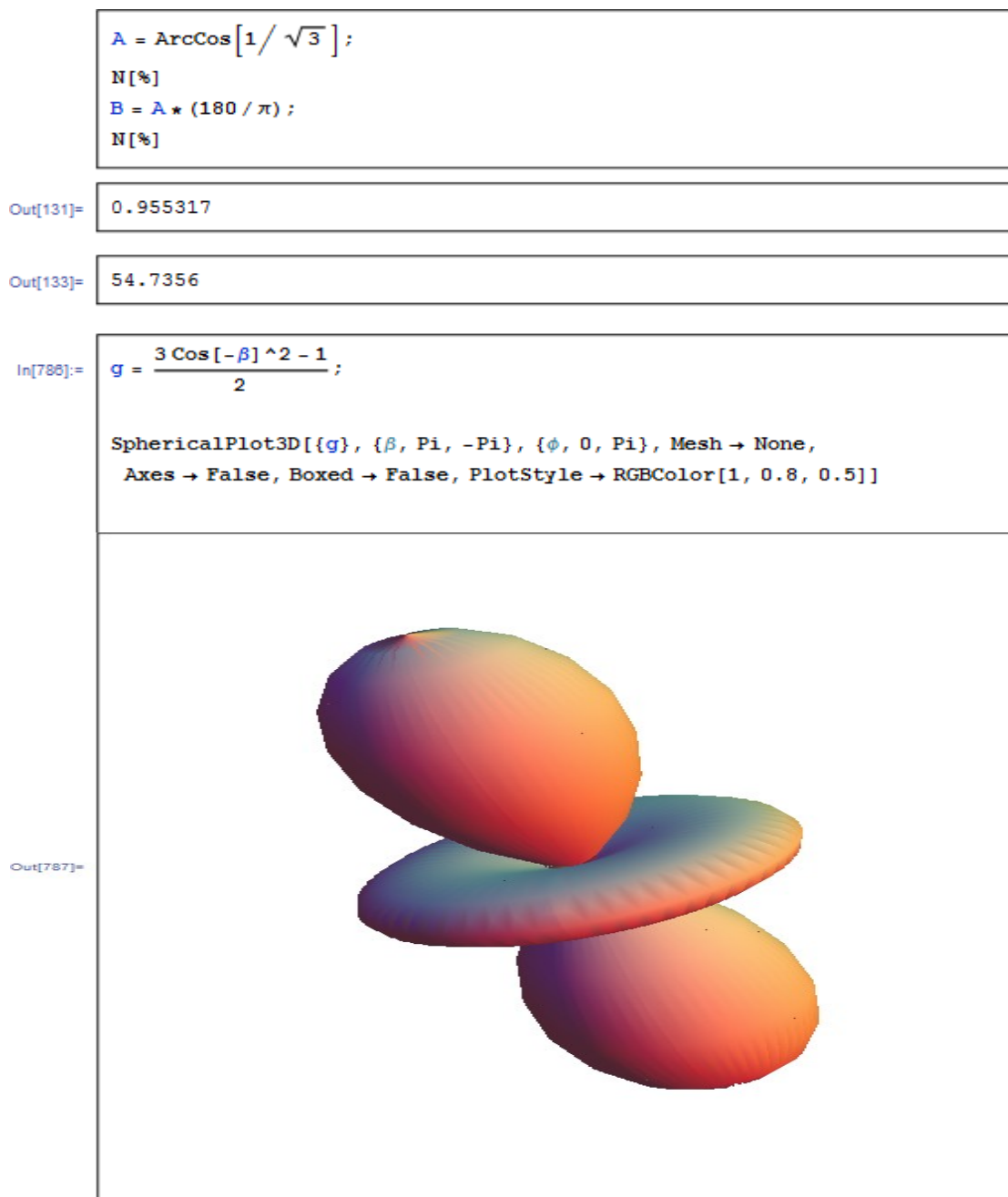


Figure 2. Mathematica output showing the factor associated with magic angle spinning in ssNMR. The magic angle is important for the measurement of anisotropic contributions in solid samples and is not limited to ssNMR because anisotropy exists in other fields as well (i.e. time resolved fluorescence spectroscopy). In the space filled graphic at the bottom of the figure (Out[787]) the filled space is where a spectroscopy signal is greatest, so placing the sample at an angle that coincides with the magic angle maximizes the anisotropic signal. If a sample were simply placed along the z axis, there would be a loss in total return because there is no information, or signal response, at 54.7°.

Schaefer and Stejskal successfully demonstrated that MAS could be used to average chemical shift anisotropy.¹² It was later determined that all interactions described, as the dipole-dipole part of the Hamiltonian, by a second rank tensor term involve the same angular dependence as the dipole-dipole interaction.¹³ Therefore, MAS may average out five important interactions; 1) heteronuclear dipole-dipole interactions, 2) chemical shift anisotropy (CSA), 3) magnetic susceptibility inhomogeneities, 4) first order quadrupole interactions, and 5) the homonuclear dipole-dipole interactions. This has made it possible to perform heteronuclear experiments by decoupling protons to remove the dipolar interaction and leaving chemical shift anisotropy as the only remaining interaction (source of sidebands that may still be eliminated at higher speeds, in most cases). Currently, MAS ssNMR is a widely accepted method to study soft matter and heterogeneous materials.

Although spinning at the magic angle is important for the previously described reasons, there is an added advantage to controlling the MAS rate. Varying MAS rates will reveal the rigidity of a sample by observing the change in the width of a signal. The nuclei in solid samples are usually in rigid environments, thus solid materials will give broad NMR signals, due to the anisotropic contributions for each of the nuclei in a chemical shift environment. Liquid samples usually contain enough molecular motion to minimize chemical shift anisotropy and sharp (isotropic) signals are typically observed. To obtain sharper lines in ssNMR the MAS rate can be increased, and the isotropic signal becomes more defined. For example, a copolymer of polystyrene (PS) with a T_g of 100°C and polybutadiene (PB) with a T_g of -90°C will have different line widths in a ^1H NMR spectrum at 25°C. The PS will give a broad signal in the aromatic range and the PB component will give sharper signals in the olefinic and aliphatic regions. Figure 3 shows the effect of different spinning speeds on the ^1H spectra of an example PS/PB copolymer sample (commonly called Styrene Butadiene Rubber, SBR). The 5kHz spectrum has much broader peaks than the 25kHz spectra due to

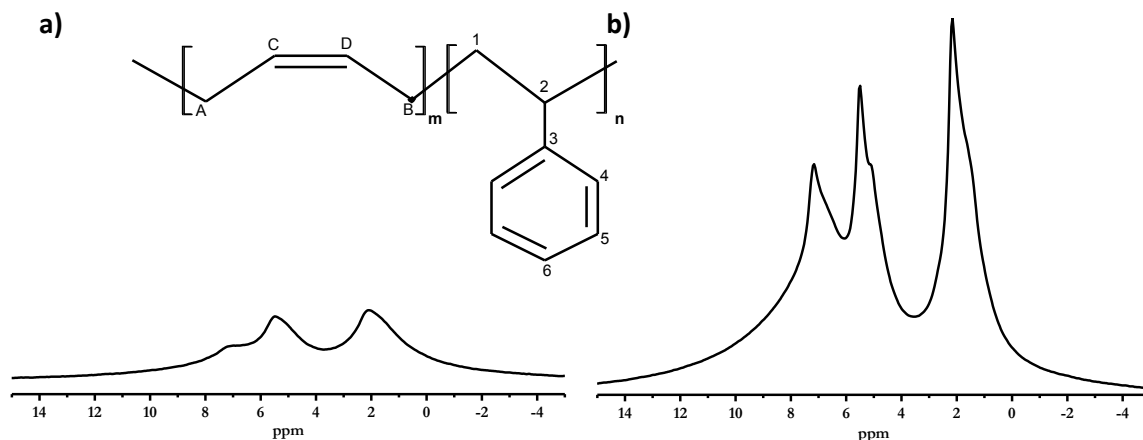


Figure 3. Normalized ^1H spectra of a PS/PB copolymer (SBR) at two different MAS rates. In a) the spectrum was taken at 5 kHz, and b) is the spectrum taken at 20 kHz. The PS resonance at ~ 7 ppm (protons at 4,5, and 6) is the most affected by the MAS rate. The PB peaks are at 2 ppm (aliphatic; A and B) and 5.5 ppm (olefinic; C and D) are affected as well but the 5 kHz spectrum does show that PB is above its T_g for these room temperature experiments (294 K). The chemical structure of a non-composition weighted SBR is given for reference.

the rigidity of the system. The spectra can be fit and the integrated areas of each species can be used to calculate a normalized rigid percentage for the bulk system using equation 1.

$$\frac{\text{Styrene Butadiene Rubber (SBR) @20k spinning} - \text{SBR@5k}}{\text{SBR@20k}} = \% \text{ rigid SBR} \quad 1)$$

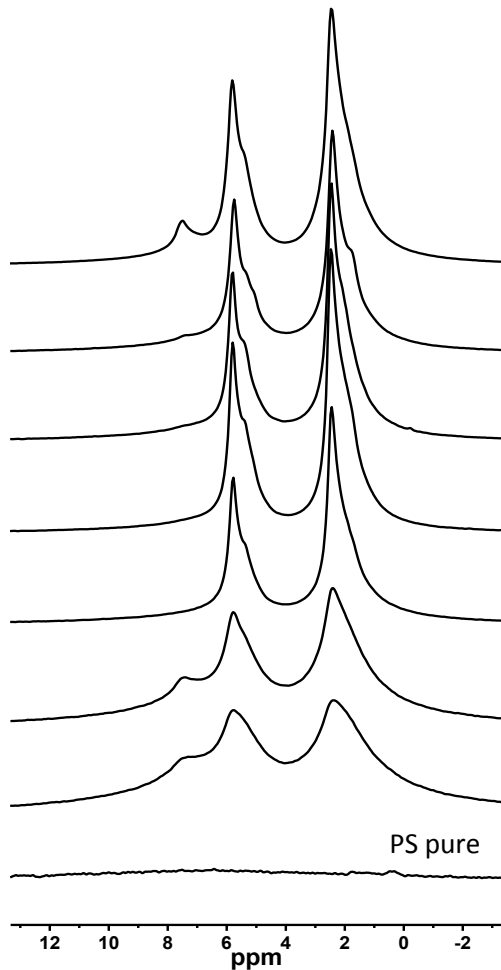
The quantitative composition analysis is also possible using the 25kHz spectrum using equation 2.

$$\frac{\text{normalized area of PS}}{\Sigma \text{PS \& PB}} = \text{mole \% PS} \quad 2)$$

This approach is extremely useful for determining the influence of the copolymerization on bulk PS. The copolymer properties are sensitive to % PB, and the copolymerization method. Figure 4 shows how using different MAS speeds will provide a distinct response based on the %PB of the method of

copolymerization. Furthermore, if the composition of a particular copolymer is not known, a standard addition (spin-counting) experiment can be done. When using a known amount of standard added

a) 5kHz



b) 20kHz

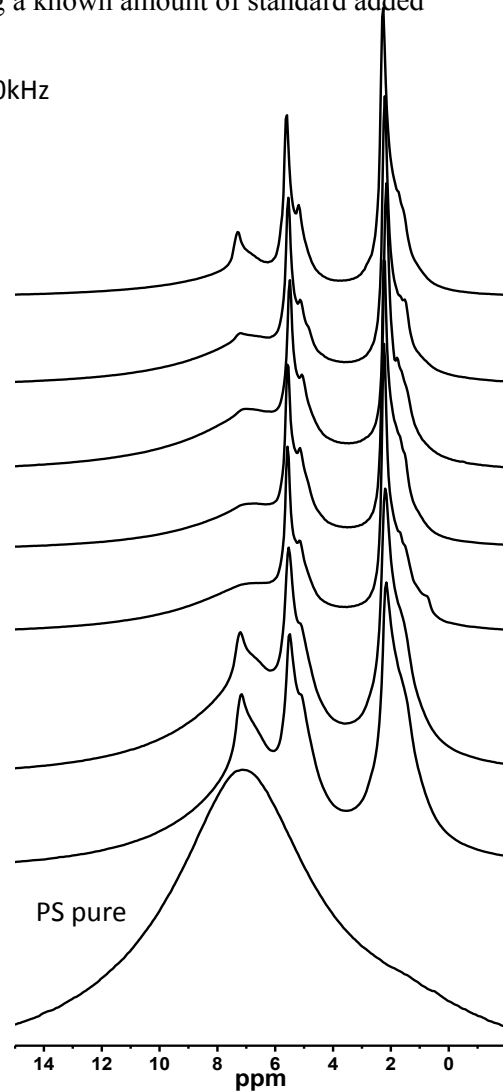


Figure 4. A stack plot of several example SBR's with different PS:PB compositions at different MAS rates.

to the sample, the molar ¹H contribution can be determined using the example given for a polybutadiene/polydimethyl siloxane (PB/PDMS) mixture in equation 3.

$${}^1H \text{ mole } \% \text{ PDMS} = \frac{\text{integrated area PDMS}}{\text{integrated area PDMS} + \text{integrated area PB}} \quad 3)$$

This strategy can be used for any system provided the integrated area for each species can be determined, but caution must be exercised when selecting the spin-counting substance. PDMS is a good choice as a spin-counting measure for ssNMR because it is a viscous liquid at room temperature that gives a quantitatively resolved peak at 0.2 ppm, which serves a chemical shift reference.

Using MAS for ^1H ssNMR can yield important information about these systems. Figure 4 shows an example that shows how the varying the MAS rate can provide information about the physical state of polymer samples using simple and abundant ^1H nuclei in ssNMR. Given that line widths change for a sample in a given physical state (i.e. solid, rubbery, or liquid), these phases and phase transitions can be studied with variable temperature experiments for the determination of the glass transition. It is also possible to measure how each species in a copolymer is affected by the physical or chemical properties of the other. Information about this influence can be determined with the use of variable temperature, MAS rates, and an added spin-counting measure. The integrated ^1H peak areas are quantitative with respect to the molar ^1H contribution for each component of the copolymer, and the ratio of these peak areas should match the theoretical molar ^1H percentages calculated from the composition. At certain temperatures and MAS rates, the theoretical integrated areas indeed equal the experimentally determined areas in the SBR example in figure 3. Deviations between the quantitative NMR analysis and theoretical could be due to many things including the presence of non-uniform properties at the boundaries between the different copolymer species. This can be calculated using the example in equation 4.

$$\% PB \text{ missing} = \frac{\text{theoretical integrated area PB} - \text{integrated area PB} (^1\text{H NMR})}{\text{theoretical integrated area PB}} \quad 4)$$

Proton experiments using MAS ssNMR are very useful, but heteronuclear experiments contain much more information about solid samples and polymeric materials. Many are familiar with

^{13}C NMR and the use of ^1H decoupling for liquid samples. This simple Bloch decay experiment is also available in ssNMR, albeit requiring much greater decoupling power for solid samples. However, ssNMR has the added advantage of readily exploiting the heteronuclear dipole interaction via cross-polarization (CP). As a reminder, this dipole interaction can be dependent upon MAS and caution must be exercised for CP experiments that the MAS rate is not equal to or greater than the heteronuclear dipole frequency ($\sim 20\text{kHz}$).¹⁴ CP is a ssNMR technique that allows for increasing the sensitivity to the ^{13}C nuclei, or other low- γ (i.e. low natural abundance) nuclear spin. This sensitivity arises from making use of the heteronuclear dipole interaction of 1.1% abundant ^{13}C nuclei with 99.99% abundant ^1H nuclei via polarization transfer. The CP experiment increases the difference in the spin up and spin down ^{13}C populations by creating an artificially low temperature abundant spin system and then allowing the low abundant spin system to come in contact with the low temperature abundant spin system. This produces a drop in the temperature of low abundant ^{13}C system because the heat capacity is much greater for the abundant ^1H system, and that results in greater population difference between the higher and lower energy spin states. Therefore, the CP experiment cuts down on the time between FID acquisitions, which shortens the total time needed to acquire a carbon spectrum. A more elaborate explanation of the theory for CP experiments can be found in reference 14 and others^{15-15b} on ssNMR.

It is also important to recognize that, even with the benefit of increased sensitivity and shortened acquisition time, the CP efficiency is dependent upon the physical state of a sample. Solid samples are more susceptible to cross-polarization, than soft or liquid samples. This might be intuitive given previous explanations about the comparison between MAS and liquid experiments. For example, liquid samples contain enough motion to eliminate much of the five interactions described on page 7 that MAS was designed to mimic via solid sample rotation, and intermediate or rubbery samples would be in the intermediate regime for such interactions. Therefore, CP

experiments are useful for monitoring phase behavior over a wide temperature range including the glass transition¹⁶.

The CP experiment provides more information about the dynamics associated with the glass transition than DSC, but is limited in the ability to measure atomic level chain motion directly. Many investigators have employed ^2H NMR to get more detailed chain-level information. Deuterium NMR has been used to determine the glass transition temperature for pure polymers as well as for the individual components in a binary blend through isotopic labeling. Each component must be individually labeled, but still leads to the ability to measure the chain level dynamics associated with the glass transition for each isotopic labeled species. Chain dynamics are only observable for polymer segments the length of several chemical monomers termed the Kuhn monomer. Kuhn segments are of a length great enough for conformational changes about the polymer backbone without violating conformational change thermodynamics. If a polymer is in its glassy state, no conformational changes occur during the mixing time of a deuterium NMR experiment and powder pattern, “horns”, is observed for this quadrupolar nucleus. At discrete temperatures throughout the glass transition this powder pattern changes with mixing time and allows for determination of the correlation time for polymer backbone motions, conformational changes, of the deuterated species. There are some issues with using ^2H labeling, such as 1) ^2H NMR probes faster time scales than our approach, 2) there is a known isotope affect for deuterium labeling, and 3) both components in a blend cannot be labeled at the same time. Thus, the modern Centerband Only DEtectect Exchange (CODEX) ssNMR experiment has been implemented as part of our approach to investigate these materials and overcome the issues associated with isotope labeling.

CODEX – Centerband Only Detected Exchange

The CODEX experiment is a one-dimensional (1D) constant-time version of classic two-dimensional exchange experiments that exploits the anisotropy of the chemical shift interaction to detect movement (in real time) of polymer chain segments. The dynamics of chain segment reorientation have typically been studied using multidimensional exchange techniques on solid materials. The multidimensional techniques are informative, but there are resolution problems and sensitivity issues that result from the requirements of anisotropically broadened lineshapes and sidebands. The 1D CODEX relies on signal decay from magnetization dephasing due to molecular motion (conformational changes along the polymer backbone) during the mixing time. This allows for the acquisition of high resolution spectra without isotopic labeling. The rotor synchronized CODEX pulse sequence with decoupling is shown in Figure 5. Pure CODEX will only contain signal intensity differences for chain segments that have reoriented during the allowed exchange/mixing time. The result is a different chemical shift anisotropy magnitude not refocused during the second recoupling period consequently generating a signal difference between a reference spectrum and CODEX spectrum.

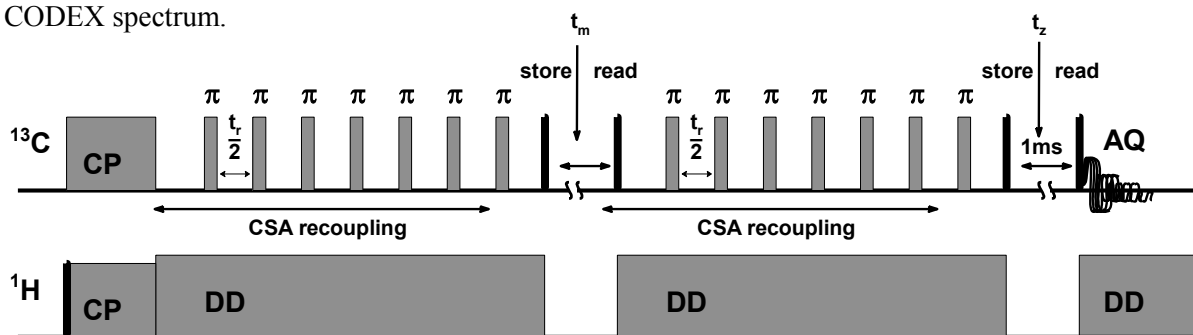


Figure 5. CODEX experimental pulse sequence applied under MAS conditions.^{50, 51} The value of the mixing time (t_m) may range from 50 milliseconds to many seconds. The reference time is typically 1ms so that the experiment is specific to slow motions. DD is high power decoupling on the proton channel. Dark pulse lines are 90 degree ($\pi/2$) pulses, shaded boxes are 180 degree (π) pulses, and CP is cross-polarization pulses of 1ms. CSA is recoupled by applying a π pulse synchronized with the MAS rate (rotor period, t_r). When the t_z is in the middle of the recoupling periods the spectrum “reference” spectrum is acquired. When the t_m is between the recoupling periods the “CODEX” spectrum is acquired. The reference time (t_m) and t_m are swapped every 256 scans to account for spectrometer drift.

The CODEX experiment collects transients in alternating acquisition blocks for each of a reference (S_0) spectrum and a CODEX spectrum (S). The sum of these acquisition blocks are then compared as a normalized exchange intensity (E); and $E = \Delta S/S$, $\Delta S = S_0 - S$. ΔS is a consequence of dephasing of the magnetization if the orientation-dependent chemical shift (CS) frequencies are different before and after the mixing time. In order to eliminate the T_1 , T_2 relaxation effects the reference spectrum (S_0) is measured so that it has the same T_1 , T_2 relaxation factors but no motion during mixing time. Figure 6 shows an example of CODEX results where there is clearly a difference

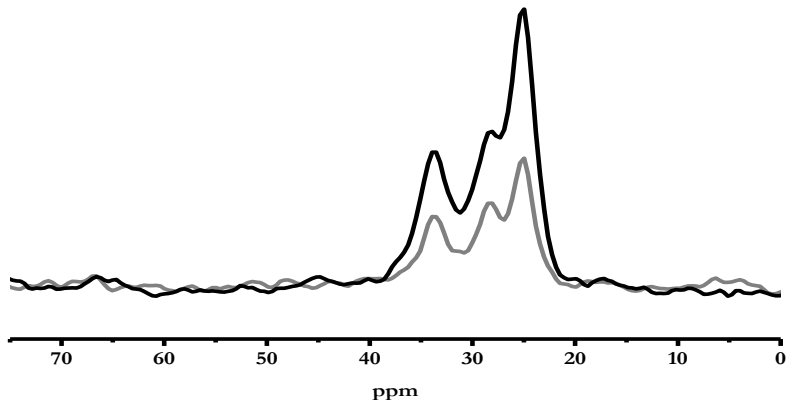


Figure 6. An example of the reference (S_0 , **black** line) and CODEX (S , **gray** line) spectra stacked to show the exchange intensity (E). The integrated areas of each spectrum are used to determine the normalized E by $E = (S_0 - S)/S_0$.

in the magnitude of the refocused isotropic shift between S_0 and S . The exchange intensity (E) is dependent on CSA recoupling time (τ_{CSA}), mixing time (t_m), and temperature (T). The flexibility of each experimental CODEX parameter gives site specific information about slow conformational changes for polymers below, at, and above T_g . The next few paragraphs will discuss the significance of these parameters in more detail.

In order to reintroduce the chemical shift anisotropy (CSA), a $180 (\pi)$ pulse must be applied every half rotation of the sample rotor ($t_r/2$) since, as stated earlier, MAS can average the chemical shift interaction. This is shown pictorially in Figure 6. The CSA recoupling period is established by

adjusting the number ($2N$) of π pulses and/or changing the sample spinning speed (t_r) to determine the CSA time constant (τ_{CSA}) at a fixed mixing time (t_m). The τ_{CSA} is then dependent on the CSA recoupling time by $N \cdot t_r$. For example, if in Figure 6 the MAS rate is 4500 Hz, $t_r = 222 \mu\text{s}$, and there are 4 periods before the mixing time and after the mixing time ($N=8$), then $N \cdot t_r = 1.778 \text{ ms}$. The $N \cdot t_r$ dependence is typically determined at a discrete temperature, usually the DSC T_g , for each pure polymer and the lowest value is used for all experiments conducted on binary blend systems.

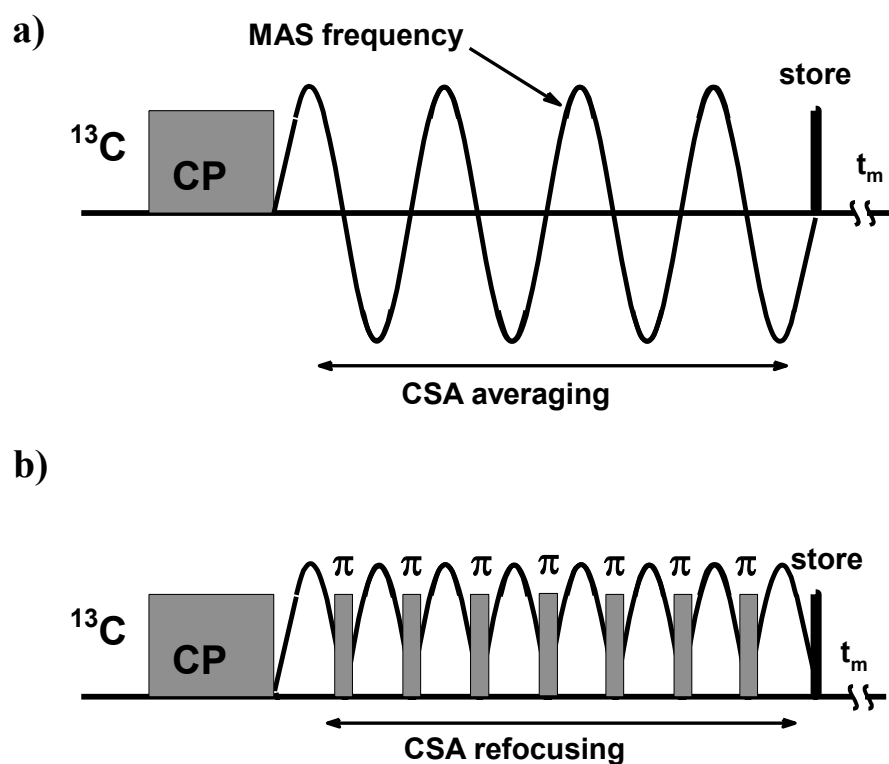


Figure 7. The ^{13}C isolated portion of the CODEX pulse sequence. In a) the CSA is averaged by the magic angle spinning, as shown by the sine wave representing the MAS frequency (t_r). In b) the CSA is refocused, or recoupled, by the rotor synchronized π pulses at $t_r/2$.

The mixing time dependence is determined by varying the mixing time, usually from 10 ms to 3 or 400 ms, at DSC T_g . The maximum t_m could theoretically be much greater for more persistent chemical shift interactions, but when comparing the time scales available using CODEX, the time

scales are considerably greater than those achieved by other multidimensional methods. The value of determining the t_m dependent exchange intensity $[E(t_m)]$ is obtaining an experimental correlation time constant (τ_c) at a discrete temperature, and it is directly comparable with methods used in multidimensional studies. However, even though the CP alleviates some experiment time, conducting a mixing time dependence experiment at several different temperatures would be quite time consuming. Each experimental point can take up to 8 hours to acquire, and it could take 40+ hours to obtain Figure 8. Therefore, a single experimentally determined correlation time can be used to verify correlation times calculated with widely accepted polymer physics models that predict a correlation time distribution over a broad temperature range using temperature dependent exchange data $[E(T)]$ obtained using CODEX.

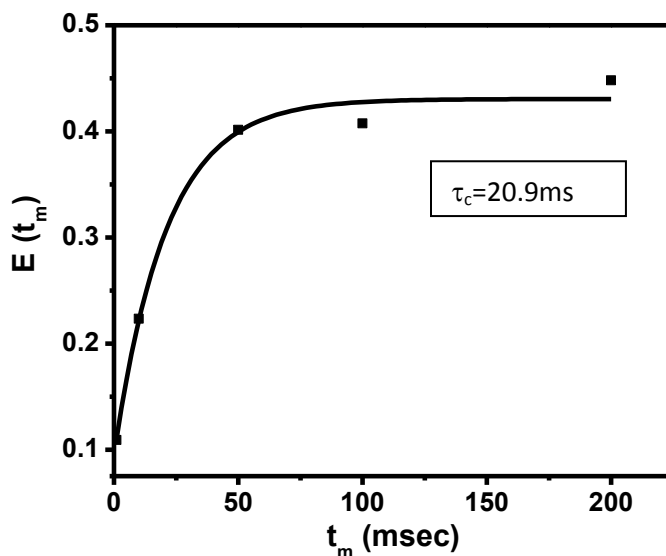


Figure 8. CODEX mixing time dependence $E(t_m)$ for a 1,2-polybutadiene sample. Varying the mixing time in the CODEX experiment at a discrete temperature value gives an experimentally determined correlation time constant (τ_c) that is independent of the model used to calculate the correlation time values for $E(T)$.

The effect of temperature on amorphous macromolecules through the glass transition can be observed using CP experiments, as discussed earlier, but site specific information for segmental

relaxations cannot be measured directly. The CODEX experiment resolves that issue by directly observing polymer dynamics as they occur during the allowed mixing time over a broad temperature range, as long as time scale of those motions is greater than 1ms (t_z). Figure 9 shows the $E(T)$ CODEX data for two different homopolymers over a their respective T_g ranges using data similar to that in Figure 6. Each point on the graph is determined by $E(T) = (S_0 - S)/S_0$. The experimentally

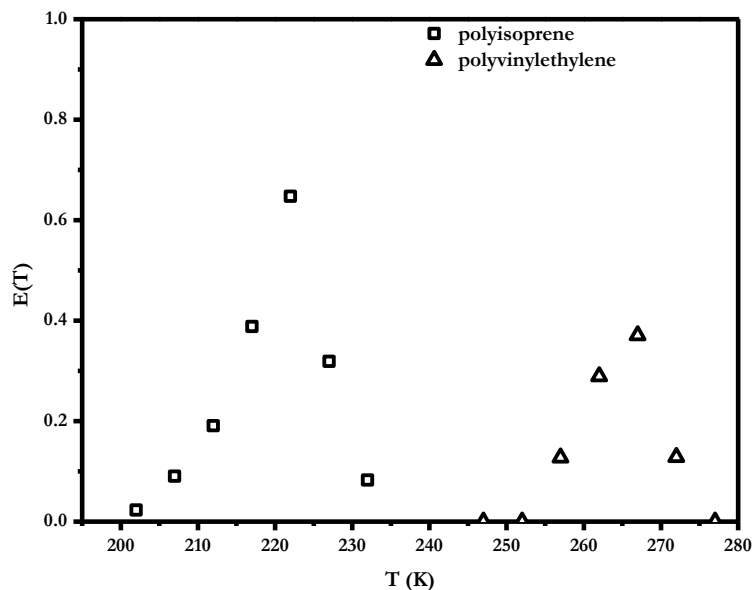


Figure 9. Normalized ($t_m=50\text{ms}$) experimental exchange intensity $E(T)$ data for pure PI and PVE.

determined exchange intensity $E(T)$ points are fit using theoretical Arrhenius and Williams-Landel-Ferry polymer (WLF) physics models.

Theoretical calculation of normalized exchange intensity $E(T)$

As show in a recent publication¹⁷, in the completely rotor-synchronized MAS experiment an effective (recoupled) CSA tensor can be approximately modeled by a static CSA tensor. This approximation holds for a small-angle rotational-diffusion model. The temperature dependence of normalized pure-exchange intensity, $E(T)$, in the case of motions with a distribution of correlation times, can then be calculated as in the PUREX experiment.¹⁸

$$E(T) = \frac{S_0 - S}{S_0} = \frac{\int_0^\infty \{\text{Re}[G_-(t_z, \tau, T)] - \text{Re}[G_-(t_m, \tau, T)]\} g(\tau) d\tau}{\int_0^\infty \text{Re}[G_-(t_z, \tau, T)] g(\tau) d\tau} \quad (5)$$

where $g(\tau)$ is a scaling factor from a distribution of correlation times [e.g. log-Gaussian, Kohlrausch–Williams–Watts (KWW) distribution]. We can restrict ourselves to calculation of magnetization after the second recoupling period since all the exchange effects are encoded at that point¹⁹, consequently the G_- functions are defined by:¹⁷

$$\mathbf{G}_-(\mathbf{t}_x) = \langle 1 | \exp \left[(\tilde{\Pi} - i\tilde{\omega}) \frac{\tau_{\text{CSA}}}{2} \right] \exp \left[(\tilde{\Pi} \mathbf{t}_x) \right] \exp \left[(\tilde{\Pi} + i\tilde{\omega}) \frac{\tau_{\text{CSA}}}{2} \right] \tilde{\mathbf{P}}^{\text{eq}} | 1 \rangle \quad (6)$$

where t_m refers to the mixing time used to obtain the exchange spectrum S ($t_m = 200$ or 50 ms) and reference spectrum S_0 ($t_z = 1$ ms). $\tilde{\Pi}$ is the exchange matrix of jump rates between N sites defined by a given model of molecular reorientation (i.e. the matrix element $(\tilde{\Pi})_{ij}$ describes the probability per unit time for exchange from site ‘j’ to ‘i’). $\tilde{\mathbf{P}}^{\text{eq}}$ is the matrix of equilibrium populations of those N sites, and $|1\rangle$ is the $(1, 1, 1, \dots, 1)$ vector needed to obtain the sum of contributions of all sites participating in the exchange. The total time of chemical shift anisotropy (CSA) evolution is τ_{CSA} , and $\tilde{\omega}$ is the matrix of NMR resonance frequencies that depend on the orientation of a chemical shift tensor at a given site relative to the external magnetic field B_0 .

The chain dynamics of amorphous polymers used in this study were modeled using the isotropic rotational diffusion model²⁰ which assumes that molecular reorientations occur via small-angle jumps to nearby sites, and further sites can be reached after several jumps if the experimental mixing time is long enough. The longer the mixing time, i.e. the greater the t_m/τ_c ratio, the more distant sites can be populated (with τ_c being the correlation time of the motion).

A previous publication³ shows that the results of Eq. (6) are comparable with calculations obtained using the following formula where brackets denote powder average.⁸

$$\left\langle \mathbf{P}_{ij}(\mathbf{t}_m) \mathbf{P}_j^{\text{eq}} \cos\left(\frac{\mathbf{N}}{2} \Phi_j - \frac{\mathbf{N}}{2} \Phi_i\right) \right\rangle = \left\langle \left(\mathbf{e}^{\tilde{\Pi} \mathbf{t}_m}\right)_{ij} \mathbf{P}_j(0) \cos\left(\frac{\mathbf{N}}{2} \Phi_j - \frac{\mathbf{N}}{2} \Phi_i\right) \right\rangle \quad (7)$$

$\mathbf{P}_{ij}(\mathbf{t}_m) = \left(\mathbf{e}^{\tilde{\Pi} \mathbf{t}_m}\right)_{ij}$ is conditional probability that the spin is in the site “i” after the mixing time, provided that it was in site “j” before \mathbf{t}_m . $\mathbf{P}_j^{\text{eq}} = \mathbf{P}_j(0)$ is the equilibrium population of site “j”, and $\Phi(t)$ is the expression for the phase accumulated during one rotor period, t_r , when CSA recoupling π -pulses are applied every $1/2 t_r$.⁹

$$\frac{\mathbf{N}}{2} \Phi(t) = \frac{\mathbf{N}}{2} \left(4 \frac{S_1}{\omega_R} \cos(\gamma + \omega_R t) - 4 \frac{C_1}{\omega_R} \sin(\gamma + \omega_R t) \right) \quad (8)$$

with \mathbf{N} being the total number of rotor periods, ω_R equal to spinning frequency and expressions for S_1, C_1 coefficients as given by Luz *et al.*²¹ In the case of completely rotor-synchronized experiments the parameter t is the starting point of the π -pulse train and is set to zero.

The exchange matrix $\tilde{\Pi}$ for the isotropic rotational diffusion model is tri-diagonal^{5a}:

$$\tilde{\Pi} = \begin{bmatrix} \Pi_{1,1} & \Pi_{1,2} & 0 & 0 & 0 & 0 \\ \Pi_{2,1} & \Pi_{2,2} & \Pi_{2,3} & 0 & 0 & 0 \\ 0 & \Pi_{3,2} & \Pi_{3,3} & \ddots & 0 & 0 \\ 0 & 0 & \ddots & \ddots & \Pi_{m-1,m} & 0 \\ 0 & 0 & 0 & \Pi_{m,m-1} & \Pi_{m,m} & \Pi_{m,m+1} \\ 0 & 0 & 0 & 0 & \Pi_{m+1,m} & \Pi_{m+1,m+1} \end{bmatrix} \quad \text{for } m = 1, 2, \dots, N-1 \quad (9)$$

and the super- and sub-diagonal elements are given by:

$$\Pi_{m,m+1} = \frac{1}{6 \tau_c \Delta^2} \frac{\sin(m\Delta)}{\sin[(m+1/2)\Delta]}, \quad \Pi_{m+1,m} = \frac{1}{6 \tau_c \Delta^2} \frac{\sin(m\Delta)}{\sin[(m-1/2)\Delta]}, \quad (10)$$

where τ_c is the correlation time and $\Delta = \pi/N$ is the angular interval. The diagonal elements are obtained as a negative sum of all non-diagonal elements of a given column:

$$\Pi_{m,m} = \frac{-1}{3\tau_c\Delta^2} \cos\left(\frac{\Delta}{2}\right) \quad (11)$$

The matrix calculations were performed using Mathematica[®] (Wolfram Research, Inc.)

The equilibrium population of site ‘j’ in the isotropic rotational diffusion model is given by^{5c}:

$$P_j^{\text{eq}} = \frac{\sin[(j-0.5)\Delta]}{\sum_{i=1}^N \sin[(i-0.5)\Delta]} = \sin[(j-0.5)\Delta] \sin\left(\frac{\Delta}{2}\right) \quad \text{for } j = 1, 2, 3, \dots, N \quad (12)$$

leading to the following diagonal matrix:

$$\tilde{P}^{\text{eq}} = \begin{bmatrix} P_1^{\text{eq}} & 0 & 0 & 0 & 0 & 0 & 0 \\ 0 & P_2^{\text{eq}} & 0 & 0 & 0 & 0 & 0 \\ 0 & 0 & P_3^{\text{eq}} & 0 & 0 & 0 & 0 \\ 0 & 0 & 0 & \ddots & 0 & 0 & 0 \\ 0 & 0 & 0 & 0 & P_j^{\text{eq}} & 0 & 0 \\ 0 & 0 & 0 & 0 & 0 & \ddots & 0 \\ 0 & 0 & 0 & 0 & 0 & 0 & P_N^{\text{eq}} \end{bmatrix} \quad \text{with normalization conditions } \sum_{j=1}^N P_j^{\text{eq}} = 1. \quad (13)$$

The matrix of NMR frequencies of the accessible sites is diagonal

$$\tilde{\omega} = \begin{bmatrix} \omega_1 & 0 & 0 & 0 & 0 & 0 & 0 \\ 0 & \omega_2 & 0 & 0 & 0 & 0 & 0 \\ 0 & 0 & \omega_3 & 0 & 0 & 0 & 0 \\ 0 & 0 & 0 & \ddots & 0 & 0 & 0 \\ 0 & 0 & 0 & 0 & \omega_i & 0 & 0 \\ 0 & 0 & 0 & 0 & 0 & \ddots & 0 \\ 0 & 0 & 0 & 0 & 0 & 0 & \omega_N \end{bmatrix} \quad (14)$$

with elements representing the frequency in the laboratory frame for spins at site ‘i’

$$\omega_i = \omega_L \left[\frac{1}{3} (\delta_{11}^{i, MF} + \delta_{22}^{i, MF} + \delta_{33}^{i, MF}) + C_2^i \cos(2\omega_R t + 2\gamma) + S_2^i \sin(2\omega_R t + 2\gamma) + C_1^i \cos(\omega_R t + \gamma) + S_1^i \sin(\omega_R t + \gamma) \right] \quad (15)$$

where ω_L is resonance frequency, ω_R is sample spinning speed, and parameters C_2^i , S_2^i , C_1^i , S_1^i depend on components of chemical shift tensor in molecular frame (MF) $\delta_{11}^{i, MF}$, $\delta_{22}^{i, MF}$, $\delta_{33}^{i, MF}$ and the Euler angles α , β , γ transforming the chemical shift tensor from MF to rotor frame (RF). The exact expressions are given by Luz *et al.* ⁶ Powder averaging involves numerical integration over angles α , β , γ in steps of $\Delta\alpha$, $\Delta\beta$, $\Delta\gamma$.

In the isotropic rotational diffusion model the N accessible sites correspond to N different orientations of principal axis system (PAS) of chemical shift tensor relative to MF. The change of orientation of PAS occurs in a number of individual steps. In case of N = 20 sites the angular interval is $\Delta = 9^\circ$. The chemical shift tensor elements in the MF, $\tilde{\delta}^{i, MF}$, for a given site 'i' can be obtained from the diagonal chemical shift tensor in PAS, $\tilde{\delta}^{PAS}$, via a series of rotations about angles a^i , b^i , c^i ,

$$\tilde{\delta}^{i, MF} = \tilde{R}^{PAS \rightarrow MF}(a^i, b^i, c^i) \tilde{\delta}^{PAS} \tilde{R}^{PAS \rightarrow MF}(a^i, b^i, c^i)^{-1} \quad (16)$$

where the transformation angle ' a^i ' represents the initial rotation around 'z' axis of PAS, ' b^i ' is the angle between 'z' axes of PAS and MF, whereas ' c^i ' is the final rotation angle about the 'z' axis of MF. $\tilde{R}^{PAS \rightarrow MF}$ in Eq. (16) represents a 3 x 3 transformation matrix with elements depending on angles a^i , b^i , c^i as given by Luz *et al.* ⁶

The following chemical shift tensor values were used in calculating the normalized exchange intensity for the PI methyl groups: $\delta_{11}^{PAS} = 28.5 \text{ ppm}$, $\delta_{22}^{PAS} = 26.3 \text{ ppm}$, and $\delta_{33}^{PAS} = 8 \text{ ppm}$, which give a typical methyl CS tensor anisotropy and isotropic shift $\delta_{iso} = 24.9 \text{ ppm}$. For the methine group of polyvinylethylene (PVE), the tensor anisotropy was estimated using Herzfeld-Berger

analysis (HBA) at 716Hz, 331Hz, and 190Hz MAS rates. The average of the MAS rate CS tensor values were used for calculations. $\delta_{11}^{PAS} = 52.01 ppm$, $\delta_{22}^{PAS} = 38.94 ppm$, and $\delta_{33}^{PAS} = 27.10 ppm$ resulting in the experimentally observed isotropic value $\delta_{iso} = 39.5 ppm$. The HBA analysis was done using software from Eichele, K, *version 1.6.9, January 6, 1999*. The HBA software estimates the CS tensor from sideband intensities at different spinning speeds. The spectra used to obtain sideband intensities at different spinning speeds for the PVE methine are shown in figure 10. Also, it is a practical example of how magic-angle spinning solid-state NMR refocuses CS anisotropy to obtain an isotropic signal at higher spinning speeds.

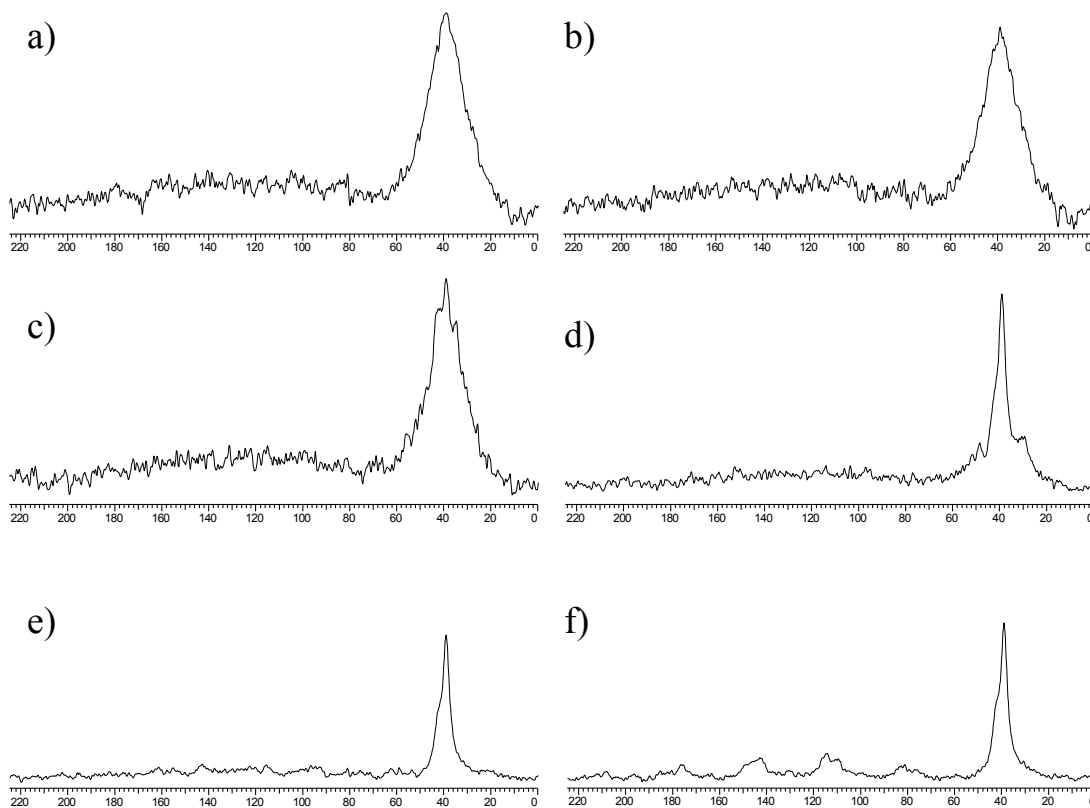


Figure 10. CP spectra of PVE at different spinning speeds for Herzfeld-Berger analysis and estimation of the CSA tensor. The spinning speeds were a) static, b) 190Hz, c) 331Hz, d) 716Hz, e) 1500Hz, and f) 2500Hz. The static spectrum and the 190Hz spectrum show no spinning sidebands for the PVE methine group. Spinning sidebands begin to appear in the 331Hz and 716Hz spectra.

Distribution of correlation times

It is recognized that the molecular dynamics in polymers slow down dramatically in the proximity of glass transition leading, overall, to an Arrhenius temperature dependence of correlation times. The empirical Williams-Landel-Ferry (WLF) model can be used to describe the experimental data at over a broader temperature range. The Arrhenius model can be used as a linear approximation (when plotted in $\log(\tau)$ vs. $1000/T$ scale) in a relatively narrow temperature range just above the T_g . The advantage of an Arrhenius model is that only two parameters are needed in comparison to 4 parameters in the WLF model. These two models are compared in the fitting of normalized CODEX exchange intensity $E(T)$ data for the homopolymers, and the individual components for each polymer in the blend, to evaluate temperature dependence and distribution of correlation times. The comparison was applied as follows: A) Arrhenius model of temperature dependence with log-Gaussian distribution, B) WLF model with Kohlrausch–Williams–Watts (KWW) distribution.

In the calculations of $E(T)$ the discrete version of log-Gaussian distribution was used with 17 points equally spaced over 5 decades in the logarithmic scale (from $0.002 \tau_c$ to $400 \tau_c$, where τ_c is the correlation time at the center of the distribution), similar to O'Connor *et al.*⁷ It is assumed that the width of the distribution is temperature dependent and decreases with increasing temperature, accompanied by a shift of τ_c toward smaller values.²⁴ The weighting factors $g(\tau, T)$ are calculated according to:

$$g(\tau, T) = \frac{1}{\sigma(T)\sqrt{2\pi}} \exp\left[-\frac{(\ln(\tau) - \ln(\tau_c(T)))^2}{2\sigma^2(T)}\right] \quad (18)$$

and the width of the distribution experiences changes linear with temperature, $\sigma(T) = a k_B T + \sigma_0$. The mean correlation time, $\tau_c(T)$, follows Arrhenius behavior and k_B is Boltzmann constant. In the discrete version of log-Gaussian distribution only three points per decade are considered, and one effectively obtains a single correlation time for values of σ smaller than 0.28.

To observe the temperature dependence, $E(T)$ calculations were performed for 20 values of temperature, in intervals of 2 – 2.5 K. For each temperature the powder-average of $G_{-}(t_z, \tau, T)$ and $G_{-}(t_m, \tau, T)$ was computed for 17 values of correlation time τ centered at τ_c , followed by calculation of weighting factors $g(\tau, T)$ corresponding to the a given width $\sigma(T)$ of the distribution. Finally, the normalized exchange intensity $E(T)$ was calculated using eq. (5).

In a previous work¹⁷ this model was applied to hhPP/PIB blend and the resulting plots of hhPP correlation times can be compared with recently published dielectric spectroscopy (DS) data for pure hhPP and hhPP in the hhPP/PIB blend.²⁵ Although NMR and DS may probe a different time scale, a similar ~ 3 decade shift of hhPP correlation time values upon blend formation is detected by both methods as shown in Figure 11.

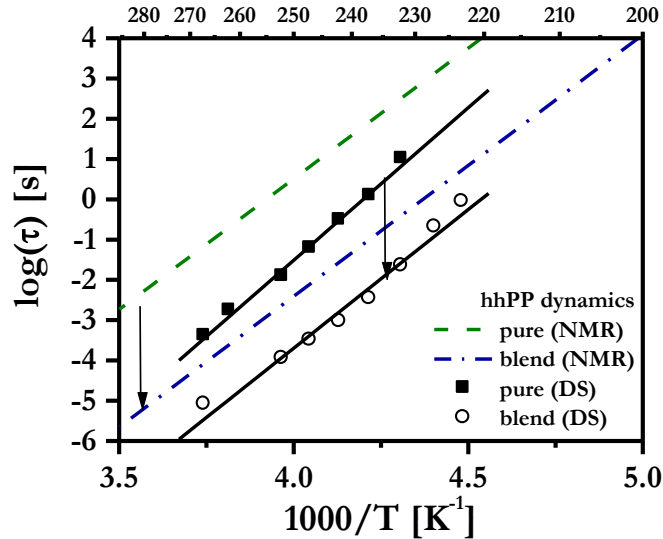


Figure 11. Plots of mean correlation time for pure hhPP and hhPP in the hhPP/PIB blend as obtained from CODEX NMR and dielectric spectroscopy experiments.

The KWW function $\exp[-(\tau/\tau)^\beta]$ with $0 < \beta \leq 1$, a stretched exponential, is used to fit the time dependent quantities that exhibit non-exponential behavior. For $\beta < 1$ it is assumed that a distribution of correlation times is present. The actual shape of that distribution, $g(\tau)_{\text{KWW}}$, can be calculated as²⁶

$$g(\tau, T)_{\text{KWW}} = -\frac{\tau_c(T)}{\pi\tau^2} \sum_{k=0}^{\infty} \frac{(-1)^k}{k!} \sin(\pi\beta k) \Gamma(\beta k + 1) \left(\frac{\tau}{\tau_c(T)} \right)^{\beta k + 1} \quad (19)$$

where Γ is the gamma function. Two examples of asymmetric shapes of KWW distribution for $\beta=0.5$ and 0.3 are show in Figure 12. The temperature dependence of correlation time $\tau_c(T)$ in Eq. (19) is usually given by WLF model ²⁷

$$\tau_c(T)_{\text{WLF}} = \tau_{T_g} 10^{\frac{-C_1(T-T_g)}{C_2+(T-T_g)}} \quad (20)$$

where C_1 and C_2 are empirical parameters and τ_{T_g} is the correlation time at T_g , usually assumed to be greater than or equal to 100s.

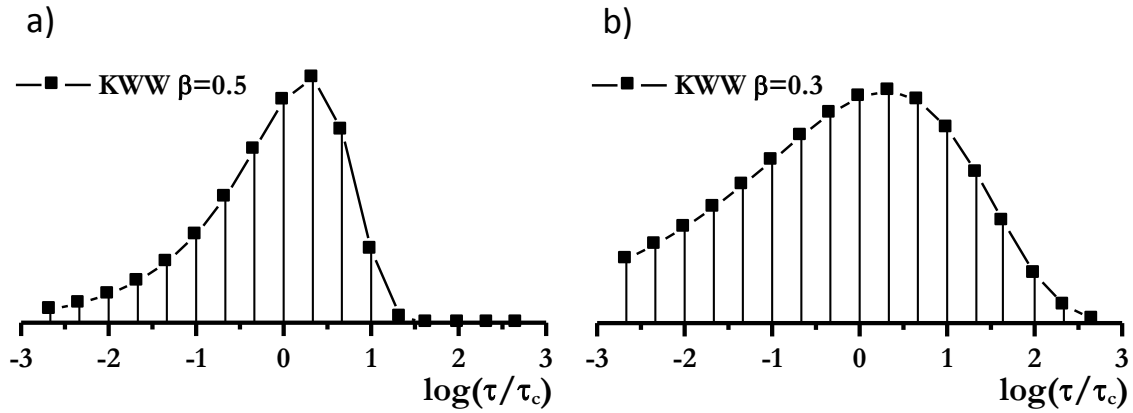


Figure 12. Plots of discrete 17-points KWW distribution $g(\tau)_{\text{KWW}}$ for a) $\beta_{\text{KWW}} = 0.5$ and b) $\beta_{\text{KWW}} = 0.3$ calculated according to Eq. (19)

The approximate relationship between β_{KWW} parameter from KWW distribution and width of log-Gaussian distribution in decades $\Delta_\sigma = \log_{10}(e^{2\sigma})$ as reported by Zemke *et al.*,¹² and Pascui *et al.*²⁸ is presented in Figure 13.

The experimental CODEX data represented in Figure 9 can be fit using the theoretical calculation of normalized exchange intensity $E(T)$ with the model appropriate distribution of correlation times as described. These models eliminate the need for experimentally determining the

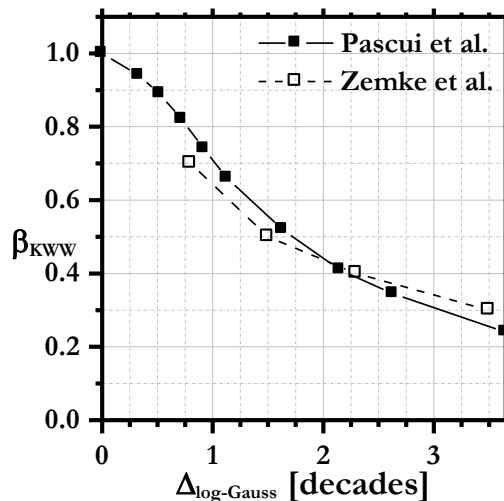


Figure 13. Relationship between β_{KWW} parameter of KWW distribution and half-height width of log-Gaussian distribution.²⁸

correlation time value at each temperature, as in Figure 8, over the entire $E(T)$ range. The theoretically calculated fit using the Arrhenius model with the log-Gaussian distribution is shown in Figure 14. The model and the experimental data ($t_m=50\text{ms}$) are plotted with the respective DSC T_g ranges for each of the pure polymers, showing that the CODEX experiment is observing molecular motion associated with the glass transition for each material.

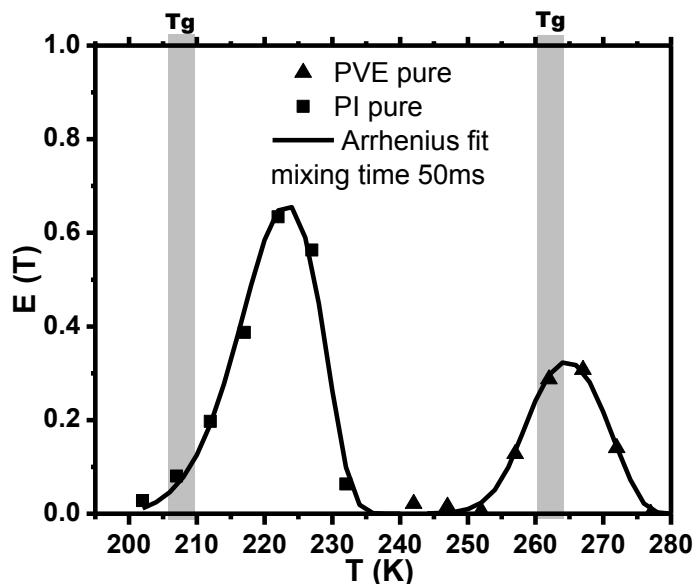


Figure 14. Normalized 50ms exchange intensity $E(T)$ curves for the total aliphatic region integrated intensity. The solid lines represent the Arrhenius model with log-Gaussian distribution to the experimental data.

CHAPTER II

POLYPROPYLENE AND POLYETHYLENE COPOLYMER BLEND MISCIBILITY: SLOW CHAIN DYNAMICS IN INDIVIDUAL BLEND COMPONENTS NEAR THE GLASS TRANSITION*

Introduction

Several key questions relevant to the design, synthesis, and application of heterogeneous polymer materials can be addressed experimentally using binary blends of polyolefins. Although polyolefins are the most chemically “simple” polymers, the complexities of phase behavior over an almost endless array of economically important blend, copolymer, and nanocomposite applications is reflected in the lack of understanding about miscibility in simple binary mixtures of polyolefins.²⁹⁻³³ Stated simply, one cannot predict a priori if two synthetic polyolefins will form a miscible mixture, and therefore from a mechanical properties perspective, a new material. Recently, several groups including our own have investigated these questions using polyolefin blends as a limiting class of macromolecules in which specific chemical interactions are minimized due to their completely saturated sp^3 carbon structure.³⁴⁻³⁹ Chain organization and dynamics control the observed mechanical properties, and while many polyolefin blends are semicrystalline, important limits on phase behavior can be established by examination of amorphous blends. From a practical perspective, new materials are often desired with properties

**The content of this Chapter has been published in Macromolecules, 2008, 41, 2832-2838.*

intermediate between the two constituent polymers, which is often characterized by the difference in their glass transition temperatures T_g . There has been considerable attention in the literature regarding mechanically relevant chain dynamics in amorphous polymers and their blends (with component polymers exhibiting large T_g differences), although in many cases, at temperatures well above T_g . Specifically, the relative contributions of self-concentration (i.e. intrachain) and concentration fluctuation effects to segmental dynamics in pure and mixed polymers, as well as their effects on the cooperative rearrangements near T_g , have been discussed.⁴⁰⁻⁴⁸ Key differences in these models lie in the details regarding temperature dependence of characteristic segmental relaxation lengths, length scales for the glass transition, and intrachain versus interchain contributions.

In a recent paper,⁴⁹ it was shown by direct chain measurement solid-state NMR experiments that the polyolefin blend PIB/hhPP (polyisobutylene/head-to-head polypropylene) is intimately mixed at the chain level, that the mixing is driven by increased configurational entropy in the blend, and the individual slow segmental chain dynamics ($1 \text{ ms} < \tau_c < 1000 \text{ ms}$) near T_g respond in a non-linear fashion upon mixing and are characterized by unique changes in correlation time distributions. This contribution represents the examination of more commercially relevant blend systems involving atactic polypropylene (aPP) and polyethylene-1-butene copolymers (PEB) containing differing amounts of butene comonomer. The model-free experimental observations based on a similar direct/selective chain-measurement strategy are that aPP is intimately mixed with PEB containing 66 wt% 1-butene comonomer, and at or near T_g , slow segmental dynamics become even more heterogeneous in the miscible blend than in the pure polymers, particularly for the high- T_g aPP component. The experiments spanned the full range of temperatures for each pure component glass transition, and that of the blend. Through comparative application of Arrhenius/log-Gaussian versus WLF/KWW models for analysis of the temperature dependent CODEX^{50, 51} exchange intensities, it is determined that in the miscible

aPP/PEB-66 blend, the central correlation time constants τ_c converge to essentially identical values at a common intermediate temperature relative to the unmixed components, but that the correlation time distributions widths diverge from one another in the blend, and from their pure component values. This is particularly evident for the high- T_g aPP component, which exhibits a ca. 3-decade increase in its correlation time distribution in the blend relative to its pure state, far exceeding the ca. 1-decade increase for the low- T_g PEB66 component in the blend. The pure polymers themselves are characterized by 1-2 decade wide correlation time distributions near T_g , decreasing as temperature is increased. Quantitative analysis of all of the temperature-dependent correlation time data in the unmixed and blended polymers reveals that the total configurational entropy increases by 15% in the blend relative to the pure polymer components.

Experimental

Samples and Data Collection. Atactic polypropylene (aPP) was acquired from Eastman, with a molecular weight $M_w = 29600$ and DSC $T_g = -11^\circ\text{C}$. The PEB-66 ($M_w = 114,000$, $T_g = -54^\circ\text{C}$) is the same polymer previously referenced as HPB66 by Graessley and coworkers, and is a monodisperse ethylene-butene copolymer obtained by anionic polymerization of butadiene, followed by hydrogenation.⁵² The degree to which the diene polymerizes 1,2 vs. 1,4 addition determines the butene and ethylene concentrations, respectively, as has been extensively discussed in previous papers.^{52,53} The PEB-23 sample is a commercial ethylene-butene copolymer made via metallocene polymerization ($M_w = 79,000$), and sold as Exact 4041 by ExxonMobil. Other PEB copolymers mentioned in Figure 2 are a combination of commercial or anionically polymerized materials, and are denoted numerically by their percent weight butene comonomer content. The 50:50 weight % blends were prepared from dissolution in toluene for 24-48 hours, followed by solvent evaporation, and then vacuum drying to 10^{-2} torr for 4 days or longer. The DSC T_g for the blend was -36°C (5 K/min scan).

All ^{13}C and ^1H measurements were collected on a Bruker DSX-300 with field strength equal to 7.05T. Solid-state CODEX NMR experiments were performed on a 4-mm double-resonance magic-angle spinning probe using the pulse sequence in Figure 1, previously described in detail by Schmidt-Rohr.^{50,51} The probe temperature was calibrated using PbNO_3 to within ± 1 K. All CODEX exchange data was acquired with an actively-controlled 4 kHz MAS speed, a 1-ms cross-polarization contact time, rotor synchronization, and as a precaution, measurements were altered between the CODEX and reference signal every 256 scans to eliminate spectrometer drift. All CODEX slow exchange data was acquired using a 50-ms exchange time, unless otherwise noted. Total experiment times typically ranged between 8-12 hours for a single measurement, depending on the temperature.

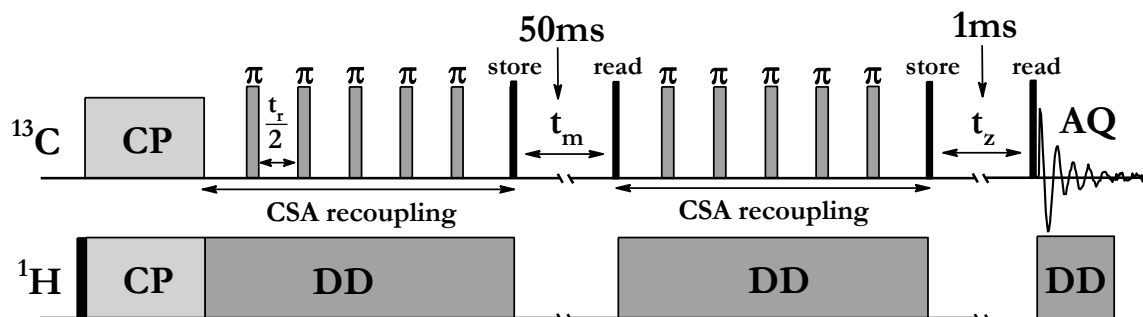


Figure 1. CODEX experiment pulse sequence applied under conditions of MAS. The value of the exchange mixing time $t_m = 50$ ms for all aPP, PEB, and blend data reported in this paper. The total CSA evolution time corresponding to the sum of the first and second recoupling period $2(3t_r) = 1.5$ ms.

Calculations and Theory. The data analysis methods used here are the same as those recently described for a different polyolefin blend system,⁴⁹ and are described in detail in the introduction. Chain conformational exchange data from variable temperature CODEX experiments were analyzed to extract correlation time constants, activation energies for chain reorientation, and quantitative correlation time distributions. An isotropic rotational diffusion

model (employing 20 discrete conformer populations as an approximation to the heterogeneous backbone conformer distribution) was used to simulate the experimental data and solve the overall equilibrium exchange matrix as a function of the exchange mixing time in the CODEX experiment and the correlation time constant for the specific polymer at each temperature. A discrete log-Gaussian correlation time distribution function was analyzed with respect to temperature using both Arrhenius and WLF models. Powder averaged values of the chemical shift anisotropy, reflecting the distribution of tensor orientations in the amorphous polymers, were included in all calculated fits of the data. The *Mathematica*[®] program (version 5.2) was used for all calculations. The theory regarding exchange intensities has been previously developed for static samples, and the incorporation of the additional terms arising from the time-dependence of the frequency introduced by MAS has also been described.^{54,55} Complete details for all calculations as implemented for the pure polymers and their blends are described in Reference 49 and in the introduction. For convenience, the equation describing the quantitative evolution of the normalized exchange intensity **E** as a function of exchange time and temperature for a distribution of correlation times $g(\tau)$ is reproduced here in Equation 1:⁵⁴

$$E(t_m, \tau_c, T) = \frac{S_0 - S}{S_0} = \frac{\int_0^\infty \{\text{Re}[G_-(t_z, \tau, T)] - \text{Re}[G_-(t_m, \tau, T)]\} g(\tau) d\tau}{\int_0^\infty \text{Re}[G_-(t_z, \tau, T)] g(\tau) d\tau} \quad \text{Eq. 1}$$

All additional terms are defined and described in the introduction section, but the reader can quickly note the time dependencies for the specific delays in the Figure 1 pulse sequence from this equation.

Results and Discussion

Candidates for a Miscible aPP/PEB System. In order to determine if PP and PE-copolymers can form miscible, intimately mixed chain-level blends, and more importantly, understand why they do or do not exhibit such behavior, one must first narrow the field of all

possible choices reported in the recent literature.^{36,52,56-58} In this investigation, the focus is on amorphous systems, since phase separation in amorphous binary blends typically implies phase separation in their crystalline counterparts. ¹²⁹Xe NMR diffusion/equilibration experiments can indicate which blends are intimately mixed, albeit with a minimum length scale much longer than constituent radii of gyration, as we previously demonstrated for PIB/PEB blends.⁵⁹ In other words, it is a quick and reliable test for microphase separation for blends, since the observation of distinct peaks for Xe in each polymer component in the blend indicates regions of single-component density whose dimensions exceed that of the Xe diffusion coefficient length scale (ca. ≥ 35 nm).^{59,60} While this is a relatively coarse-grained experimental probe compared to molecular/chain dimensions, it does provide valuable limiting information. Figure 2 shows a series of static ¹²⁹Xe NMR spectra for several pure PEB copolymers (2a) and for blends of aPP with the same PEB copolymers (2b).

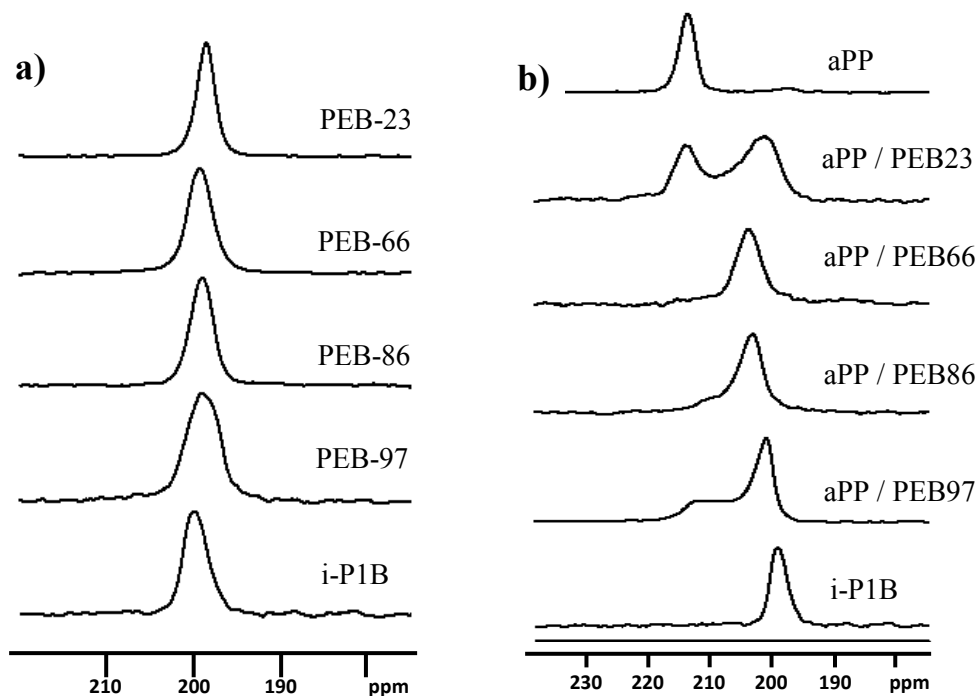


Figure 2. ¹²⁹Xe static NMR results for xenon gas absorbed in (a) a series of pure PEB-xx copolymers, with xx indicating the weight percent of 1-butene content, and (b) the blend of aPP with the same PEB copolymers. Pure isotactic poly-1-butene is denoted i-P1B. Details of the Xe NMR experimental conditions may be found in Reference 31.

Figure 2a shows the results of a control experiment used to verify that the xenon shielding environment is insensitive to comonomer concentration in the PEB-copolymer series ranging from 23 to 97 wt% butene comonomer. As shown in 2a, all PEB copolymers, as well as pure isotactic poly-1-butene, exhibit a similar ^{129}Xe chemical shift of 197-198 ppm. In contrast, Figure 2b indicates that the shift for xenon gas in pure aPP is 215 ppm, an expected result given the well-known sensitivity of xenon gas to different polymer densities. Most importantly, the spectra in 2b for blends of aPP with the different PEB copolymers clearly indicate that the only blend where Xe is sampling a homogeneous polymer environment on the timescale defined by its diffusion coefficient (ca. $2 \times 10^{-7} \text{ cm}^2\text{s}^{-1}$) is the blend of aPP with PEB-66; the other three blends show two well-defined peaks consistent with the same peaks observed in the pure polymer components. The center of mass for the aPP/PEB-66 peak is 205 ppm; the expected composition-weighted average for the 50:50 wt:wt% blend is 206 ppm. Of the various PEB copolymers in Figure 2, most of which have been previously discussed as candidates for miscible blends with aPP, Figure 2b indicates that only PEB-66 is a viable possibility. For this reason, detailed investigations of individual chain mixing and dynamics using more advanced and time-consuming CODEX methods will be limited to the aPP/PEB-66 blend in the remainder of this contribution.

Slow Chain Dynamics near T_g in aPP, PEB-66, and aPP/PEB-66 Blend by CODEX NMR. The CODEX experiment is a one-dimensional constant-time version of classic two-dimensional exchange experiments that exploits the anisotropy of the chemical shift interaction to detect movement (in real time) of polymer chain segments.⁵⁰ The experiment is run in duplicate to generate two data sets, which differ in that the t_m and t_z periods are interchanged, generating what is known as the exchange spectrum $S(t_m \text{ and } t_z)$ positioned as shown in Figure 1) versus the reference spectrum S_0 (no mixing; t_m and t_z switched from that shown in Figure 1). The pure

exchange spectrum is the difference between these two results, denoted as $\Delta S = S_o - S$. From Equation 1, the amplitude of this signal is related to the normalized exchange intensity as $E(t_m, \tau, T) = \Delta S/S$. Systematic comparisons of E as a function of temperature for pure polymers versus the same polymers in the binary blend can reveal quantitative changes in slow chain dynamics and their distributions (1 – 1000 ms correlation time constants) upon blend formation. Figure 3a and 3b provide the results of mixing time and recoupling time dependencies for these polymers.

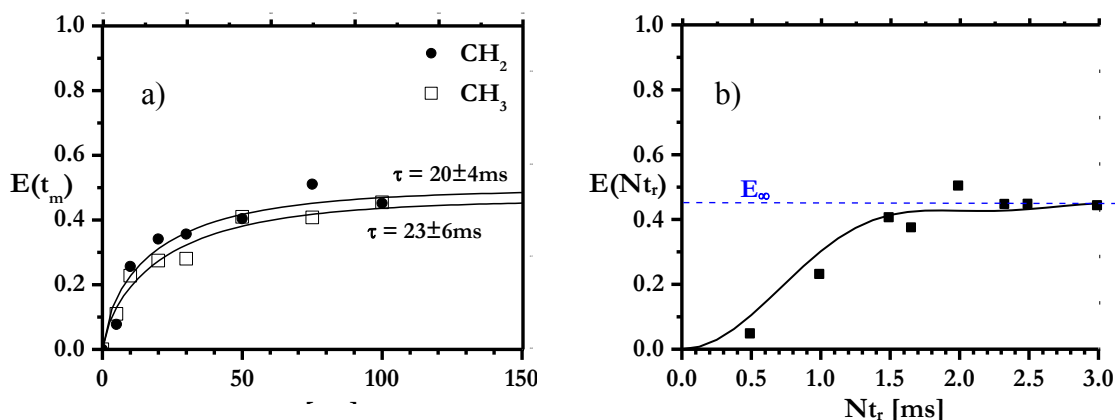


Figure 3. **a)** The mixing time dependence of normalized exchange intensity $E(t_m)$ for methyl and methylene resonances of aPP at 274K. Solid lines represent the KWW fit with $\beta_{KWW} = 0.7$. **b)** The recoupling time dependence of normalized exchange intensity $E(Nt_r)$ for methyl group of aPP, solid line represents the fit obtained using the same model we used to fit the temperature dependence of $E(T)$ at fixed $Nt_r = 1.5$ but using 30% smaller CSA.

Figure 4 shows representative results for pure PEB-66, pure aPP, and their blend at temperatures near the maximum exchange intensity for each sample. As discussed previously, when the temperature is low compared to the polymer T_g , no chain motion occurs and the exchange intensity is zero. The CODEX experiment detects chain dynamics as the polymer proceeds through T_g , with a characteristic exchange frequency window of 1 – 1000 Hz. At high temperatures, chain reorientation occurs with a correlation exchange frequency greater than that of the chemical shift anisotropy mechanism by which the CODEX sequence detects motion

through echo attenuation. If the polymers become too mobile at high temperatures, then the ability to detect chain motion is precluded and the exchange intensity vanishes. For the

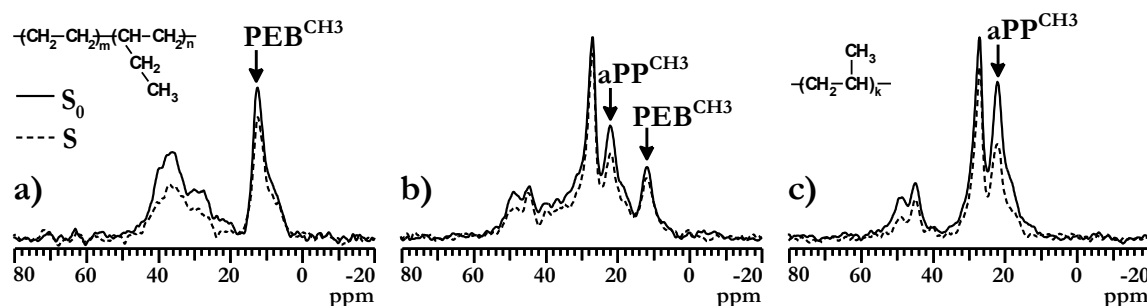


Figure 4. Example ^{13}C CODEX spectra for (a) pure PEB66 at 225 K, (b) aPP/PEB66 50/50 wt. % blend at 250 K, and (c) pure aPP at 274 K. Solid line is the reference spectrum S_0 , whereas the dashed line corresponds to the spectrum obtained with mixing time = 50 ms (S).

amorphous polyolefins used here, the magnitude of the chemical shift anisotropy was estimated from static lineshape experiments to be equal to 1.5 - 2 kHz. From the pure polymer results in 4a and 4c, one can extract exchange intensities $E(T)$ versus temperature for chain specific locations, i.e., backbone CH_2 versus side-group CH_3 . This is an important control experiment, since it eliminates any uncertainty associated with additional side group dynamics that might

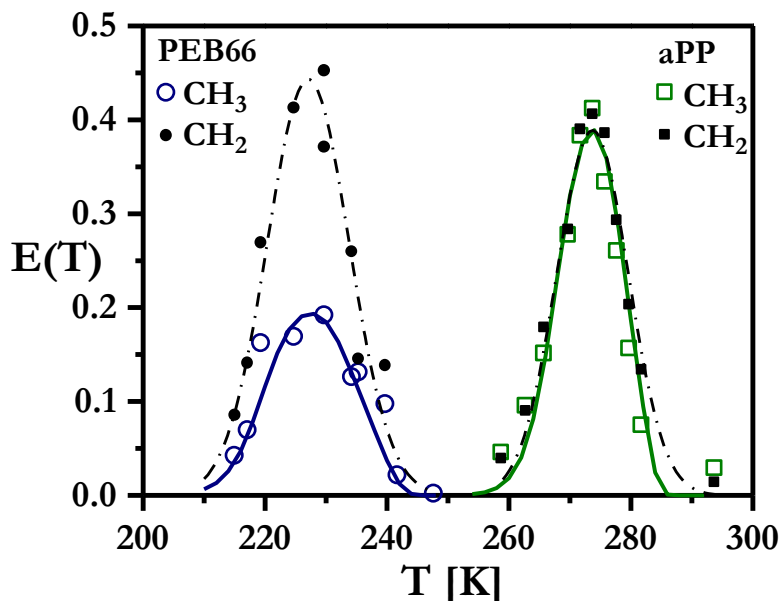


Figure 5. Normalized exchange intensities $E(T)$ for methyl and methylene signals of pure PEB66 and pure aPP. The solid lines are Arrhenius model fits (see below) to methyl data points, whereas the dash-dot lines are drawn through the methylene experimental points only to guide the eye.

influence the interpretation of the CODEX results in the blend. Figure 5 shows systematic comparisons of CODEX exchange intensities measured from backbone CH₂ versus side-group CH₃ in the two pure polymers over the entire temperature range for which a measurable exchange signal is detected. The onset of detectable exchange intensity for either functional group, as well as the temperature of the maximum E(T) value, is identical within each polymer. The absolute value of the maximum E(T) is markedly different for the CH₂ vs. CH₃ signals in the PEB-66 polymer, indicative of additional ethyl branch motions which further reduce the magnitude of the chemical shift anisotropy for that pendant methyl group relative to backbone moieties, thereby decreasing E(T) values compared to the backbone CH₂. The exchange intensity for this CH₃ group did increase in experiments with longer recoupling times (not shown), as previously demonstrated on another polyolefin blend system.⁴⁹ Since only a single carbon-carbon bond separates the CH₃ group from the main-chain in aPP, this dramatic difference in exchange intensity relative to the backbone is not observed. Two important points from this control experiment are: (1) the temperature of the maximum E(T) value is independent of which group is measured, which means that the CH₃ signals can accurately report conformational exchange in the blend, an advantage given that they are better resolved than their respective CH or CH₂ backbone counterparts and can be deconvoluted accurately; (2) the onset of detectable E(T) signal in the CODEX experiment agrees with DSC data, in that the first one or two data points on the low temperature side of each curve coincide with the DSC T_g (PEB66 = 219 K and aPP = 262 K).

Large changes in the temperature dependence of slow conformational exchange are observed for each pure polymer following formation of the blend, as summarized by the pure CODEX exchange intensity E(T) versus temperature in Figure 6. Figure 6 represents the outcome of three independent temperature dependent experiments; one each for the two pure polymers and a single experiment for the blend from which polymer specific exchange intensities were extracted at each temperature. Prior to any consideration of a quantitative model to fit the

results, several key points may be discerned via simple inspection of the raw data in Figure 6, comparing the response of the CH₃ signal in the CODEX experiment for each pure polymer to the response of that same polymer in the blend. First, the PEB66 exchange intensity curve shifts to higher temperature in the blend relative to pure chains (PEB66 is the lower T_g component). Similarly, the exchange intensity curve shifts to lower temperature for the aPP in the blend compared to its pure response. For the PEB66, the $E(T)$ maximum shifts from 227 K to 247 K upon blend formation, while the aPP $E(T)$ maximum changes from the pure value of 273 K to 253 K in the blend. So, while each curve exhibits an identical 20 K change, they do not converge to an identical common value (5-7 K difference in $E(T)$ maxima), as we previously observed for the PIB/hhPP polyolefin blend.⁴⁹ While omitted from the figure in order to maintain clarity, the $E(T)$ versus T curve for the backbone CH₂ peak of aPP *in the blend* has a maximum at the same 252-253 K position as the CH₃ peak shown in Figure 6 (see Figure 9). Secondly, the breadth of

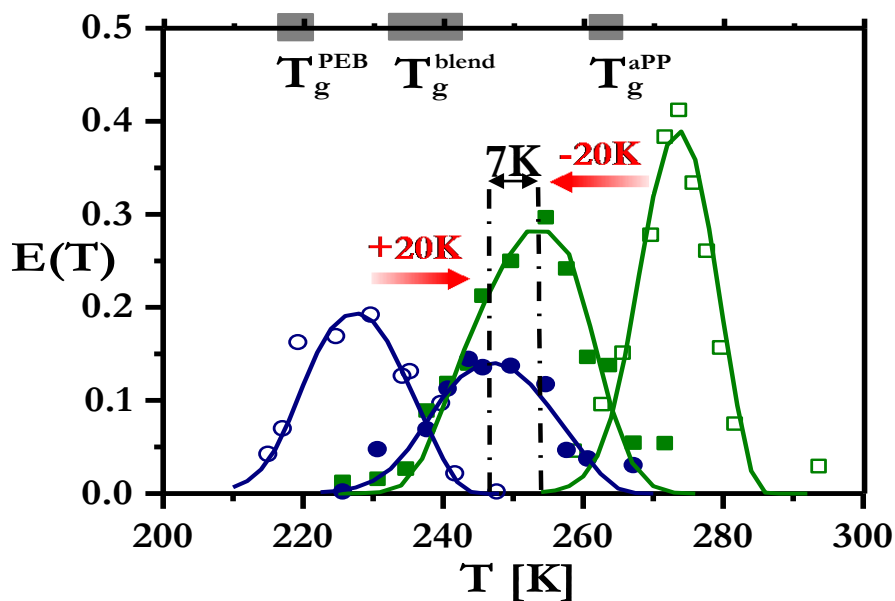


Figure 6. Normalized exchange intensities $E(T)$ for pure PEB66 (\bullet), PEB66 in the blend (\bullet), pure aPP (\square), and aPP in the blend (\blacksquare). The smooth lines are fits to the data using an Arrhenius model as described in the text. Note shifts of equal but opposite magnitude for each component upon blend formation, but a lack of complete convergence to a common temperature for the exchange intensity maximum of each polymer in the blend. The 5K/min scan DSC T_g range for each polymer and the blend is plotted for reference on the top of the figure, with the box length representing the beginning and end of the endotherm.

each $E(T)$ curve increases for either component in the blend relative to the pure polymer, especially for aPP. Finally, the absolute value of $E(T)$ at each temperature across the detectable range decreases in the blend relative to the unmixed result for both polymer components. Although each temperature dependent exchange intensity curve decreases in intensity and increases in breadth for the polymers in the blend compared to the pure polymers, the overall integrated area under the curve fits (vide infra) remains constant for each polymer, within the error of the data analysis. While the intermediate temperature values for the $E(T)$ curves are reminiscent of DSC results on blends, the ability to extract these specific details for each polymer in an amorphous mixture by simultaneous detection of the two unique $E(T)$ curves is difficult using traditional thermal analysis methods. From these points it can be concluded that the overall dynamic heterogeneity for both polymer chains increases in the blend, and in addition, it is also known that the CODEX exchange intensity decreases with increasing number of sites involved in the exchange process for a fixed recoupling and mixing time.⁵⁴ The details specifying exactly how the dynamic heterogeneity increases for both chains will be discussed in the following sections.

Data Analysis via Correlation Time Distribution and Arrhenius vs. WLF Models.

The fits to the experimental data shown in Figures 4 and 5 were obtained by combining isotropic rotational diffusion with a temperature-dependent discrete log Gaussian correlation time distribution/Arrhenius model, as described briefly in the Experimental section, in Reference 49, and in detail in the introduction. The absolute value of the exchange intensity $E(T)$ at each temperature, for a fixed recoupling and mixing time, depends on the correlation time constant characteristic of the motion modulating the chemical shift anisotropy as well as the distribution of correlation time constants for all of the segments in the amorphous polymer or polymer mixture. Figure 7 shows calculated correlation time distributions from the fits to data in Figures 5 and 6

for the aPP component, and demonstrating how the $g(\tau)$ function in Equation 1 can influence $E(T)$. We note how much broader the correlation time distributions become upon formation of the blend, and also, the increased distribution width near the T_g value (low T) for a pure polymer.

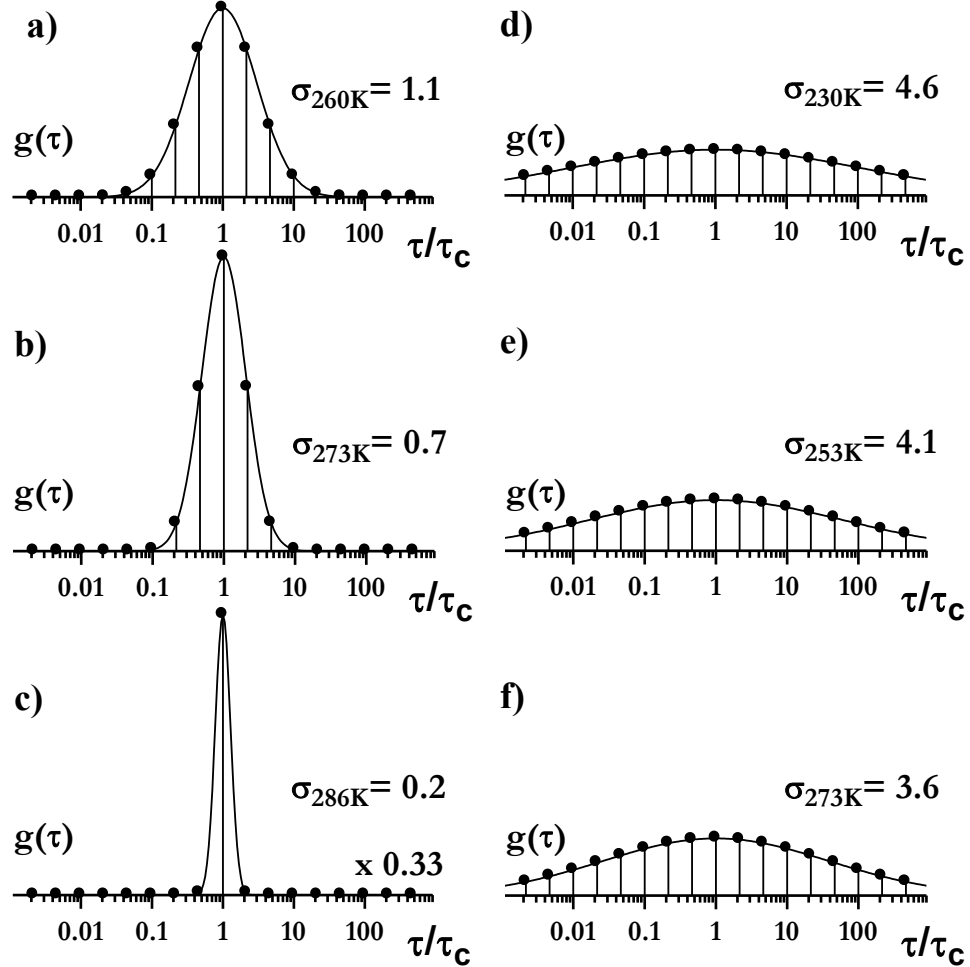


Figure 7. Discrete version of log-Gaussian correlation time distribution for aPP, with different widths σ following a linear temperature dependence $\sigma(T) = a k_B T + \sigma_0$, at key temperatures previously shown in Figure 5. Each distribution is centered at τ_c and consists of 17 points equally spaced over approximately 6 decades. (a) pure aPP at 260K, (b) pure aPP at 273K, (c) pure aPP at 286K, (d) aPP in blend at 230K, (e) aPP in blend at 253K, (f) aPP in blend at 273K. The $\sigma = 0.2$ distribution (c) was scaled by 0.33 to allow comparison with the other temperatures.

Figure 8 summarizes the temperature dependence of the correlation time distributions for both aPP and PEB66, pure and in the blend, over the entire temperature range for which an exchange signal is detected. The linear temperature dependence of $\sigma(T)$ is apparent from the

figure, as is the increase in absolute value of $\sigma(T)$ for both polymers once they are in the blend. Figure 8 shows that the width of the correlation time distributions versus temperature increases much more for aPP, the high T_g component in the blend, than that for PEB66. A similar result was recently reported for the miscible binary blend of PIB (polyisobutylene) and hhPP, where again, the hhPP (head-to-head PP) was the high T_g component and exhibited the largest perturbation in σ upon blend formation.⁴⁹

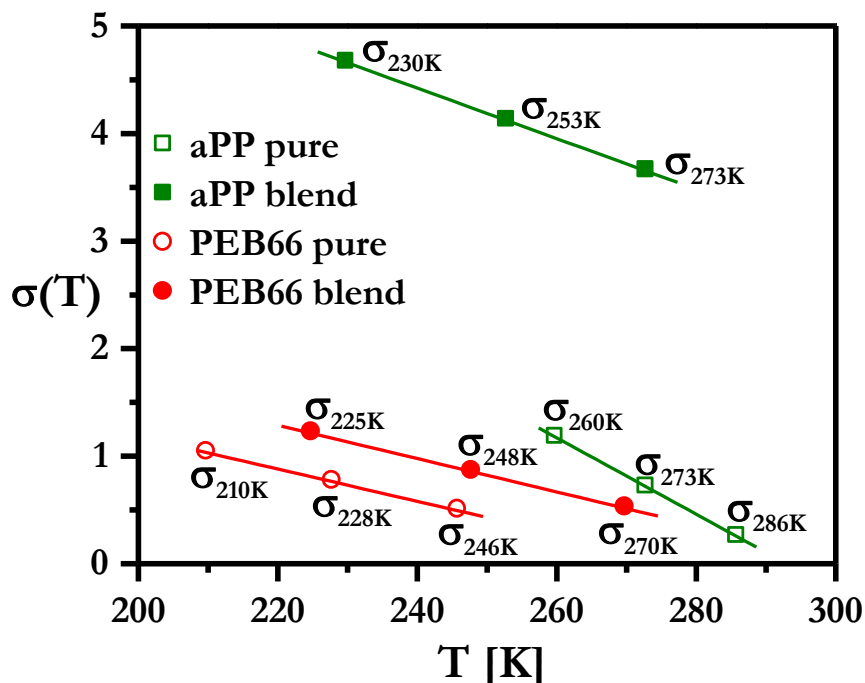


Figure 8. Temperature dependence of correlation time distribution widths for pure versus blended aPP and PEB66.

While the primary goal is not to validate the absolute accuracy of one model versus another, but rather to understand why certain polymer chains form intimate mixtures while others do not, it is recognized that other temperature dependent models may be more familiar to the reader. Figure 9 shows a comparison of the correlation time distribution/log Gaussian/Arrhenius model discussed in Figures 5-7 with a KWW/WLF analysis for the exchange intensity data from pure aPP and aPP in the blend; this is the same aPP raw data shown in Figure 6. The KWW/WLF

fitting parameters are reported in the captions to Figures 9 and 10; and excellent agreement between the two models in terms of correlation time values over the temperature range of this data. Such low β values upon blend formation are consistent with increased dynamic heterogeneity in aPP, as recently discussed by deAzevedo using similar experiments on pure aPP,⁵⁴ and as is also readily apparent from direct inspection of the $E(T)$ exchange curve intensities in Figure 9. Comparisons of KWW β values to corresponding values of the correlation time distribution widths $g(\tau)$ are provided in the introduction.

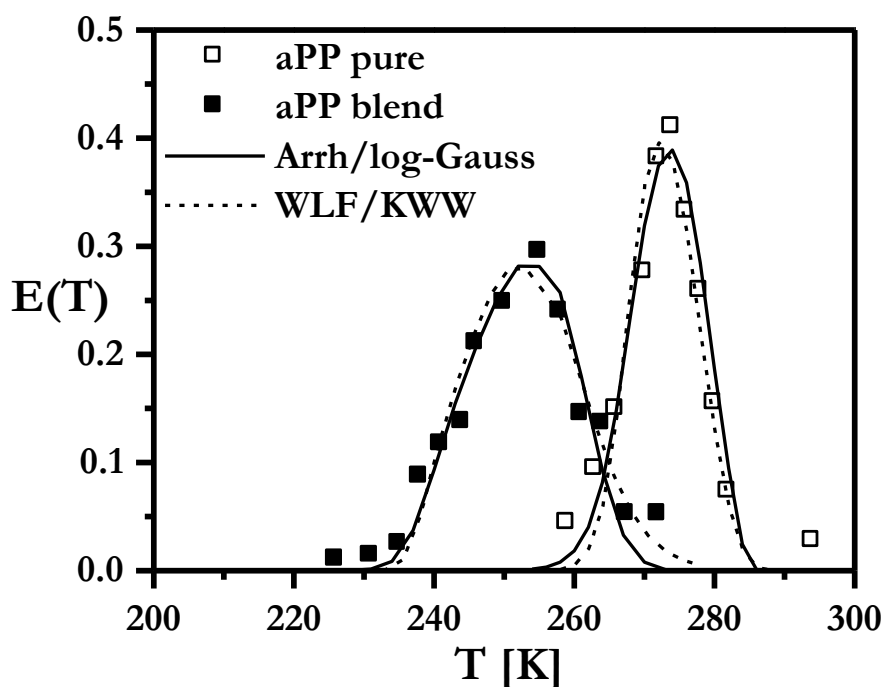


Figure 9. Comparison of fits to the aPP exchange data obtained using two different models: (1) Arrhenius temperature dependence of correlation times with variable-width log-Gaussian distribution, and (2) WLF temperature dependence combined with KWW distribution. The WLF/KWW parameters for pure aPP were $C_1 = 15.5$, $C_2 = 41$ K, $\tau(T_g) = 100$ s, $T_g = 259$ K, $\beta = 0.8$, whereas for aPP in blend $T_g = 237$ K and $\beta = 0.2$ was used.

That equivalent correlation times for the center of the distribution (τ_c) are obtained using either model is more clearly evident by the representation of their temperature dependence for both polymer components in Figure 10. One observes that the temperature dependence of the slow chain dynamics for PEB66 and aPP are very different. Figure 10 also shows that while the

magnitude of the change in τ_c values upon blend formation differs between the two polymers significantly at any temperature (ca. 5 decade decrease in aPP versus ca. 2.5-3 decade increase in PEB66), the two polymer components *in the blend* have identical values of τ_c near 250 K. The

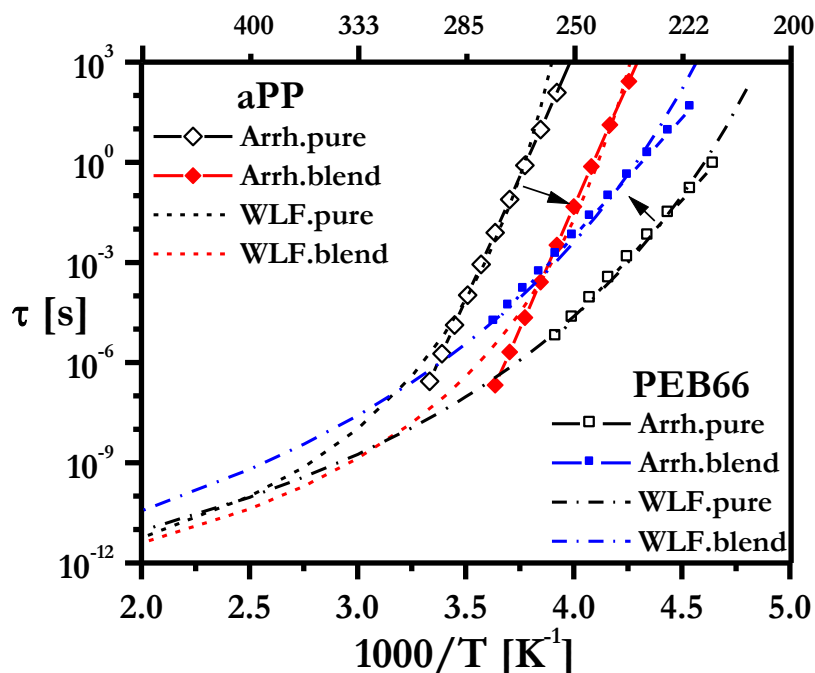


Figure 10. Temperature dependence of correlation times obtained using Arrhenius and WLF models. The WLF parameters for pure aPP were: $C_1 = 15.5$, $C_2 = 41$ K, $\tau(T_g) = 100$ s, $T_g = 259$ K, whereas for aPP in blend $T_g = 237$ K was used. For pure PEB66 we used $C_1 = 15.5$, $C_2 = 55$ K, $\tau(T_g) = 100$ s, $T_g = 210$ K, and the best fit for PEB66 in blend was obtained with $C_2 = 68$ K and $T_g = 224$ K. An Arrhenius model can be treated as linear approximation to the WLF curve, since both Arrhenius and WLF models give similar results over the temperature range for slow motions near T_g .

entire range of temperatures exhibiting equal correlation times and overlapping distributions is more evident in Figure 11, in which correlation time distributions for each polymer in the blend are shown at selected temperatures spanning the entire temperature range of interest. At the two intermediate temperatures shown in Figure 11, the two correlation time distributions completely overlap, and the central correlation time constants are essentially equal at 253 K. In total, these data indicated **(1)** that in a miscible polymer blend, the central correlation time constants τ_c converge to the same or nearly the same value, but **(2)** the widths of the correlation time

distributions do not. For comparative purposes, Figure 12 shows overlapping symmetrical correlation time distributions for the PIB/hhPP blend discussed previously in Reference 49, at the common temperature of the maximum value of $E(T)$ for each component in the miscible blend.

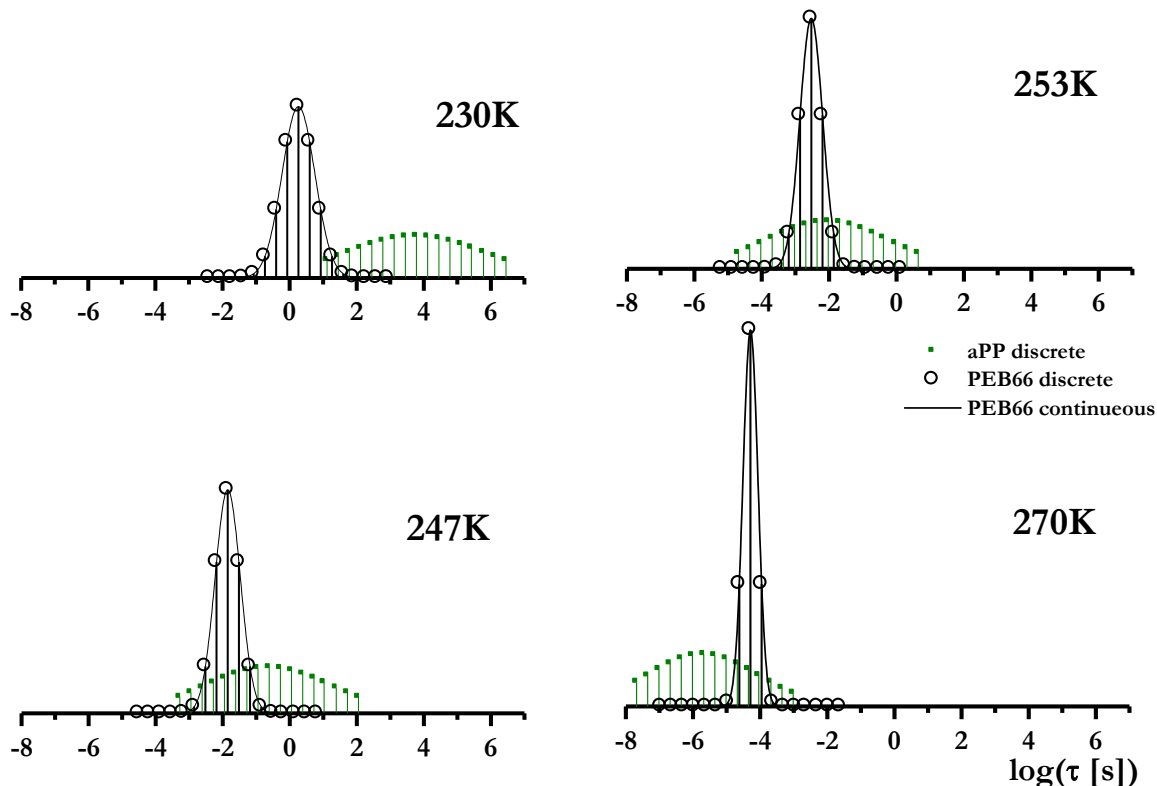


Figure 11. Correlation time distributions for aPP and PEB66 in the blend at selected temperatures spanning the range of detectable CODEX exchange intensity.

Conclusions

The data from Figures 6-11 indicate that: **(1)** in a miscible polymer blend, the central correlation time constants τ_c converge to the same value, but **(2)** the relative widths of the correlation time distributions actually diverge dramatically (even though both do increase) compared to the pure polymer results. In addition, and in agreement with the previously published work on miscible PIB/hhPP blends (see Figure 12 below, and Figures 7-10 in Reference 49), it is the high T_g component that exhibits the largest change in absolute value of

central correlation time constants and in the width correlation time distributions. Figures 6 and 9 above show that the $E(T)$ vs. T curve is the most asymmetric for the high T_g aPP component in the blend, even though its pure component curve is symmetric about the $E(T)_{\max}$ temperature value. Also, and in agreement with that previous study, the limiting values of the correlation time distribution width σ at T_g for any of the four pure amorphous polymers studied to date by this experimental approach (PIB, hhPP, aPP, and PEB66) are between 1.1 and 1.4 (see Figure 8). This value corresponds to approximately one decade of dynamic heterogeneity in slow segmental dynamics (correlation time constants $1 \text{ ms} \leq \tau_c \leq 1000 \text{ ms}$) of the pure amorphous polymers.

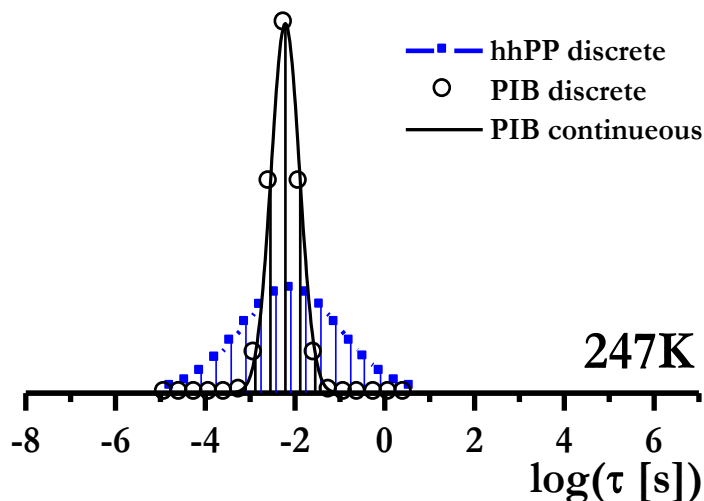


Figure 12. Correlation time distributions for individual polymer components in the miscible hhPP/PIB blend of Reference 49, at the temperature of maximum exchange intensity $E(T)_{\max}$, showing the same central correlation time value τ_c but largely different correlation time distribution widths σ .

Each of the points raised in the preceding paragraph address key questions recently raised in the literature about the dynamics of miscible polymer blends, and also reveal by experiment the details of slow segmental dynamics of both pure and mixed polymers near the glass transition temperature.^{40-48,61} While previous two-dimensional site-specific exchange experiments indicate that conformational trans-gauche isomerizations take place in polyolefin chains over the temperature ranges where we detect a CODEX exchange signal,^{38,39} such motions cannot simply occur for two adjacent monomers, as a trans diad is longer than a gauche, for example. Since all

monomers are connected in the chain, the rest of the chain and its immediate environment through space must accommodate the resulting change in length for even a single trans-gauche jump. At temperatures below T_g , such events occur with very long time constants; Figure 6 indicates that the onset of detectable numbers of these events for aPP, PEB66, and their blend occurs at essentially identical temperatures in the CODEX NMR experiment and DSC (for the specific experimental parameters used here). Although the experimental data reported here do not reveal the exact size of the rearranging regions, the quantitative values of their central correlation time constants τ_c and the temperature dependence of the correlation time distributions are in every way consistent with recent models invoking characteristic lengths of dynamic heterogeneities or cooperatively rearranging regions which increase as the temperature increases above T_g .^{41,42,61} Without question, the fact that individual trans-gauche conformational exchange does occur for amorphous polyolefins indicates a minimum length scale from a purely intrachain perspective of 2-3 monomer units, but does not reveal the maximum length of concerted conformational events within or among several nearby chain segments. The current view in the literature is that the characteristic length of the cooperatively rearranging regions near T_g range from 1-5 nm, inclusive of the Kuhn length which would be polymer-specific.⁴⁰⁻⁴⁸

The direct observation chain-specific CODEX experiments clearly show that irrespective of the characteristic lengths of the cooperatively rearranging regions near T_g for either of the four polyolefins studied to date, the heterogeneity in the dynamics associated with this latent “structure” increases upon miscible blend formation. The convergence in central correlation time constants τ_c but large divergence in the correlation time distribution widths for the miscible blends is unequivocal. The degree to which recently discussed ideas regarding “self-concentration” and “concentration fluctuation” contribute to this increased heterogeneity is

unclear, however; our experiments certainly are consistent with an increased “concentration fluctuation” contribution in the miscible blends.⁴⁸

Our conclusions regarding the larger questions of why only a few polyolefin pairs form a miscible binary blend, based on these results for the aPP/PEB66 system, remain unchanged from our previous publications in which PIB was always one blend component.^{38,39,49} As previously discussed, the increased width in the correlation time distributions in the blend, particularly for the high- T_g component, are consistent with an increased configurational entropy model and concomitant increased size of the characteristic dynamic heterogeneity near T_g relative to either of the unmixed components. Quantitatively, the change can be evaluated using the Adams-Gibbs equation,⁶³

$$\tau_{\text{ex}} = \tau_o \exp(c/TS_c),$$

where τ_{ex} is equated to τ_c , the value of the correlation time at the center of the distribution at the temperature of maximum CODEX exchange intensity in the blend $(T_{\text{em}})_{\text{blend}}$. Using Figures 6 and 10, and assuming τ_o ranging from 10^{-12} s to 10^{-15} s and c as constant for each polymer in pure versus mixed state at the temperature $(T_{\text{em}})_{\text{blend}} = 248\text{-}253$ K, it is determined that the change in configurational entropy for PEB66 chains ranges from -0.81 to -0.85 upon blend formation, while the corresponding range for aPP is $+1.35$ to $+1.28$. In total for both PEB66 and aPP, $(S_c)_{\text{blend}}$ ranges from $1.16(S_c)_{\text{unmixed}}$ to $1.13(S_c)_{\text{unmixed}}$, meaning that there is approximately a 15% increase in the total configurational entropy of the miscible blend compared to the two unmixed components. This is considered a lower limit, since as applied to only the central correlation time constant, it does not capture the large increases in correlation time distributions for both polymer components, and particularly aPP, upon formation of the miscible blend. Although their work focused on isotactic PP/PEE blends in the melt, these conclusions regarding miscibility for aPP/PEB66 qualitatively agree with those of Bates and coworkers, in which conformational

asymmetry leads to excess entropies of mixing in the blend if appropriate branch concentrations exist in the PEB copolymer.³⁴ While the previous conclusions on entropic contributions to polyolefin miscibility were derived from experiments on polyolefin blends in which PIB was always one of the components (PIB/PEB66 and PIB/hhPP), and given that PIB has been considered an anomalous blend component, the conclusions from this study on aPP/PEB66 suggest a more widespread phenomenon for polyolefin blends specifically, and for weakly interacting amorphous macromolecules in general.

CHAPTER III

POLYOLEFIN BLEND MISCIBILITY: POLARIZATION TRANSFER VERSUS DIRECT EXCITATION EXCHANGE NMR*

Introduction

Relatively simple chemical constituents in polyolefin macromolecules belie the fact that their phase behavior in mixture can be complex.⁶⁵ Polyolefins are obviously important economically as commodity polymers, but many specialty applications require unique formulations of multiple polyolefins with slightly different chemical structures. Predicting the details of the ultimate phase mixing is difficult and nonintuitive, and experimental verification of chain level behavior is challenging due to similar chemical and physical properties among varying polyolefin chain structures. Many investigators have approached this problem through multiple theoretical and experimental avenues in recent years.⁶⁶⁻⁷¹ The aspects of binary polyolefin blend phase behavior has been recently described, relying extensively on advanced solid-state NMR methods to show configurational entropy is an important thermodynamic parameter in controlling miscibility between different polyolefin structures.⁷²⁻⁷⁴ Important general conclusions based on these advanced NMR experiments are often complicated by complex pulse sequences that employ an initial polarization transfer step. CODEX NMR

**The content of this Chapter has been published in Macromolecules, 2009, 42, 553-555.*

experiments have proven particularly powerful for direct chain level interrogation of mixing and dynamics in amorphous polyolefin blends, but to date, all work has involved polarization transfer from protons to carbons (cross-polarization or CP) to generate the initial signal in the CODEX experiment.^{75,76} Concerns about nonrepresentative sampling of a subset of polymer chains by polarization transfer steps can arise in cross-polarization solid-state NMR methods; differential polymer chain dynamics may lead to nonuniform polarization transfer efficiency in that step, often preferentially emphasizing the more spatially constrained or rigid regions of the sample which preserve larger heteronuclear dipolar couplings.^{77,78} To address this in the context of amorphous polyolefin blend miscibility, a modified version of the experiment is devised that employs only direct carbon polarization as the initial step in the experiment. On the basis of quantitative comparisons of the modified direct polarization versus CP-based CODEX results over a wide temperature range (including T_g) for atactic polypropylene (aPP), it is demonstrated that results representative of all polymer chains in the sample are obtained here as well as in previously published polarization-transfer-based results. This work shows that CODEX-based exchange methods can provide chain-level information representative of the bulk mixing and miscibility in amorphous polyolefin blends.

Experimental Section

Atactic polypropylene (aPP) was a commercial sample acquired from Eastman, characterized by a DSC $T_g = -11\text{ }^{\circ}\text{C}$ and $M_n = 2600$. Solid-state NMR measurements were collected on a Bruker DSX-300 with field strength equal to 7.05T and using a 4mm double resonance magic-angle spinning probe with the probe temperature calibrated to within $\pm 1\text{ K}$ using $\text{Pb}(\text{NO}_3)_2$. All CODEX exchange data were acquired with active MAS speed control and rotor synchronization, and as a precaution, measurements were between CODEX and reference every 256 scans to eliminate spectrometer drift. Slow exchange data were acquired using a 50ms

exchange time, unless otherwise noted. Total experiment times typically ranged from 8 and 12 h for a single measurement, depending on the temperature.

The modified direct excitation CODEX experiment devised for this work is shown in Figure 1, and as stated earlier, a single ^{13}C 90° pulse is used to directly excite the carbon signals from the polymer chains. While this experiment obviously suffers from sensitivity loss relative to the original CP-based sequence, it eliminates any possibility of selection of subsets of polymer chains based on differential cross-polarization dynamics.^{77,78} In acquiring data for the aPP sample using in this study, ^{13}C T_1 time constants were measured using the Torchia method⁷⁹ and found to equal 0.77s for the CH_3 carbons at 274K. Since previously reported data on the aPP CH_3 carbons

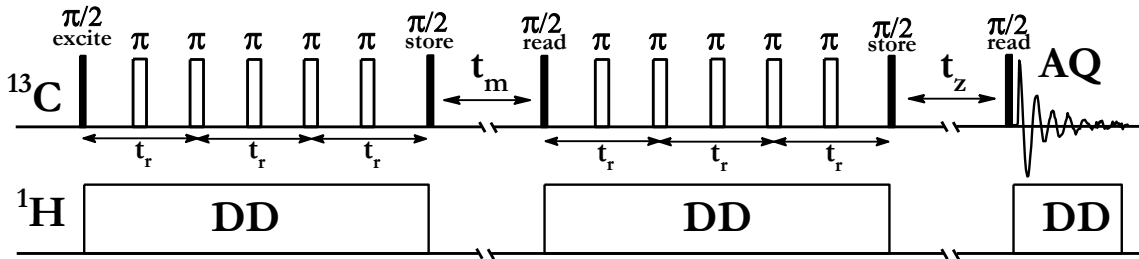


Figure 1. Pulse sequence diagram for direct excitation ^{13}C CODEX experiment, based on a modified version of the original sequence.^{11,12} The modified phase cycling scheme for all $\pi/2$ pulses, which includes required changes in the receiver phase due to elimination of the CP step, is shown in Table 1. The phase alteration for the π pulses in the first and second evolution windows follows the xy-8 phase cycling scheme.¹⁶ The exchange mixing time $t_m = 50\text{ms}$ in this work and the relationship between the exchange signal intensity measured by CODEX and the length of the evolution/refocusing windows (Nt_r) has been presented earlier for aPP.¹⁰ DD denotes dipolar decoupling.

| Table 1. Modified Phase Table for the $\pi/2$ Pulses in the Direct Excitation CODEX Experiment shown in Figure 1 | | | | | |
|--|---------------------|--------------------|----------------------|---------------------|-----------|
| $\pi/2$ excite | First $\pi/2$ store | First $\pi/2$ read | Second $\pi/2$ store | Second $\pi/2$ read | receiver |
| y -x -y x | -y x y -x | y -x -y x | -y x y -x | y -x -y x | -y x y -x |
| | -y x y -x | -y x y -x | | | y -x -y x |
| | -x -y x y | x y -x -y | | | -y x y -x |
| | -x -y x y | -x -y x y | | | y -x -y x |
| | y -x -y x | | | | y -x -y x |
| | y -x -y x | | | | -y x y -x |
| | x y -x -y | | | | y -x -y x |
| | x y -x -y | | | | -y x y -x |

in polyolefin blends via the CP CODEX approach, this is the relevant structural moiety to consider here. In acquiring data using the direct excitation CODEX experiment, 4s repetition times were used to ensure adequate relaxation of ^{13}C methyl group polarization.

Results and Discussion

Polypropylene (aPP) has been discussed as a key component in many polyolefin blends, is economically important, and was included in recent work involving blends with polyethylene copolymers.⁷⁴ For these reasons, atactic polypropylene (aPP) was selected as a relevant test material in this work. Figure 2a,b shows a comparison of direct excitation ^{13}C MAS and direct excitation CODEX for aPP with their respective CP-based counterparts in Figure 2c,d.

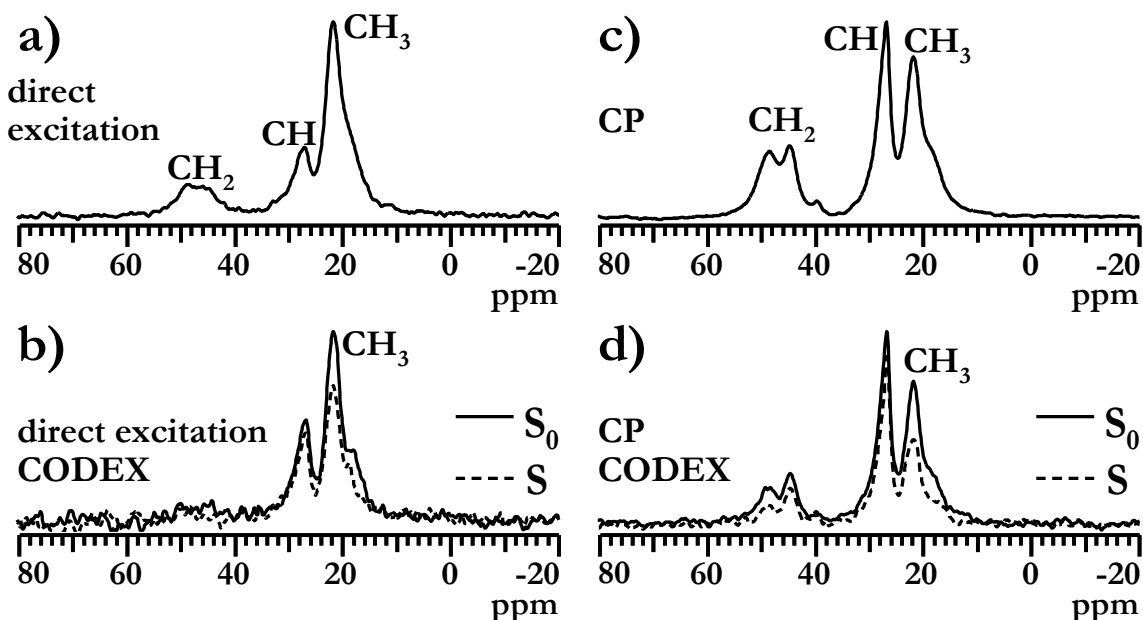


Figure 2. ^{13}C NMR MAS spectra of aPP at 274K: (a) single-pulse spectrum, 128 scans; (b) corresponding direct excitation CODEX spectra with 50ms exchange time and 4096 scans; (c) CP spectrum with 1ms polarization transfer time and 128 scans; (d) corresponding CP CODEX spectra with 50ms exchange time and 4096 scans. S_0 is the reference spectrum in each of the two CODEX results, and S is the exchange spectrum.

The data were acquired at 274K, since this corresponds to the previously published exchange maximum for aPP.⁷⁴ Relative peak intensities differ dramatically in the normal Bloch decay (i.e., direct or single-pulse excitation) and CP/MAS spectra (Figure 2a,c) due to the combined

differences in the heteronuclear dipolar couplings and concomitant CP efficiency as well as simple ^{13}C T_1 effects.^{77,78} For example, the relative height of the backbone CH_2 group compared to more mobile CH_3 side group is enhanced in the CP/MAS spectrum (Figure 2C) compared to that observed in the Bloch decay spectrum (Figure 2a).

As expected, the different excitation methods produce different reference spectra S_0 in the CODEX results of Figure 2b,d. The key question is whether the details of polymer chain reorientation as measured during the 50ms exchange time manifest themselves in a quantitatively similar way independent of the initial excitation method. This question cannot be answered by direct inspection of the S_0 and S spectra in Figure 2b,d, as this is only a single result at one temperature. Since in reference 73 and Chapter II a detailed analysis of the CP CODEX results on the methyl group of pure aPP and aPP in blends over a wide temperature range, including the glass transition temperature, new data were acquired using the modified direct excitation CODEX experiment over an identical temperature range for the same aPP polymer.

Figure 3 shows comparative data for the direct excitation CODEX and the CP-based CODEX for the aPP CH_3 group over its complete temperature range, beginning slightly below T_g and increasing to temperature high enough to eliminate (via motional averaging) the chemical shift anisotropy interaction which is required to monitor exchange during the evolution and refocusing windows of the CODEX experiment. Since the overall sensitivity decreases for the direct excitation version, we have plotted only the temperature-dependent response of the CH_3 group here, instead of the much weaker backbone CH_2 signal. However, we showed earlier that identical results are obtained for both CH_2 or CH_3 groups in aPP.⁷⁴ As previously discussed, the fact that the detectable CODEX exchange intensity coincides with the T_g by DSC shows that each experiment is probing the onset of slow chain dynamics in polyolefins in the 1-100Hz frequency range. The advantage of the CODEX approach for polyolefin work is site resolution

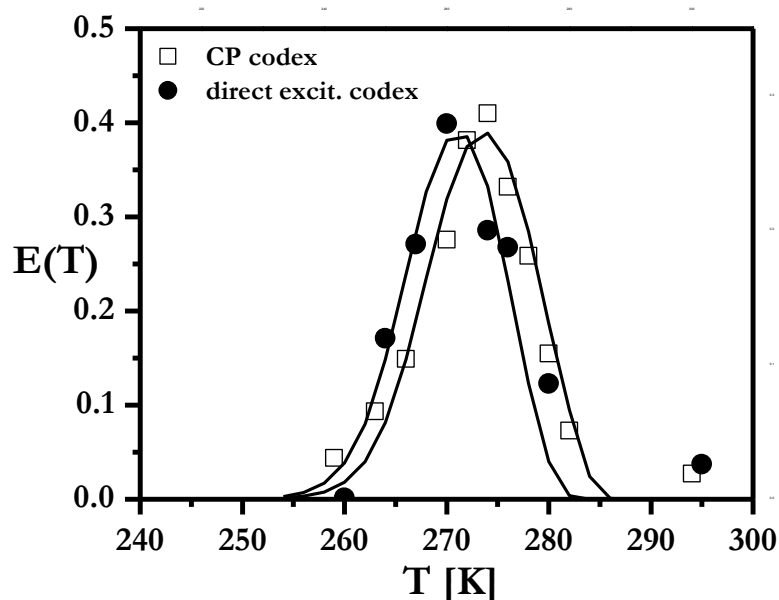


Figure 3. Normalized exchange intensities $E(T)$ for methyl carbon signal of pure aPP obtained by cross-polarization CODEX (□) versus direct excitation CODEX (●). The smooth lines are fits to the data using the same isotropic rotational diffusion/Arrhenius model (as described in detail previously in refs 9 and 10) for either experiment. For reference, the T_g by DSC occurred at 262 K. The 1–2 K low-temperature shift observed for the direct excitation points relative to the CP CODEX points is attributed to the use of a much larger heat exchanging coil in the variable-temperature setup for the former; this was required since the experimental acquisition time per point was 3 times longer for the direct excitation data.

which allows chain-specific information before and after blend formation, instead of an average response. In Figure 3, a negative 1–2 K per point shift in the direct excitation data is observed relative to the CP-based CODEX results. While there is a ± 1 K uncertainty in the temperature calibration using PbNO_3 chemical shift thermometry, the systematic low-temperature shift here arises from the use of a much larger heat exchanger in the variable temperature equipment for acquisition of the direct excitation data. This change was necessary due to the factor of 3 longer data acquisition time per point for the direct excitation CODEX results compared to the CP-based CODEX data. Even with this small temperature offset, one observes that the exchange intensity representative of slow chain dynamics with central correlation time constants ranging from 1s to 1ms, i.e., the $E(T)$ vs T curve in Figure 3, is essentially identical. Quantitative analysis of each

curve using either Arrhenius or KWW/WLF model gives the same activation energies, central correlation time constants, correlation time distributions, β values, etc., for chain reorientation as previously reported for aPP using the CP-based CODEX.⁷⁴ Given the reduced sensitivity in the direct excitation CODEX results (compare b and d of Figure 2), the absolute error in each measurement is higher than the CP CODEX results; the fact that the same exchange intensity curve is reproduced from the individual pure exchange difference at each temperature indicates that results are representative of the behavior of aPP polymer chains, irrespective of excitation method. As mentioned earlier, 4 second repetition times allowed uniform sampling of all aPP methyl carbon groups in the direct excitation experiment. Also, the CP CODEX results were obtained using a 1ms cross-polarization time, which is near the maximum in a T_{CH} experiment and therefore should provide the most uniform sampling of all polymer chains. One could use the polarization method as a more discriminating initial selection method in the CODEX approach, if desired, by employing well-known adjustments in either experimental method. For example, the direct excitation method used in conjunction with a short repetition time (e.g., 0.5—1 s) between each transient would select for the most mobile regions, while the CP CODEX approach with a very short polarization transfer time (e.g., 50—100 μ s) would skew the response to the most constrained subset of chains. Sensitivity losses would ultimately limit the degree to which either type of severe polarization discrimination was practical, even though the level of selectivity could prove especially informative for semicrystalline blends of polyolefin nano-composites.

In conclusion, a modified CODEX experiment has been devised employing direct ^{13}C excitation as the first step in the experiment to show that the CODEX strategy does provide information on slow chain dynamics and miscibility in polyolefin blends which is representative of the bulk polymer behavior. Detailed comparison of amorphous polypropylene exchange data

obtained with either the direct excitation CODEX or the original CP CODEX method gives essentially identical results over a wide temperature range, including T_g .

CHAPTER IV

GLASS TRANSITIONS, SEGMENTAL DYNAMICS, AND FRICTION COEFFICIENTS FOR INDIVIDUAL POLYMERS IN MULTICOMPONENT POLYMER SYSTEMS BY CHAIN- LEVEL EXPERIMENTS*

Introduction

Miscible polymer blends present significant challenges to our fundamental understanding of the connections between molecular and macroscopic properties in macromolecular mixtures. While many commercial polymer blend applications exist, their discovery and optimization have essentially followed empirical methods. Recently, the polymer blend literature has addressed deficiencies in the predictive understanding of binary miscible blends by focusing on the temperature and composition dependence of chain dynamics in their mixed and unmixed states, as well as the failure of empirical time-temperature superposition relationships, via a variety of experimental and computational approaches. Key aspects of recent discussions surrounding miscible blends include dynamic heterogeneity,^{81,82} different effective glass transitions for the polymer constituents in the blend, particularly for blends whose components have large differences in the Tg's,^{83,84} the characteristic minimum length scale for cooperative chain rearrangements,^{85,86} local composition variations and the role they play in differential chain behavior, or as stated in the recent language found in the literature, the relative contributions of

**The content of this Chapter has been published in Macromolecules, 2010, 43, 3903-3910.*

“self-concentration” and “concentration fluctuations” and the failure of time-temperature superposition.⁸⁷⁻⁹² A recent review has summarized some of the progress towards addressing many of these key outstanding questions.⁹³

Experimental work in chapter 2 and 3 and references 94 and 95, has relied heavily on advanced solid-state NMR methods, revealed new information regarding the formation of miscible polyolefin blends and their individual segmental dynamics at or near the glass transition temperature. Specifically, chain-level experiments on this class of athermal polymer mixtures indicated that (1) configurational entropy can drive mixing in miscible polyolefin blends, (2) the effective Tg’s of each polymer component in the miscible blend may or may not be identical and must be evaluated on a case-by-case basis, and (3) dynamic heterogeneity exists and upon formation of a miscible polyolefin blend, the dynamic heterogeneity significantly increases for the high-Tg blend component while the low-Tg blend component experiences much smaller perturbations in chain dynamic heterogeneity. These previous experiments focused on slow chain dynamics near the glass transition, i.e., segmental dynamics, and did not address terminal dynamics accessed at much higher temperatures. In the course of pursuing direct experimental evidence for why polyolefin blends exhibit such unique mixing behavior, it is recognized that the experimental approach utilizing temperature dependent CODEX NMR^{98,99} was equally well-suited for addressing many of the larger, general questions surrounding miscible polymer blends as described in the preceding paragraph. Indeed, the experimental approach offers some important advantages that allow general application to any polymer blend or composite system. These advantages include: (1) no isotopic labeling is required; (2) no physical modification of the material is required, e.g., solvent or small molecule addition; (3) the individual blend components do not have to have an electric dipole moment, as is required for dielectric spectroscopy (which becomes complicated if both species are dielectrically active); (4) chain-specific resolution even in the blend, unlike typical calorimetric methods; (5) raw data which is amenable to treatment

using models familiar to the broader polymer science community, including those which capture spatially and temporally heterogeneous chain behavior; and (6) the ability to interrogate chain behavior below, at, or above the glass transition temperature. These advantages have recently been discussed in previous publications for binary blends containing various combinations of polyethylene, atactic polypropylene, polyisobutylene, polyethylene-co-butene, and head-to-head polypropylene.⁹⁴⁻⁹⁷ Here, it is important to discuss recent experimental results and their implications in the context of the larger questions surrounding polymer blend science for the PI (polyisoprene) and PVE (polyvinylethylene or poly-1,2-butadiene) blend, a classic ideal miscible blend whose pure polymers have > 50 K difference in their individual Tg's, and which are known to be intimately mixed when the PVE 1,2-diene content exceeds ca. 85%. The PI/PVE blend system (50/50 mole %) was chosen since it has been studied extensively by many researchers using a variety of methods and theory,¹⁰⁰⁻¹¹³ including several key ²H labeling wide-line NMR experiments by Kornfield and coworkers that helped generate significant interest in the blend.¹¹⁴⁻¹¹⁶ Based on this wealth of published data, the PI/PVE blend will serve as an excellent baseline for validating the experimental approach as generally applicable to any mixed polymer or composite system without the aforementioned limitations often encountered with other experimental strategies.

The specific chain-level NMR experiments discussed below for PI/PVE quantitatively reveal (1) the length scales of mixing in the polymer mixture; (2) distinct effective Tg's for each component; (3) central correlation times characteristic of slow segmental dynamics over a wide temperature range (beginning at or below Tg) for each polymer before and after blending; (4) the breadth of the correlation time distribution before and after formation of the miscible blend; and (5) friction coefficients for each blend component before and after blend formation. Agreement exists between our results and previously published results on this blend system. It is observed that the individual blend components do not exhibit the same effective Tg in the miscible blend,

and the high-T_g blend component (PVE) experiences a significantly larger change in its temperature-dependent central correlation time and correlation time distribution (characteristic of slow segmental dynamics) versus the low-T_g PI. These chain-level experiments reinforce the emerging picture of inequivalent individual chain dynamics in miscible polymer blends. These results will be discussed in detail relative to the extensive literature on this blend system, the comparison of which demonstrates the overall validity of our experimental design as a general strategy for essentially any polymer blend or polymer composite/nanocomposite system from which one can obtain an NMR signal.

Experimental Section

Samples and Data Collection. A commercial polyisoprene (PI) sample was obtained from Aldrich, with MW ~800,000 and microstructure corresponding to 97% cis-1,4 enchainment (catalog #182141). Polyvinylethylene (PVE) was purchased from Polymer Source, Inc (catalog #P390-Bd). The molecular weight and polydispersity index (PDI) was obtained by size exclusion chromatography (SEC) in THF. SEC analysis was performed on a Varian gel-permeation chromatograph equipped with refractive and UV light scattering detectors. The PVE sample has Mw/Mn ratio of 1.04 (Mw = 11450) and 88% 1,2 polybutadiene enchainment. The percent 1,4 enchainment in PVE was calculated using integration of the olefinic region of the ¹³C single-pulse experiment, yielding 12% 1,4 isomer. Equimolar PI/PVE blends were made via toluene dissolution for 24 hours and then mixed for 72 hours to form the blend.

Thermal analysis of the samples was completed using a TA Q2000 differential scanning calorimeter (DSC), with a 10°K/min heating rate. The endotherm midpoint from the second heating scan was assigned as the calorimetric glass transition (T_g) temperature. Solid-state NMR T_{1ρH} measurements confirmed intimate mixing for the blended components, and experimental

results were compared to simple mixtures of the same polymers. The experimental DSC and $T_{1\rho\text{H}}$ data are reported in Table 1.

All ^{13}C and ^1H measurements were collected on a Bruker DSX-300 with field strength equal to 7.05T. Solid-state CODEX NMR experiments were performed on a 4-mm double-resonance magic-angle spinning probe using the pulse sequence in Figure 1, previously described in detail by deAzevedo and Schmidt-Rohr.^{98,99} The probe temperature was calibrated using PbNO_3 to within ± 1 K. All CODEX exchange data was acquired with an actively-controlled 4.5 kHz MAS speed, a 1-ms cross-polarization contact time, rotor synchronization, and acquisitions were alternated between the exchange and reference signal every 256 scans to eliminate spectrometer drift. All slow exchange data were acquired using a 200-ms exchange time. Total experiment times typically ranged between 8-20 hours for a single measurement, depending on the temperature.

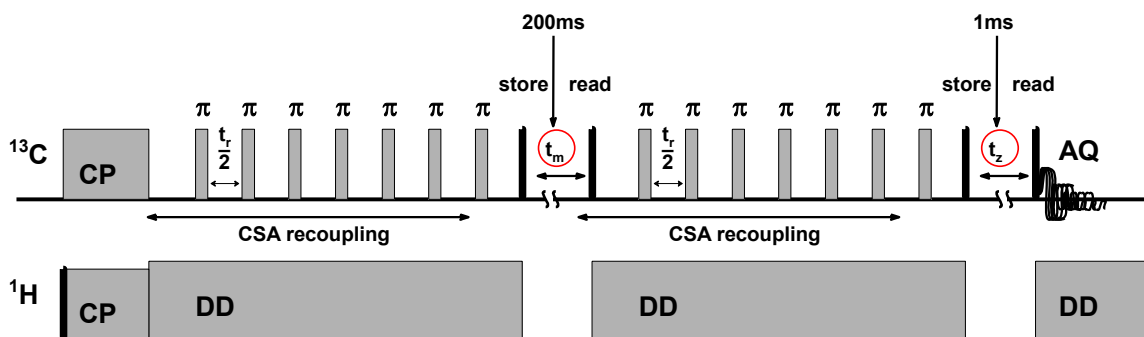


Figure 1. CODEX experiment pulse sequence applied under conditions of MAS. The value of the exchange mixing time $t_m = 0.2$ s for all data reported in this paper, unless specifically noted. The total CSA evolution time corresponding to the sum of the first and second recoupling period was $2Nt_r = (2)(4)(0.22 \text{ ms}) = 1.78 \text{ ms}$.

Experimental Verification of Blend Miscibility. Table 1 shows results from DSC and ^1H $T_{1\rho}$ NMR measurements. As expected, the DSC measurements agree with multiple reports in the previous literature; a broad, featureless endotherm was observed for the blend, whereas the

mixed sample exhibited distinct individual pure component transitions. Using known spin-diffusion length scale equations, the essentially equivalent ^1H $T_{1\rho}$ time constants for the blend ($T = 230$ K, where spin-diffusion is efficient) indicate miscibility at a length scale of mixing equal to 1.8 – 2.2 nm, which is significantly smaller than chain dimensions for either polymer component, and indeed on the order of accepted Kuhn lengths for these polymers.¹¹⁷

Table 1. DSC T_g values for the polymers and blends acquired using a 10°K/min rate, and $T_{1\rho\text{H}}$ measurements obtained at 230 K. The pure polymers have essentially identical $T_{1\rho\text{H}}$ values at 198K.

| | <u>PI pure</u> | <u>PVE pure</u> | <u>PI blend</u> | <u>PI mixed</u> | <u>PVE blend</u> | <u>PVE mixed</u> |
|---------------------------------------|----------------|-----------------|-----------------|-----------------|------------------|------------------|
| DSC T_g | 208 K | 263 K | 214 K | 208 K | 224 K | 263 K |
| $T_{1\rho\text{H}}$ | 1.9ms | 13.8ms | 5.1ms | 1.5ms | 6.5ms | 13.1ms |

Calculations and Theory. Data analysis methods used for this miscible blend system are the same as applied to the previously published aPP/PEB66 and hhPP/PIB polyolefin systems.⁹⁵⁻⁹⁷ Complete details are described in the introduction. Chain conformational exchange data from variable temperature CODEX experiments were analyzed to extract correlation time constants, activation energies for chain reorientation, and quantitative correlation time distributions. An isotropic rotational diffusion model (employing 20 discrete conformer populations as an approximation to the heterogeneous backbone conformer distribution) was used to simulate the experimental data and solve the overall equilibrium exchange matrix as a function of the exchange mixing time in the CODEX experiment and the correlation time constant for the specific polymer at each temperature. A discrete log-Gaussian correlation time distribution function was analyzed with respect to temperature using an Arrhenius model, which was also compared to results from a WLF/KWW model analysis of the experimental data. Powder averaged values of the chemical shift anisotropy, reflecting the distribution of tensor orientations

in the amorphous polymers, were included in all calculated fits of the data. The *Mathematica*[®] program (version 6.0) was used for all calculations.

Results and Discussion

Exchange Data for Pure PI and PVE. Figure 2 shows representative ¹³C CODEX NMR spectra for pure PI and PVE, and their blend. The details of the CODEX experiment itself, and the variable temperature strategy used for polymer blends has been discussed extensively in previous contributions.⁹⁵⁻⁹⁷ In summary, spectra are obtained over the entire temperature range spanning each pure polymer, and specifically for the PI/PVE system, from 193 to 280 K. The experiment is actually run in duplicate to generate two data sets at each temperature, which differ in that the t_m and t_z periods are interchanged, generating what is known as the exchange spectrum $S(t_m \text{ and } t_z \text{ positioned as shown in Figure 1})$ versus the reference spectrum S_0 (no mixing; t_m and t_z switched from that shown in Figure 1).^{98, 99} The pure exchange spectrum is the difference between these two results, denoted as $\Delta S = S_0 - S$. The amplitude of this signal is related to the normalized exchange intensity $E(t_m, \tau_c, T) = \Delta S/S$, as previously discussed,¹¹⁸ and in addition to the temperature dependence, the amplitude depends on the mixing time t_m and the correlation time τ_c characteristic of segmental dynamics. The mixing time is a real time parameter that can be varied (in practice from a few microseconds to almost one second; in theory up to several seconds if polarization can be preserved). Most importantly for this contribution, systematic comparisons of E as a function of temperature for pure polymers versus the same polymers in the binary blend can reveal quantitative changes in slow chain dynamics and their distributions upon blend formation. As a result, exchange intensity curves as a function of temperature, beginning at or below the known Tg for each component, provide the raw experimental data from which it is possible to extract correlation times and correlation time distributions characteristic of slow segmental chain reorientation for each component in the miscible blend. As stated previously, this is achieved without any isotopic labeling or tracer/probe molecule introduction.

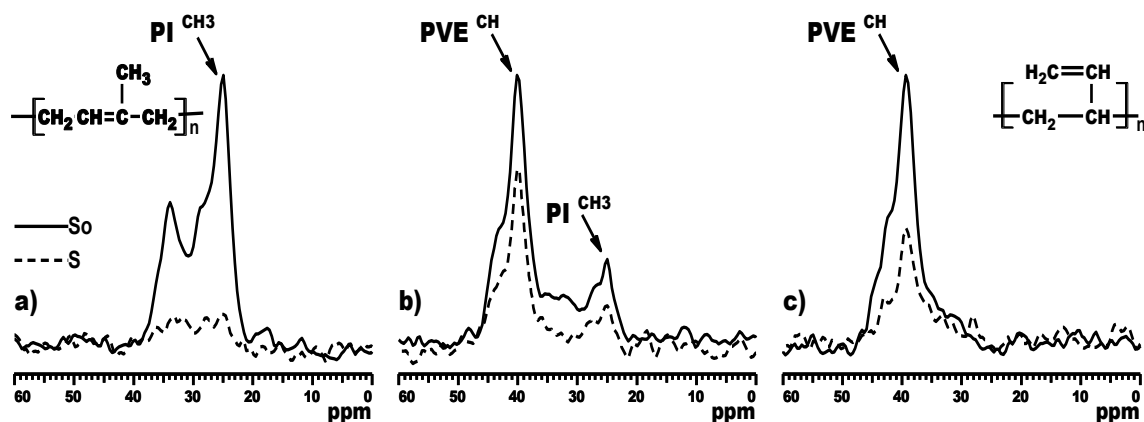


Figure 2. Example ^{13}C CODEX spectra showing only the aliphatic region, from which backbone dynamics were interrogated, for (a) pure PI at 214K, (b) PI/PVE 50/50 mole % blend at 236K, and (c) pure PVE at 263K. The solid line represents the reference spectrum with $t_z=1$ ms (S_0) and the dashed line is the codex spectrum obtained with $t_m=200$ ms (S).

Exchange intensity curves $E(T)$ for 0.2 second mixing times are shown in Figure 3 for the two pure polymers PI and PVE. Qualitatively, the curves provide the expected shape for variable-temperature CODEX experiments, as no exchange intensity is observed at very low temperatures, exchange intensity increases as the temperature increases and polymer segments begin to reorient, and finally at high temperatures, no exchange intensity remains as chain motion becomes fast enough to isotropically average the chemical shift anisotropy interaction. Using a 0.2 s mixing time, the onset of detectable slow chain dynamics occurs at temperatures lower than the 10 K/min DSC T_g (indicated by the shaded vertical stripe) for each component. However, the same effective glass transition difference (50 K) is observed from the initial temperature at which exchange intensity exists. Since multiple signals arise from each polymer component, one chooses that signal from each polymer that provides the best resolution in the blend spectrum. Often, this can be a methyl group, so it is important to verify that the temperature-dependent

CODEX response is the same for a pendant methyl as it is for the main chain carbons. Control experiments verify this is the case for PI, as shown by the open and closed symbols in Figure 3. Specific methyl group dynamics are much too fast to influence the magnitude of the exchange intensity signal, since the CODEX experiment probes the much slower 1-1000 Hz frequency regime, and while the agreement shown in Figure 3 was expected based on previous polymer systems, it is important to run the control for each polymer. Therefore, the resolved methyl signal in the blend spectra can be used with confidence as an accurate measure of slow PI main-chain segmental dynamics.

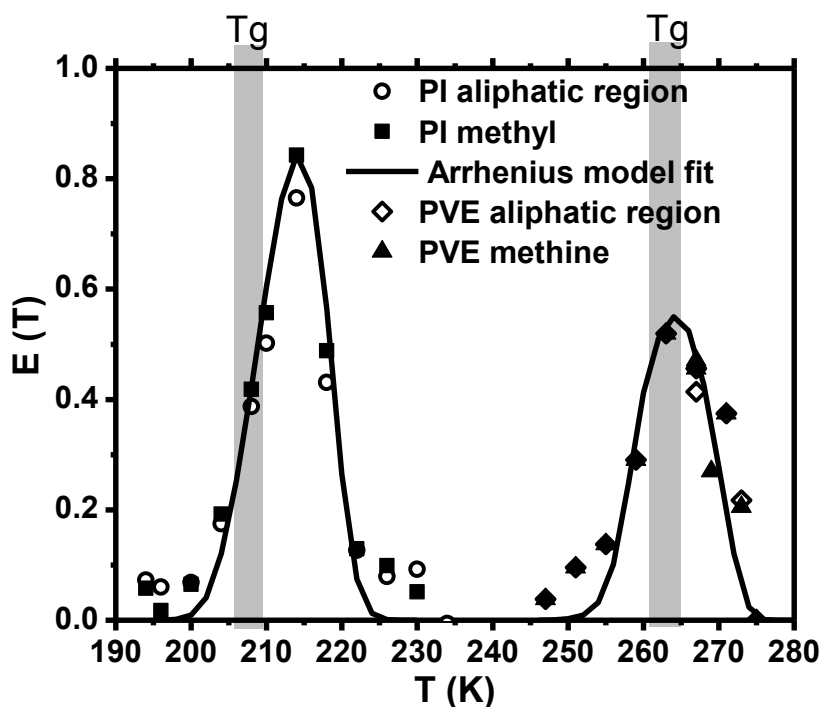


Figure 3. Normalized 200-ms exchange intensity $E(T)$ curves for the total aliphatic region integrated intensity versus only the CH_3 intensity for pure PI, and total aliphatic intensity versus backbone-CH only for PVE. The DSC value for the T_g range of the pure polymers is shown as a shaded region. The solid lines are fits to the data using an Arrhenius/log-Gaussian model described in the text.

Close examination of the first two to three points in the low temperature region of the PVE exchange curve (245-255 K) reveals additional sub-T_g dynamic modes that have not observed in previous studies of completely aliphatic polyolefins, and do not follow expected behavior for residual spin-diffusion contributions to exchange intensity.^{99, 118} Note that these points do not follow a simple monotonic intensity rise relative to the rest of the E(T) curve. There is excellent agreement between the intensity extracted from the entire aliphatic backbone signal region versus that extracted from only the backbone methine for these three points (Figure 3). This apparent premature exchange intensity gain is assigned to a neighboring group effect, since the olefinic PVE side group has a large chemical shift anisotropy and in addition, as a side chain is expected to exhibit sub-T_g dynamics prior to the onset of main-chain dynamics. Time-dependent modulation of the shielding environment (due to susceptibility anisotropy) for the directly bonded backbone methine carbon will occur even if there is no backbone chain motion during the mixing time, manifesting itself as a premature onset of detectable exchange intensity. This is confirmed by data analysis on the integrated exchange intensity for the olefinic =CH₂ signal over the 245-255 K temperature range, which mirrors that of the aliphatic backbone CH at the first three temperature points in the PVE E(T) curve (data not shown). Unfortunately, a complete exchange curve could not be constructed for the specific signals from the PVE olefinic side group, as initially anticipated, since the olefinic side-chain dynamics increase quickly and interfere with the coherent averaging from ¹H decoupling resulting in complete loss of side-chain signal intensity beginning at 260 K.¹¹⁹

Exchange Data for Polymers in the Miscible Blend: Model-Independent Conclusions. Advanced polymeric mixtures, including those with inorganic components, and particularly those composed of structurally disordered phases, require that the experimentalist understand the specific behavior of the components in that mixture in order to tailor properties and define applications for the total material. As stated in the introduction to this chapter, many

recent experiments in polymer blend science indicate that one can only assume limited information from the pure-component behaviors. Figure 4 illustrates the power of the experimental NMR approach described here to separately and quantitatively identify constituent chain behavior in mixed polymer systems, and is particularly advantageous for mixtures of amorphous polymers. The exchange intensities versus temperature for pure and blended components as measured directly from the CODEX experiment are shown, as well as fits to the raw data using Arrhenius and WLF models.

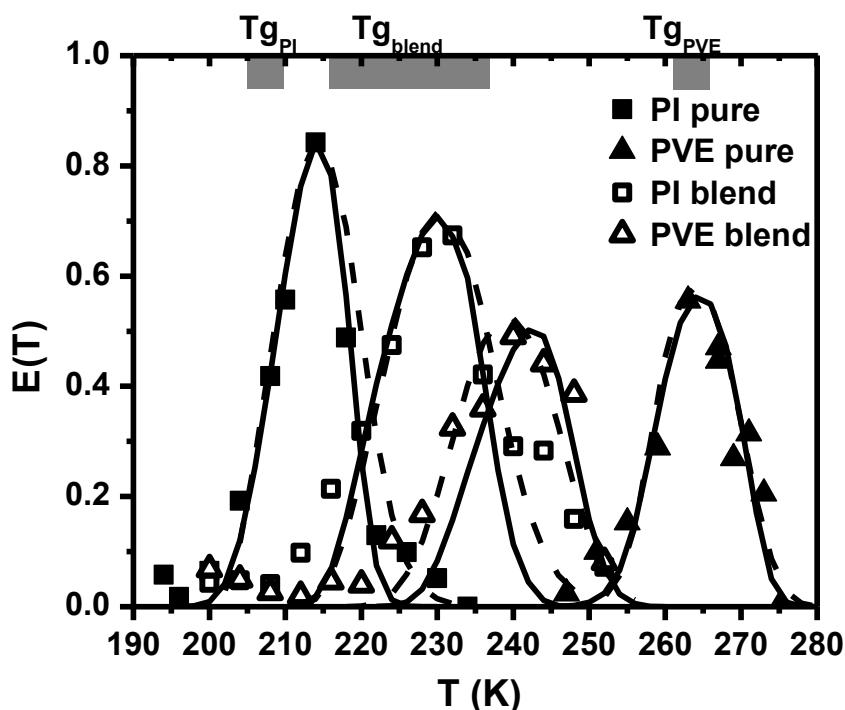


Figure 4. Normalized 200-ms exchange intensity $E(T)$ curves for the pure components and the same components measured independently in the blend. The solid lines are fits to the data using an Arrhenius model with a variable-width log-Gaussian correlation time distribution. The dashed lines are fits to the data using the WLF/KWW model. The thick gray lines at the top of the figure indicate the 10 K/min DSC T_g range for the two pure polymers and the miscible blend.

Figure 4 represents the outcome of three independent variable-temperature experiments; one each for the two pure polymers and a single experiment for the blend from which polymer

specific exchange intensities were extracted at each temperature. Prior to any consideration of a quantitative model to fit the results, several important points may be discerned via simple inspection of the raw data in Figure 4, and comparing the response of the NMR signals in the CODEX experiment for each pure polymer to the response of that same polymer in the blend. Firstly, the onset of detectable exchange intensity occurs at temperatures at or below the calorimetric T_g , indicating that the 200-ms mixing time CODEX experiment is probing the slow segmental chain dynamics (i.e., conformational reorientations) operative during the glass transition. Secondly, the PI exchange intensity curve shifts to higher temperature in the blend relative to pure chains. Similarly, the exchange intensity curve shifts to lower temperature for the PVE in the blend compared to its pure response. For PI, the $E(T)$ maximum shifts from 214 K to 230 K upon blend formation, while the PVE $E(T)$ maximum decreases from the pure value of 265 K to 240-243 K in the blend. The temperature shifts for the $E(T)$ curves of each component in the blend are not equivalent, nor do the curves converge to the same temperature range in Figure 4. The polymer components exhibit distinctly different glass transitions in the miscible blend. Thirdly, the expected temperature to observe the maximum in each $E(T)$ curve in the miscible blend, using Gordon-Taylor/Fox equations for composition weighted averaging, is 237K. Neither blend component exhibits a maximum at this temperature; the PI maximum is 7-8 degrees lower and the PVE maximum is 3-5 higher. Finally, the breadth of each $E(T)$ curve increases for either component in the blend relative to the pure polymer, clearly indicative of increased dynamic heterogeneity for blended versus pure polymers, in agreement with the observation that the absolute value of $E(T)$ at each temperature point across the detectable range decreases in the blend relative to the unmixed result for both polymer components (holding constant all other experimental parameters which could effect signal intensity). Interpretations of these direct inspection observations using quantitative physical models are presented the following sections.

Quantitative Segmental Dynamics for PI and PVE in the Miscible Blend. The fits to experimental data shown in Figures 3 and 4 were obtained using two different physical models. The $E(T)$ temperature dependence was analyzed by comparing an Arrhenius model using a discrete log-Gaussian correlation time distribution function to a WLF/KWW (Williams-Landau-Ferry/Kohlrausch–Williams–Watts) model. As previously discussed, an isotropic rotational diffusion model (employing 20 discrete conformer populations as an approximation to the heterogeneous backbone conformer distribution, and the small angle jumps between them) was used to simulate the experimental data and solve the overall equilibrium exchange matrix as a function of the exchange mixing time in the CODEX experiment and the correlation time constant for specific polymers at each temperature.⁹⁵⁻⁹⁷ Figure 4 shows the results of each approach, indicated by solid versus dashed lines, respectively. Complete details for the calculations, as well as comparisons to other possible approaches cited in the literature, are provided in the introduction. Extensive discussions of the data analysis steps for static (i.e., non-MAS) versions of this experimental approach may be found in references 118 and 120.

The absolute value of the exchange intensity $E(T)$ at each temperature, for a fixed recoupling and exchange mixing time, depends on the correlation time constant characteristic of the motion modulating the chemical shift anisotropy as well as the distribution of correlation time constants for all of the segments in the amorphous polymer or polymer mixture (described in introduction). Figure 5 shows calculated results for the temperature dependence of the central correlation time constant, i.e., the characteristic time constant at center of distribution, obtained using both the Arrhenius/log-Gaussian and WLF/KWW models. As expected, the Arrhenius model breaks down at high temperatures for macromolecules, but over the majority of the temperature range relevant for slow segmental dynamics used in this study, the model is physically reasonable and contains fewer parameters and assumptions than the WLF/KWW approach. The discrete points in Figure 5, through which the Arrhenius fits are drawn, indicate

the temperatures at which raw exchange intensity data was obtained, as in Figure 4. Figure 6 shows example calculated correlation time distributions obtained in the fitting process to the data in Figures 4 and 5 for the PVE component.

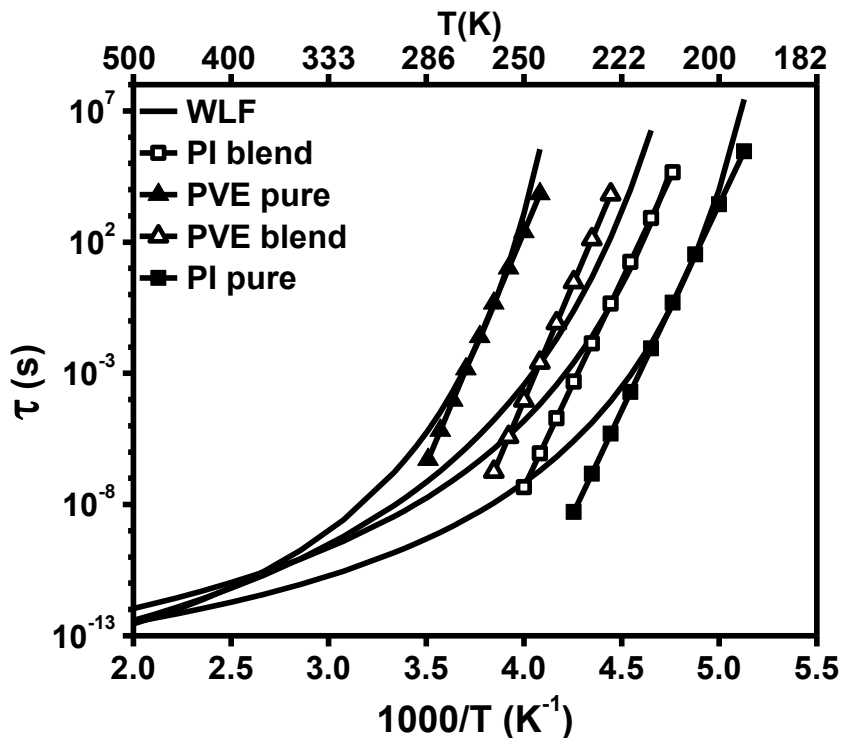


Figure 5. Temperature dependence of correlation times obtained using Arrhenius (points) and WLF (smooth line) models. The WLF parameters for pure PI were: $C_1 = 18.2$, $C_2 = 32$ K, $\tau(T_g) = 10,000$ s, and $T_g = 200$ K, whereas for PI in blend $C_2 = 41$ and $T_g = 212$ K was used. For pure PVE, $C_1 = 19.2$, $C_2 = 42$ K, $\tau(T_g) = 10,000$ s, $T_g = 248$ K, and the best fit for PVE in the blend was obtained with $C_2 = 48$ K and $T_g = 220$ K. Note the close agreement for each model in the lower temperature regions consistent with segmental dynamics, but as expected, the Arrhenius fits diverge at high temperatures. In the WLF/KWW fits, the KWW β parameters for pure PI, blend PI, pure PVE, and blend PVE were 0.33, 0.33, 0.65, and 0.46, respectively.

Figure 6 indicates that a large change in the PVE correlation time distribution width occurs once the miscible blend is formed, and also that the temperature dependence of the distribution is suppressed. Examination of the exchange intensity equations in the introduction reveals how the magnitude of the distributions shown in Figure 6 can influence each point in the $E(T)$ curves. Similar plots to those shown in Figure 6 could also be constructed for PI. A

complete comparison of the behavior of both PI and PVE are summarized by Figure 7, in which the σ values from the full $g(\tau)$ expression are plotted versus temperature.

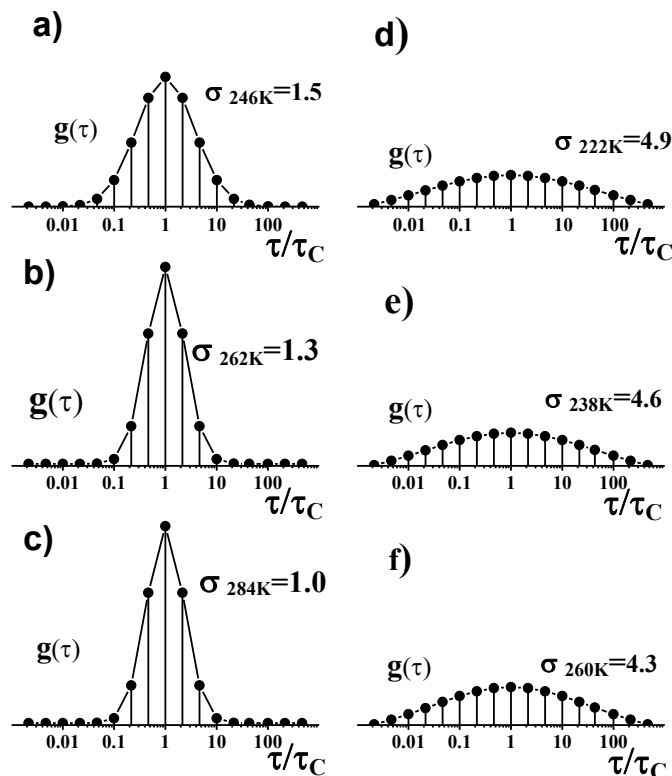


Figure 6. Example results for discrete versions of log-Gaussian correlation time distributions $g(\tau)$ for PVE, with different widths σ following a linear temperature dependence $\sigma(T) = a k_B T + \sigma_0$, at key temperatures spanning the $E(T)$ curve previously shown in Figure 4. Each distribution is centered at τ_c and consists of 17 points equally spaced over approximately 6 decades. (a) pure PVE at 246 K, (b) pure PVE at 262 K, (c) pure PVE at 284 K, (d) PVE in blend at 222 K, (e) PVE in blend at 238 K, (f) PVE in blend at 260 K.

Figure 7 indicates that pure PI and pure PVE have much different temperature dependent slopes, and also shows the large effect blend formation has on the dynamic heterogeneity characterizing segmental dynamics for each component. In particular, the high-Tg PVE component exhibits a significantly larger change in absolute value of σ in the blend relative to its pure component values, but preserves its slope. Conversely, the PI shows a relatively small

change in the absolute value of σ at any temperature over the temperature range of interest, but a much larger change in its slope. Systematic comparison of σ 's in the log-Gaussian model to KWW β parameters are discussed in support of Figure 12 of the introduction.

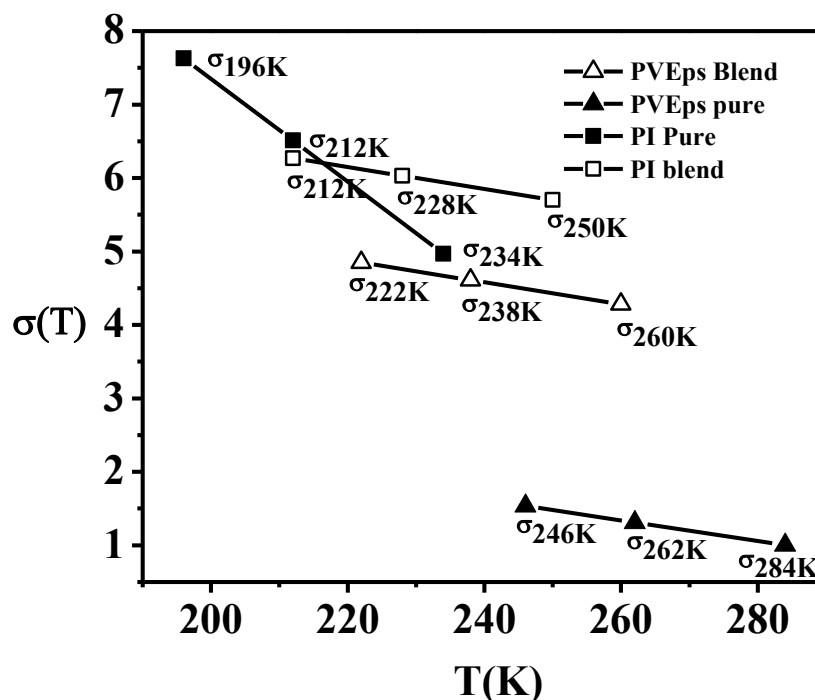


Figure 7. Temperature dependence of correlation time distribution widths σ for pure PI and pure PVE versus the same polymers in the blend, obtained using the Arrhenius/log-Gaussian model with linear temperature dependence for σ as explained in the text. Note the disparate slope for the pure components, but essentially identical slopes for the blended polymers, and the much larger change in the absolute values of σ for the high-Tg PVE blend component.

Friction coefficients for chain segmental dynamics, as referenced to a specific length or chain sub-unit, may be obtained via direct diffusion measurements,¹⁰⁸ or calculated based on measured correlation time constants characteristic of that motion.¹²¹ Direct experimental measurement of chain diffusion for high molecular weight polymers in bulk at temperatures near T_g is difficult, even via pulsed-field gradient methods, since the self-diffusion coefficients are too small. Figure 8 shows calculated friction coefficients ζ obtained from our experimental τ_c data, using the simple relationship $\zeta = \tau_c k_B T / b^2$, where $b = 1$ nm. Since the chemical shift anisotropy

modulation giving rise to finite intensity in the $E(T)$ curves originates from slow segmental dynamics involving chain sub-units, e.g. conformational reorientation, we do not scale the equation by molecular weight dependent terms as in a typical Rouse relaxation time model.

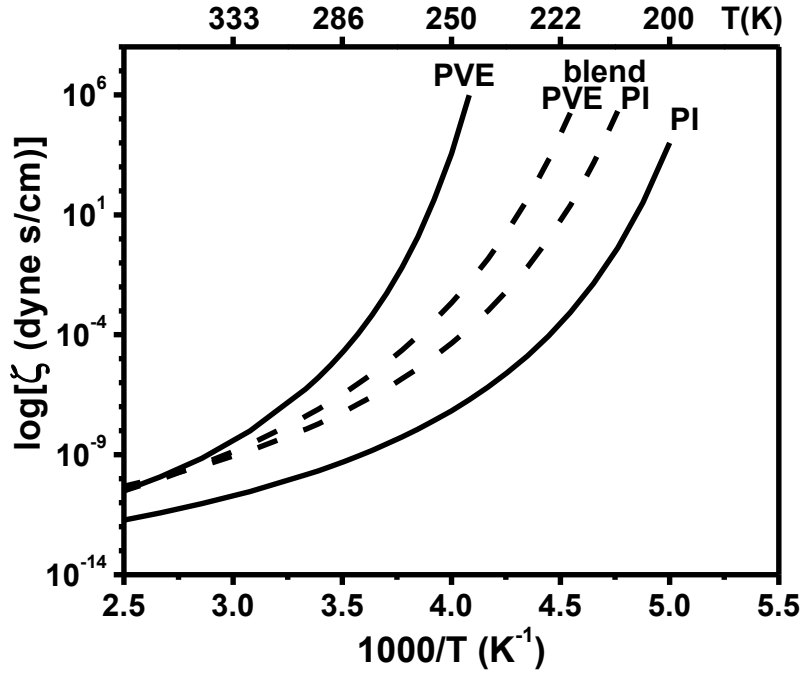


Figure 8. Calculated segmental friction coefficients using the central correlation time constants τ_c obtained from the WLF/KWW model fits to the CODEX exchange intensity data in Figure 4. The relationship $\zeta = \tau_c k_B T / b^2$ was used for the calculations, where $b = 1.1$ nm is the characteristic segment length for reorientation. The temperature range for the experimental data used to generate the curves is 196 K – 286 K.

There is some uncertainty in the literature on the magnitude of the characteristic segmental reorientation/diffusion length for amorphous polymers, with most published reports espousing values between 1 and 3 nm. The CODEX experiment probes changes in chemical shielding arising from local conformational changes of chain sub-units, and given that we are interpreting our data in the context of a rotational isotropic diffusion model (appropriate for amorphous materials), we have used a value at the lower end of the range of reported values, i.e., 1 nm, for the friction coefficient calculation.

Comparison with Previously Published Data. The PI/PVE blend system, as discussed earlier, is a well-studied system by a large variety of experimental and theoretical methods. Recently, Haley and coworkers have summarized experimental results from their own work on PI/PVE blends and also compared their results to those previously published by other groups.¹⁰⁸ In Table 1, those contributions are referenced, and compare selected values of the central correlation time constant τ_c extracted from a summary figure in Reference 108 to our values obtained in this study, for 50/50 PI/PVE blends. Inspection of Table 1 reveals close agreement between values for each of the pure polymers, as well as their individual values in the miscible blends. Exact agreement is not expected, as the WLF/KWW and Arrhenius/log-Gaussian models used here differ from the models used in the referenced work.^{108,114,115} For example, Haley and coworkers used VTF models to fit experimental data, and the WLF fits used by Kornfield and coworkers employed different fitting parameters, most notably the value of the correlation time constant at the glass transition (much smaller than the $\tau T_g = 10,000$ s that we use here), and the T_g values for the polymers in the blend. Here, the raw CODEX data was used to assign T_g 's in the blend, and there are no temperature shifts of the individual data points plotted in Figures 5 or 8. Given the large number of models pervasive in the polymer literature and the variation in fitting parameters often used within the same models, as well as small but random temperature errors in the collection of raw data by various methods, Table 2 illustrates that the experimental results obtained here are within expected agreement with previously published results on a point by point basis. More importantly, the experimentally detected changes that occur for pure versus blended polymer components, as shown in Figures 5 and 8, are in excellent agreement with these previously published results.

Table 2. Comparison of literature data previously summarized in Reference 108 with experimental results in this contribution for 50/50 PI/PVE blends.

| <u>Polymer</u> | <u>Temperature</u> (K) | <u>Literature</u> τ_c (sec) | <u>Experimental/Fit</u> τ_c (sec) |
|------------------|---------------------------|-------------------------------------|---|
| <u>PI pure</u> | 222 | 2.0 e^{-4} | 5.0 e^{-4} |
| <u>PI pure</u> | 250 | 2.0 e^{-7} | 1.0 e^{-7} |
| <u>PI pure</u> | 286 | 5.0 e^{-9} | 0.8 e^{-9} |
| <u>PI blend</u> | 222 | 0.1 | 1.0 |
| <u>PI blend</u> | 250 | 0.5 e^{-5} | 2.0 e^{-5} |
| <u>PI blend</u> | 333 | 3.0 e^{-10} | 3.0 e^{-10} |
| <u>PVE pure</u> | 286 | 0.5 e^{-5} | 1.0 e^{-5} |
| <u>PVE pure</u> | 333 | 7.0 e^{-8} | 2.0 e^{-8} |
| <u>PVE blend</u> | 235 | 5.0 | 2.0 |
| <u>PVE blend</u> | 250 | 40.0 e^{-4} | 6.0 e^{-4} |

Comparison of Correlation Time Constants Obtained from CODEX Data Analysis to Discrete Variable Mixing Time Experiments. To further validate that data obtained from the analysis of the CODEX data as a function of temperature is accurate, we compare segmental correlation time constants obtained from the temperature-dependent analysis of CODEX exchange intensity curves, like those shown in Figure 4, with the time constant for the exchange intensity as a function of mixing time, at the same temperature, obtained in separate variable mixing time experiments. Figure 9 shows the exchange intensity as a function of mixing time for four different pure polymers including PVE, atactic polypropylene (PP), head-to-head polypropylene (hhPP), and polyisobutylene (PIB) at the indicated temperatures. The correlation time constants, extracted from an exponential fit to the rising intensity curve, are indicated on each of the Figures 9a-d. (In Figures where there are multiple data points, either multiple carbon

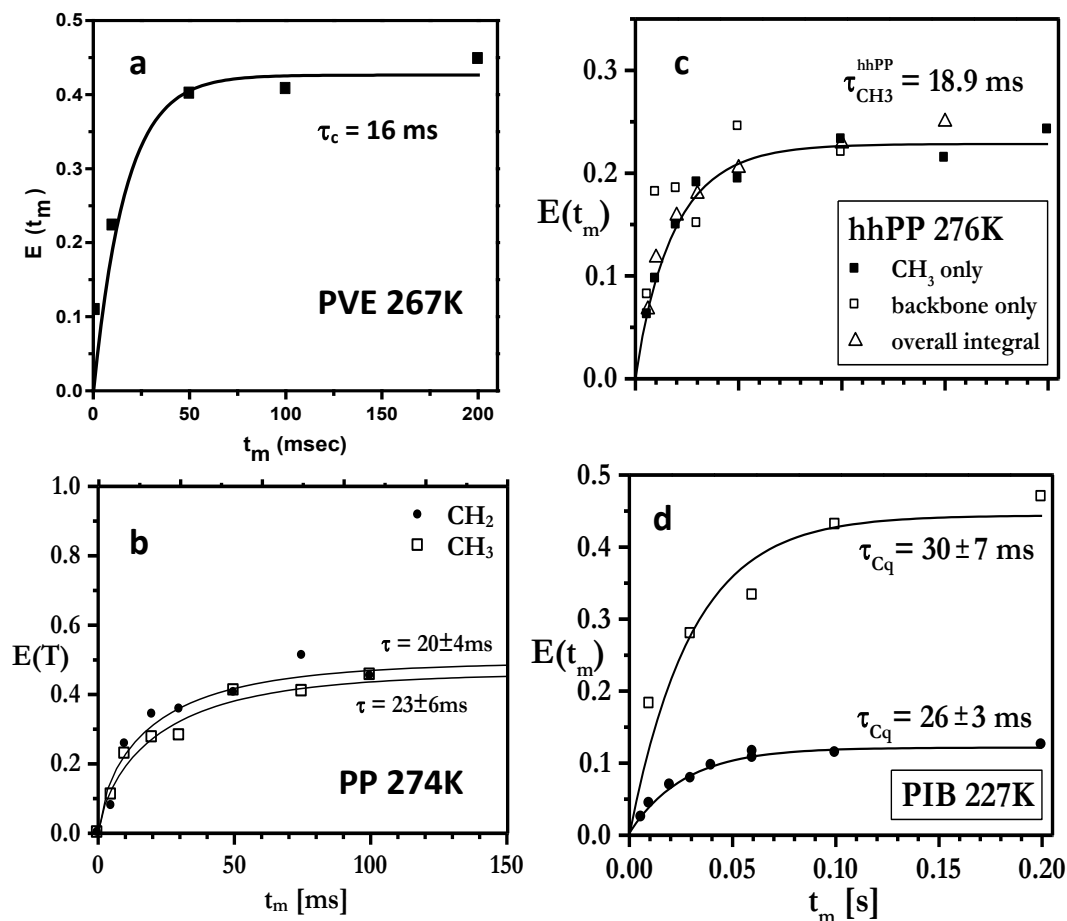


Figure 9. Exchange time constants extracted from an exponential fit to the rising exchange intensity curves are indicated on each of the Figures 8a-d for PVE, atactic PP (PP), head-to-head PP (hhPP), and polyisobutylene (PIB), respectively. For each of these same four polymers, at the same temperature as indicated on each plot, the respective central correlation time constants obtained from full analysis of the variable temperature exchange intensity curves of the type represented by the data in Figures 4 and 5, are: (a) $\tau_c = 14$ ms (b) $\tau_c = 24$ ms (c) $\tau_c = 20$ ms (d) $\tau_c = 25$ ms. The temperatures indicated in a-d are equal or very nearly equal to the exchange intensity maximum temperature for each polymer, resulting in similar values of τ_c . **Note: 9a and 9b have millisecond time axes, while 9c and 9d are displayed in seconds.**

positions in the polymer chain were probed, or as in Figure 9d, two different recoupling times in the CODEX experiment were compared.) The results in Figure 9 indicate that the correlation time constants obtained by full analysis of the raw data in Figure 4 are accurate. While the time required to generate the experimental data in Figure 4 is not trivial, such an approach is significantly shorter (by a factor of 5 to 10) than the time required to obtain full variable mixing

time exchange curves, like those shown in Figure 9, over the entire temperature range used in Figure 4.

Conclusions

A chain-specific experimental approach based on variable-temperature solid-state CODEX NMR experiments reveals that the effective glass transitions for each chain type in PI/PVE blends are inequivalent, and slow segmental dynamics for each polymer in the blend are characterized by unique central correlation times and unique correlation time distributions. Quantitative analyses of the raw data indicate that good agreement exists between effective T_g 's, central correlation time constants, correlation time distributions, and friction coefficients extracted from this approach versus those obtained by other well-documented methods. Results from an isotropic rotation diffusion model with Arrhenius/log-Gaussian or WLF/KWW treatments of temperature dependence show clear sensitivity to changes that occur upon blend formation relative to the unmixed components. That such quantitative information may be obtained for either polymer component in an amorphous mixture, without isotopic labeling, electric dipole moment constraints, or introduction of probe molecules, is a unique advantage of this experimental strategy and illustrates applicability to a wide range of mixed macromolecular systems beyond miscible blends, including polymer nanocomposites, organic/inorganic hybrids, biological macromolecules, and block copolymers.

CHAPTER V

CONCLUSIONS

Overall Conclusions

The variable-temperature solid-state CODEX experiment reveals specific information about the interactions of macromolecules at the chain level for homopolymers and for individual species in binary mixtures. Unique central correlation times and correlation time distributions are determined for pure materials and their miscible blends. The ability to extract correlation time constants for segmental motions at and around T_g , where Arrhenius behavior is followed, allows for quantitative evaluation of the entropy changes responsible for miscibility of amorphous blends using the Adams-Gibbs relationship. Correlation time distributions from the use of the Arrhenius/log-Gaussian model are real indicators of the dynamics of pure polymers, and more importantly, the dynamic heterogeneity of blended amorphous polymers, which usually exhibit an apparent single DSC glass transition. It could be concluded that even though miscible macromolecules may behave as unique materials, each component of the blend retains its own independent chain-level conformational dynamics as shown in both the aPP/PEB66 and PI/PVE blend examples where the $E(T)$ curves do not overlap as they did for hhPP/PIB (see Figure 1).

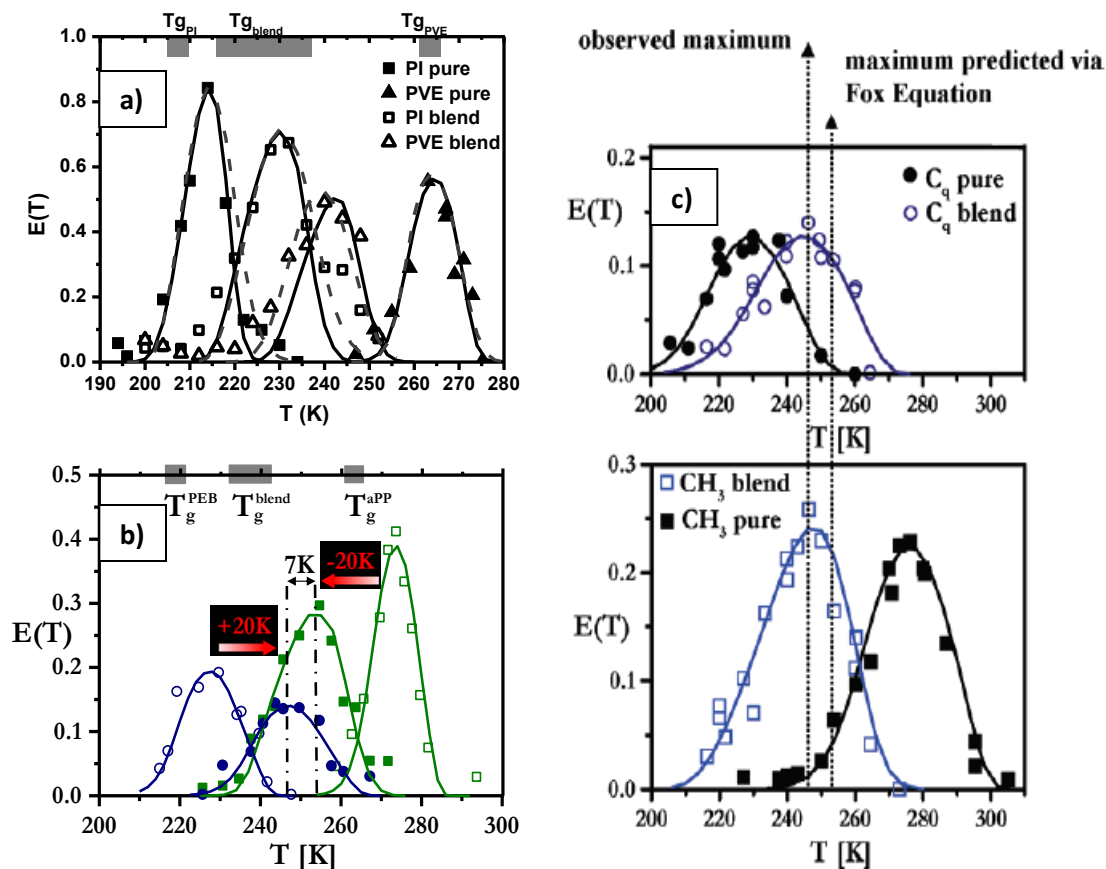


Figure 1. Normalized $E(T)$ curves for a) PI/PVE, b) aPP/PEB-66, and c) hhPP/PIB. In c) the hhPP/PIB blend maxima overlap, but there is a 7K difference in the aPP/PEB66 blend and an over 10K difference in the maxima for the PI/PVE blend.

The CODEX experiment is a true indication of the average polymer chain motions using both the Bloch decay version and the original CP-based CODEX. The development of the Bloch decay version introduces some flexibility for CODEX type experiments with the ability to incorporate more discriminating techniques. The direct excitation method can be used with variable relaxation delays to select between the most mobile regions, and the traditional CODEX can be used with varying cross-polarization transfer times to tune the response for the most rigid regions. Although each version yields essentially identical results for these materials below, at and above T_g , the original version is more economical, and one could argue more quantitative for the carbon nuclei, because it is less dependent on ^{13}C T_2 relaxations.

Given the fact that CODEX data was collected for these materials through the glass transition, where Arrhenius behavior is followed, it is possible to quantitatively evaluate the change associated with the increased width of the correlation time distributions, characteristic dynamic heterogeneity, and configurational entropy. Using the Adams-Gibbs equation [$\tau_c = \tau_0 \exp(c/TS_c)$] and the central correlation times calculated using the Arrhenius model [$\tau_c = \tau_0 \exp(E_a/RT)$] we can determine the change in configurational entropy. In chapter 2, the change in configurational entropy for PEB66 in pure vs mixed ranges from -0.81 to -0.85, and the corresponding range for aPP is +1.35 to 1.28. The total configurational entropy of the miscible aPP/PEB66 blend system results in an approximate 15% gain. For the PI/PVE blend, the configurational entropy range of PI, pure vs blend, is -0.924 to -0.933 with the corresponding range for PVE, pure vs blend, being 1.123 to 1.112. Figure 2 shows the miscible PI/PVE

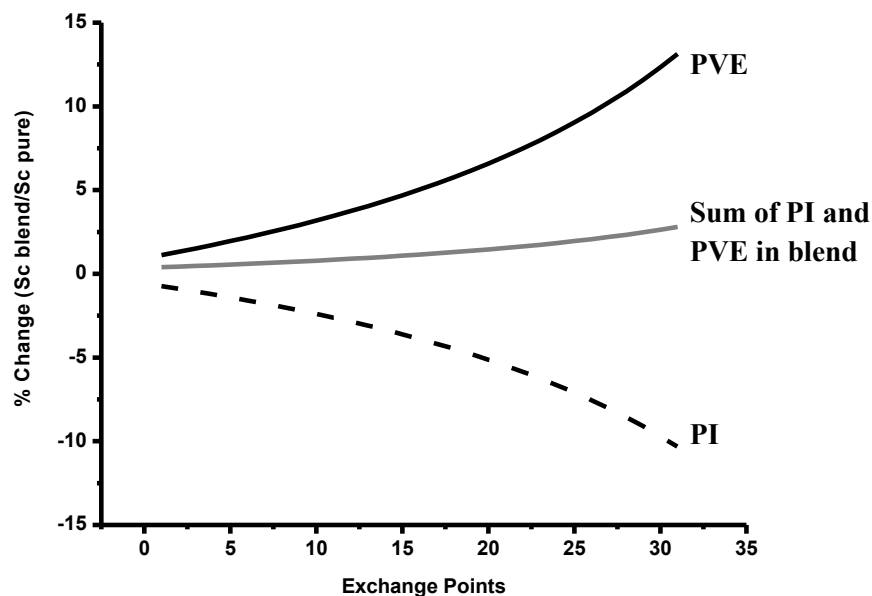


Figure 2. Calculated values of the total configurational entropy ratios in the miscible blend ($S_c \text{ Blend} / S_c \text{ Pure}$) versus the position on the exchange intensity curve shown in Figure 1a from low to high temperature. The solid line represents the percent entropy change for pure PVE versus PVE in the blend, and the dashed line represents the percent entropy change for pure PI versus PI in the blend. The gray line represents the total percent entropy gain for the PI/PVE miscible blend system. Each trace represents a calculation across the entire temperature range of the $E(T)$ curve using τ_c values from the Arrhenius model.

blend system calculations for a total configurational gain of approximately 4.6%. The small in entropy percentage for the PI/PVE blend system vs that of the aPP/PEB66 system is may be due to the number of sp² carbons along the backbone of PI and the pendant vinyl group of PVE. The low T_g blend component, PI, has an entropy change of 7 to 8%, and the high T_g blend component, PVE, experiences a much larger entropy change of 11 to 12%. This suggests that the high T_g component experiences a much larger change in dynamics compared to the low T_g component upon formation of the miscible blend. The direct observation of chain-specific information using CODEX experiments shows the dynamic heterogeneity for miscible blend systems through the divergence in correlation time distribution widths and increased configurational entropy using the approach in this work.

The CODEX experiment has been employed to obtain quantitative chain-level physical information about these blend systems, and the analysis of the raw data produces an understanding of changes in the dynamic behavior as a function of both miscible blend formation and temperature . The main objective of this project is to investigate, at the chain level, why so few amorphous macromolecules form miscible blends when a greater percentage of these materials are immiscible with one another. In each example blend studied the thermodynamic driving force for miscibility is configurational entropy. Furthermore, a miscible blend represents a new material that is separate from both of its individual components, and the blend has its own unique macroscopic glass transition. A fundamental understanding of the microscopic properties in simple miscible blends is important for engineering new raw materials and blends. The quantitative information obtained for each polymer blend component, simultaneously using CODEX ssNMR and the experimental approach developed in this work, may unlock the structure/property relationship and invoke a strategy to new materials. The benefit of this experimental methodology is that the microscopic information obtained for these important

binary blends may be applied to systems of greater complexity, such as proteins, copolymers, and polymer composites.

REFERENCES

1. Ritter, S. K., *Chemical and Engineering News* **2011**, 89 (23), 13-22.
2. Erickson, B., *Chemical and Engineering News* **2011**, 89 (42), 13.
3. Erickson, B., *Chemical and Engineering News* **2011**, 89 (25), 11.
4. Morse, P. M., *Chemical and Engineering News* **2011**, 89 (22), 28-31.
5. Tullo, A. H., *Chemical and Engineering News* **2011**, 89 (38), 10-14.
6. Cangialosi, D.; Alegría, A.; Colmenero, J., *Macromolecules* **2006**, 39, 7149-7156.
7. Donth, E., *The Glass Transition: Relaxation Dynamics in Liquids, Disordered Materials*. Springer: Berlin, 2001.
8. Heffner, S. A.; Mirau, P. A., *Macromolecules* **1994**, 27, 7283-7286.
9. Boucher, V. M.; Cangialosi, D.; Alegría, A.; Colmenero, J., *Macromolecules* **2011**, 44 (20), 8333-8342.
10. Andrew, E. R.; Bradbury, A.; Eades, R. G., *Nature* **1959**, 183, 1802-1803.
11. Lowe, I. J., *Physical Review Letters* **1959**, 2 (7), 285-287.
12. Schaefer, J.; Stejskal, E. O., *J. Am. Chem. Soc.* **1976**, 98 (Copyright (C) 2011 American Chemical Society (ACS). All Rights Reserved.), 1031-2.
13. Garroway, A. N., *J. Magn. Reson.* **1982**, 49 (Copyright (C) 2011 American Chemical Society (ACS). All Rights Reserved.), 168-71.
14. Stejskal, E. O.; Memory, J. D., *High Resolution NMR in the Solid State: Fundamentals of CP/MAS*. Oxford University Press, Inc.: New York, New York, 1994; p 189.
15. (a) Levitt, M. H., *Spin Dynamics*. Second ed.; John Wiley & Sons Ltd: USA, 2009; p 714; (b) Duer, M. J., *Introduction to Solid-State NMR Spectroscopy*. Blackwell Publishing Ltd: USA, 2004; p 349.
16. McGrath, K. J.; Roland, C. M.; Antonietti, M., *Macromolecules* **2000**, 33, 8354-8360.

17. Wachowicz, M.; White, J. L., *Macromolecules* **2007**, *40*, 5433-5440.
18. White, J. L.; Lohse, D. J., *Macromolecules* **1999**, *32*, 958-960.
19. deAzevedo, E. R.; Tozoni, J. R.; Schmidt-Rohr, K.; Bonagamba, T. J., *Journal of Chemical Physics* **2005**, *122* (15), 154506.
20. (a) Kaufmann, S.; Wefing, S.; Schaefer, D.; Spiess, H. W., *Journal of Chemical Physics* **1990**, *93*, 197-214; (b) Wefing, S.; Kaufmann, S.; Spiess, H. W., *Journal of Chemical Physics* **1988**, *89*, 1234-1247; (c) Wind, M.; Brombacher, L.; Heuer, A.; Graf, R.; Spiess, H. W., *Solid State Nucl Magn Reson* **2005**, *27* (1-2), 132-9.
21. Luz, Z.; Tekely, P.; Reichert, D., *Progress in Nuclear Magnetic Resonance Spectroscopy* **2002**, *41*, 83-113.
22. O'Connor, R. D.; Ginsburg, E. J.; Blum, F. D., *Journal of Chemical Physics* **2000**, *112* (16), 7247-7259.
23. Kumar, S. K.; Shenogin, S.; Colby, R. H., *Macromolecules* **2007**, *40* (16), 5759-5766.
24. DeAzevedo, E. R.; Reichert, D.; Vidoto, E. L. G.; Dahmouche, K.; Judeinstein, P.; Bonagamba, T. J., *Chem. Mater* **2003**, *15*, 2070-2078.
25. Saalwächter, K.; Fischbach, I., *Journal of Magnetic Resonance* **2002**, *157* (1), 17-30.
26. Lindsey, C. P.; Patterson, G. D., *Journal of Chemical Physics* **1980**, *73* (7), 3348-3357.
27. Zemke, K.; Schmidt-Rohr, K.; Magill, J. H.; Sillescu, H.; Spiess, H. W., *Molecular Physics* **1993**, *80* (6), 1317-1330.
28. Pascui, O.; Beiner, M.; Reichert, D., *Macromolecules* **2003**, *36* (11), 3992-4003.
29. Lohse, D. J.; Graessley, W. W., "Thermodynamics of Polyolefin Blends" in *Polymer Blends: Formulation and Performance*, ed. by D. R. Paul and C. B. Bucknall, Volume 1, Chapter 8, pp. 219-237, Wiley, New York, **2000**.
30. Zhang, Xiaohua; Wang, Zhigang; Han, Charles C. *Macromolecules* **2006**, *39*, 7441-7445.
31. Kaminsky, Walter; Hoff, Matthias; Derlin, Stefanie *Macromolecular Chemistry and Physics* **2007**, *208*, 1341-1348.
32. Balazs, Anna C.; Emrick, Todd; Russell, Thomas P. *Science* **2006**, *314*, 5802.
33. Rissanou, A. N.; Peristera, L. D.; Economau, I. G. *Polymer* **2007**, *48*, 3883.
34. Weimann, P. A.; Jones, T. D.; Hillmyer, M. A.; Bates, F. *Macromolecules* **1997**, *30*, 3650.

35. Graessley, W. W.; Krishnamoorti, R.; Reichart, G. C.; Balsara, N. P.; Fetter, L. J.; Lohse, D. J. *Macromolecules* **1995**, *28*, 1260.
36. Reichart, G. C.; Graessley, W. W.; Register, R. A.; Krishnamoorti, R.; Lohse, D. J., *Macromolecules* **1997**, *30*, 3036
37. Yamaguchi, M.; Miyata, H., *Macromolecules* **1999**, *32*, 5911.
38. Wolak, J.; Jia, X.; Gracz, H.; Stejskal, E. O.; Wachowicz, M.; Jurga, S. J.; White, J. L. *Macromolecules* **2003**, *36*, 4844-4850.
39. Wolak, J. E.; Jia, X.; White, J. L. *J. Am. Chem. Soc.* **2003**, *125*, 13660-13661.
40. Lodge, T.; McLeish, T. C. B. *Macromolecules* **2000**, *33*, 5278.
41. Cangialosi, D.; Alegria, A.; Colmonero, J. *Macromolecules* **2006**, *39*, 7149.
42. Cangialosi, D.; Alegria, A.; Colmonero, J. *Macromolecules* **2006**, *39*, 448.
43. Krygier, E.; Lin, G. X.; Mendes, J.; Mukandela, G.; Azar, D.; Jones, A. A.; Pathak, J. A.; Colby, R. H.; Kumar, S. K.; Floudas, G.; Krishnamoorti, R.; Faust, R. *Macromolecules* **2005**, *38*, 7721.
44. Kant, R.; Kumar, S. K.; Colby, R. H. *Macromolecules* **2003**, *36*, 10087.
45. Roland, C. M.; Casalini, R. *Macromolecules* **2007**, *40*, 3631.
46. Lutz, T. R.; He, Y.; Ediger, M. D. *Macromolecules* **2005**, *38*, 9826.
47. Lutz, T. R.; He, Y.; Ediger, M. D. *Macromolecules* **2004**, *37*, 6440.
48. Kumar, S. K.; Shenogin, S.; Colby, R. H. *Macromolecules* **2007**, *40*, 5759.
49. Wachowicz, M.; White, J. L. *Macromolecules* **2007**, *40*, 5433.
50. deAzevedo, E.; Hu, W. G.; Bonagamba, T. J; Schmidt-Rohr, K., *J. Am. Chem. Soc.* **1999**, *121*, 8411.
51. deAzevedo, E.; Hu, W. G.; Bonagamba, T. J; Schmidt-Rohr, K., *J. Chem. Phys.* **2000**, *112*, 8988.
52. Graessley, W. W.; Krishnamoorti, R.; Balsara, N. P.; Fetters, L. J.; Lohse, D. J., *Macromolecules* **1994**, *27*, 3896.
53. Krishnamoorti, R.; Graessley, W. W.; Fetters, L. J.; Garner, R. T.; Lohse, D. J., *Macromolecules* **1995**, *28*, 1252.
54. deAzevedo, E. R.; Tozoni, J. R.; Schmidt-Rohr, K.; Bonagamba, T. J. *J. Chem. Phys.* **2005**, *122*, 154506.

55. Luz, Z.; Tekely, P.; Reichert, D. *Prog. Nucl. Mag. Res. Sp.* **2002**, *41*, 83.
56. Nozue, Y.; Sakurai, T.; Hozumi, H. *Macromolecules* **2007**, *40*, 273.
57. Yamaguchi, M.; Miyata, H., *Macromolecules* **1999**, *32*, 5911.
58. Thomann, Y.; Suhm, J.; Thomann, R.; Bar, G.; Maier, R. D.; Mulhaupt, R., *Macromolecules* **1998**, *31*, 5441.
59. Wachowicz, M.; Wolak, J.; Gracz, H.; Stejskal, E. O.; Jurga, S.; White, J. L. *Macromolecules* **2004**, *37*, 4573-4579.
60. Junker, F.; Veeman, W. S. *Macromolecules* **1998**, *31*, 7010.
61. Ediger, M. D. *Ann. Rev. Phys. Chem.* **2000**, *51*, 99.
62. Vega, A.; English, A. D. *Macromolecules* **1980**, *13*, 1635.
63. Adam, G.; Gibbs, J. H. *J. Chem. Phys.* **1965**, *43*, 139.
64. Donth, E.; Huth, H.; Beiner, M. *J. Phys.: Condens. Matter* **2001**, *13*, L451.
65. Lohse, D. J., Graessley, W. M. Thermodynamics of Polyolefin Blends In *Polymer Blends: Formulation and Performance*; Paul, D. R., Bucknall, C. B., Eds.; Wiley: New York, **2000**; Vol. 1, Chapter 8, pp 219-237.
66. Zhang, X.; Wang, Z.; Han, C. C. *Macromolecules* **2006**, *39*, 7441.
67. Rissanou, A.N.; Peristera, L. D.; Economau, I. G. *Polymer* **2007**, *48*, 3883.
68. Krygier, E.; Lin, G. X.; Mendes, J.; Mukandela, G.; Azar, D.; Jones, A. A.; Pathnak, J. A.; Colby, R. H.; Kumar, S. K.; Floudas, G.; Krishnamoorti, R.; Faust, R. *Macromolecules* **2005**, *38*, 7721.
69. Wolak, J. E.; Jia, X.; Gracz, H.; Stejskal, E. O.; Wachowicz, M.; Jurga, S. J.; White, J. L. *Macromolecules* **2003**, *36*, 4844.
70. Roland, C. M.; Casalini, R. *Macromolecules* **2007**, *40*, 3631.
71. Cangialosi, D.; Alegria, A.; Colmonero, J. *Macromolecules* **2006**, *39*, 7149.
72. Wolak, J. E.; Jia, X.; White, J. L. *J. Am. Chem. Soc.* **2003**, *125*, 13660.
73. Wachowicz, M.; White, J. L., *Macromolecules* **2007**, *40*, 5433.
74. Wachowicz, M.; Gill, L.; Wolak, J. E.; White, J. L. *Macromolecules* **2008**, *41*, 2832.
75. deAzevedo, E.; Hu, W. G.; Bonagamba, T. J.; Schmidt-Rohr, K. *J. Chem. Phys.* **2000**, *112*, 8988.

76. Saalwachter, K.; Schmidt-Rohr, K. *J. Magn. Reson.* **2000**, *145*, 161-172.
77. Vanderhart, D. L.; Earl, W. L.; Garroway, A. N. *J. Magn. Reson.* **1981**, *44*, 361.
78. Schaefer, J.; Stejskal, E. O.; Buchdahl, R. *Macromolecules* **1977**, *10*, 384.
79. Torchia, D. A. *J. Magn. Reson.* **1978**, *30*, 618.
80. Gullion, T.; Baker, D. B.; Conradi, M. S. *J. Magn. Reson.* **1990**, *89*, 479.
81. Richert, R. *J. Phys. Condens. Matter*, **2002**, *14*, R703.
82. Cangialosi, D.; Colmonero, J. *Phys. Rev. E*, **2009**, *80*, 041505.
83. Lodge, T. P.; Wood, E. R.; Haley, J. C. *J. Polym. Sci. B, Polym. Phys.* **2006**, *44*, 756.
84. Gaikwad, A. N.; Wood, E. R.; Ngai, T.; Lodge, T. P. *Macromolecules*, **2008**, *41*, 2502.
85. W. Paul. and G. D. Smith, *Rep. Prog. Phys.* **2004**, *67*, 1117.
86. Ediger, M. D. *Annu. Rev. Phys. Chem.* **2000**, *51*, 99-128.
87. Lodge, T. P.; McLeish, T. C. B. *Macromolecules*, **2000**, *33*, 5278.
88. Liu, W.; Bedrov, D.; Kumar, S. K.; Veytsman, B.; Colby, R. H. *Phys. Rev. Lett.* **2009**, *103*, 037801.
89. Milner, S. T.; McLeish, T. C. B. *Phys. Rev. Lett.* **1998**, *81*, 725.
90. Kumar, S. K.; Shenogin, S.; Colby, R. H. *Macromolecules* **2007**, *40*, 5759.
91. Haley, J. C.; Lodge, T. P. *Coll. Polym. Sci.* **2004**, *82*, 793.
92. Painter P.; Coleman, M. *Macromolecules*, **2009**, *42*, 820.
93. Colmenero J.; Arbe, A. *Soft Matter* **2007**, *3*, 1474.
94. Wolak, J. E.; Jia, X.; White, J. L. *J. Am. Chem. Soc.* **2003**, *125*, 13660.
95. Wachowicz, M.; White, J. L. *Macromolecules* **2007**, *40*, 5433.
96. Wachowicz, M.; Wolak, J. E.; Gill, L.; White, J. L. *Macromolecules* **2008**, *41*, 2832.
97. Wachowicz, M.; Gill, L.; White, J. L. *Macromolecules*, **2009**, *42*, 553.
98. deAzevedo, E.; Hu, W. G.; Bonagamba, T. J.; Schmidt-Rohr, K. *J. Am. Chem. Soc.* **1999**, *121*, 8411-8412.

99. deAzevedo, E.; Hu, W. G.; Bonagamba, T. J.; Schmidt-Rohr, K. *J. Chem. Phys.* **2000**, *112*, 8988-9001.
100. Hefner, S.; Mirau, P. A. *Macromolecules*, **1994**, *27*, 7283.
101. Roovers, J.; Toporowski, P. M. *Macromolecules*, **1992**, *25*, 1096.
102. Roovers, J.; Toporowski, P. M. *Macromolecules*, **1992**, *25*, 3454.
103. Alegria, A.; Colmonero, J.; Ngai, K. L.; Roland, C. M. *Macromolecules*, **1994**, *27*, 4486.
104. Haley, J. C.; Lodge, T. P. *J. Rheology* **2005**, *49*, 1277.
105. Min, B.; Qiu, X.; Ediger, M. D.; Pitsikalis, M.; Hadjichristidis, N. *Macromolecules*, **2001**, *34*, 4466.
106. Cangialosi, D.; Alegria, A.; Colmonero, J. *Macromolecules*, **2006**, *39*, 7149.
107. Sakaguchi, T.; Taniguchi, N.; Urakawa, O.; Adachi, K. *Macromolecules*, **2005**, *38*, 422.
108. Haley, J. C.; Lodge, T. P.; He, Y.; Ediger, M. D.; von Meerwall, E. D.; Mijovic, J. *Macromolecules*, **2003**, *36*, 6142.
109. Kamath, S.; Colby, R. H.; Kumar, S. K.; Karastos, K.; Floudas, G.; Fytas, G.; Roovers, J. L. *J. Chem. Phys.* **1999**, *111*, 6121.
110. Trask, C. A.; Roland, C. M. *Macromolecules*, **1989**, *22*, 256.
111. Bahani, M.; Laupretre, F.; Monnerie, L.; *J. Polym. Sci. B, Polym. Phys.* **1995**, *33*, 167.
112. Colby, R. H.; Lipson, J. E. G. *Macromolecules*, **2005**, *38*, 4919.
113. Ambler, M. R. *J. Appl. Polym. Sci.* **2008**, *109*, 2029.
114. Chung, G. C.; Kornfield, J. A.; Smith, S. D. *Macromolecules* **1994**, *27*, 964.
115. Chung, G. C.; Kornfield, J. A.; Smith, S. D. *Macromolecules* **1994**, *27*, 5729.
116. Saxena, S.; Cizmeciyan, D.; Kornfield, J. A. *Solid State Nuclear Magnetic Resonance* **1998**, *12*, 165.
117. Fetters, L. J.; Lohse, D. J.; Colby, R. H. in “*Physical Properties of Polymers Handbook*”, J. E. Mark, Editor, **2007**, p. 447, Springer, New York, NY.
118. deAzevedo, E. R.; Tozoni, J. R.; Schmidt-Rohr, K.; Bonagamba, T. J. *J. Chem. Phys.* **2005**, *122*, 154506.
119. Rothwell, W. P.; Waugh, J. S. *J. Chem. Phys.* **1981**, *74*, 2721-2732.

120. Kaufmann, S.; Wefing, S.; Schaefer, D.; Spiess, H. W. *Journal of Chemical Physics* **1990**, 93, (1), 197-214.
121. Rubenstein, M.; Colby, R. H. *Polymer Physics* **2003**, Oxford University Press, New York, NY.

APPENDICES

A.1 CODEX Pulse Sequence

;1.7) Program: RIDER (Relaxation-Induced Dipolar Exchange with Recoupling)

;Description: Selects C bonded to N (and slowly rotating segments)

;Requires: !!; Same pulse sequence as CODEX; in contrast to SPIDER, only 1H-13C double-res. ;equipment is needed; but slow dynamics will produce artifacts.

;Reference(s): Saalwachter & KSR, J. Magn. Reson. 145, 161-172 (2000).

;srcodex.toss

;from srcodex.ksr (no TOSS)

;from srcodex.ksr on SGI with modifications

;centerband-only detection of exchange

;Detlef's phase cycle put in (from ercodexmh.ksr, dated 5-24-2000)

;with multiple power levels on 13C (p11/p111) and 1H (p12/p112/p122)

;1H at p122 during 13C 180 pulses

define delay cd15mp1

define delay cd15m1h

define delay cd15mp2

"l20=aq/(p8*2)" ;loop for tppm dec

"d15=0.25s/l31-2u" .

"cd15mp1=0.25s/l31-p1-2u"

"cd15m1h=0.25s/l31-p1-p1/2-2u"

"cd15mp2=0.25s/l31-p2-2u"

"d30=p3+d19+p15-p1-2u" ;rotor synch.delay in tm

"d25=(1s/l31)*0.1226-(p2/2)-2u-3u"

"d26=(1s/l31)*0.0773-p2" ;too short for power level switch

"d27=(1s/l31)*0.2236-p2-6u"

"d28=(1s/l31)*1.0433-p2-6u"

"d29=(1s/l31)*0.7744-(p2/2)-3u-d13"

"l3=ns/l0"

;-----

1 ze

2 10m rf #0

3 d1 do:f2 ;recycle delay, turn the decoupler off

10u pl1:f1 ;preselect pl1 drive power level for F1

10u pl2:f2 ;preselect pl2 drive power for F2

1u:f2 ph1

1u:f1 ph2

rpp5 ;reset phase lists for xy-8

1u trigpe1 ;record rotor phase

p3:f2 ph1 ;proton 90 pulse

d19 ;allow time for the phase shift on F2

(p15 ph2):f1 (p15 ph17):f2 ;contact pulse

1u cw:f2 ;turn on F2 decoupling

1u pl12:f2 ;set decoupling drive power level

cd15mp1 pl11:f1 ;tr/4

d15:f1 ph5 ;tr/4

2u pl22:f2 ;high 1H power during 13C pulse

p2:f1 ph5^ ;13C 180 deg. pulse

2u pl12:f2

d15

4 cd15mp2:f1 ph5

2u pl22:f2 ;high 1H power during 13C pulse

p2:f1 ph5^ ;13C 180 deg. pulse

2u pl12:f2

d15

lo to 4 times l1 ;an even number

cd15m1h pl1:f1 ;tr/4

2u pl22:f2 ;high 1H power during 13C pulse

p1:f1 ph8 ;first mixing time

d6 do:f2

1u trigpe1 ;same phase as above

d30:f1 ph9

2u cw:f2 pl22:f2

p1:f1 ph9

2u pl12:f2

cd15m1h pl11:f1 ;tr/4

5 d15:f1 ph5

2u pl22:f2 ;high 1H power during 13C pulse

p2:f1 ph5^ ;13C 180 deg. pulse

```

2u pl12:f2
cd15mp2
lo to 5 times l1      ;an even number
d15:f1 ph5            ;tr/4
2u pl22:f2            ;high 1H power during 13C pulse
p2:f1 ph5^            ;13C 180 deg. pulse
2u pl12:f2
d15
cd15mp1 pl1:f1        ;tr/4
2u pl22:f2
p1:f1 ph3             ; second z-filter
d16 do:f2
1u trigpe1            ;same phase as above
d30:f1 ph4
2u cw:f2 pl12:f2
p1:f1 ph4
2u:f1 ph0             ;dead time delay, reset RF phase to detect
gosc ph31             ;do NS scans
10u do:f2             ;turn decoupler off
10m id18
lo to 3 times l0
30m wr #0 if #0

=====

13 d1 do:f2           ;recycle delay, turn the decoupler off
10u pl1:f1            ;preselect pl1 drive power level for F1
10u pl2:f2            ;preselect pl2 drive power for F2
1u:f2 ph1
1u:f1 ph2

```



```

rpp5                      ;reset phase lists for xy-8
1u trigpe1                ;record rotor phase

p3:f2 ph1                 ;proton 90 pulse
d19                       ;allow time for the phase shift on F2
(p15 ph2):f1 (p15 ph17):f2 ;contact pulse

1u cw:f2                  ;turn on F2 decoupling
1u pl12:f2                ;set decoupling drive power level
cd15mp1 pl11:f1           ;tr/4
d15:f1 ph5                ;tr/4
2u pl22:f2                ;high 1H power during 13C pulse
p2:f1 ph5^                ;13C 180 deg. pulse
2u pl12:f2
d15

14 cd15mp2:f1 ph5
2u pl22:f2                ;high 1H power during 13C pulse
p2:f1 ph5^                ;13C 180 deg. pulse
2u pl12:f2
d15

lo to 14 times l1         ;an even number
cd15m1h pl1:f1           ;tr/4
2u pl22:f2                ;high 1H power during 13C pulse
p1:f1 ph8                 ;first mixing time
d7 do:f2
1u trigpe1                ;same phase as above
d30:f1 ph9
2u cw:f2 pl22:f2

```

```

p1:f1 ph9
2u pl12:f2
cd15m1h pl11:f1 ;tr/4
15 d15:f1 ph5
2u pl22:f2 ;high 1H power during 13C pulse
p2:f1 ph5^ ;13C 180 deg. pulse
2u pl12:f2
cd15mp2
lo to 15 times l1 ;an even number
d15:f1 ph5 ;tr/4
2u pl22:f2 ;high 1H power during 13C pulse
p2:f1 ph5^ ;13C 180 deg. pulse
2u pl12:f2
d15
cd15mp1 pl1:f1 ;tr/4
2u pl22:f2
p1:f1 ph3 ; second z-filter
d17 do:f2
1u trigpe1 ;same phase as above
d30:f1 ph4
2u cw:f2 pl12:f2
p1:f1 ph4

2u:f1 ph0 ;dead time delay, reset RF phase to detect
gosc ph3 l ;do NS scans
10u do:f2 ;turn decoupler off
10m id18
lo to 13 times l0
30m wr #0 rf #0 zd

```

10m

lo to 2 times l3

exit

ph0= 0 ;reference phase for detection

ph1= 0 2 ;1H 90 excitation

ph2= 0 0 1 1 2 2 3 3 ;13C CP

ph3= 3 3 0 0 1 1 2 2

ph4= 1 1 2 2 3 3 0 0 ;readout after 2nd z period

ph5= 0 1 0 1 1 0 1 0 ;xy-8

ph8= 3 3 0 0 1 1 2 2

3 3 0 0 1 1 2 2

2 2 3 3 0 0 1 1

2 2 3 3 0 0 1 1

1 1 2 2 3 3 0 0

1 1 2 2 3 3 0 0

0 0 1 1 2 2 3 3

0 0 1 1 2 2 3 3

ph9= 1 1 2 2 3 3 0 0

3 3 0 0 1 1 2 2

0 0 1 1 2 2 3 3

2 2 3 3 0 0 1 1

ph13= (360) 10

ph14= (360) 0

ph17= 1 ;1H CP

ph23= 1 1 2 2 3 3 0 0 ;180 13C #1 TOSS

ph24= 3 3 0 0 1 1 2 2 ;180 13C #2

ph25= 1 1 2 2 3 3 0 0 ;180 13C #3

3 3 0 0 1 1 2 2

ph26= 2 2 1 1 0 0 3 3 ;180 13C #4

0 0 3 3 2 2 1 1

ph31= 0 2 1 3 2 0 3 1 ;receiver phase

2 0 3 1 0 2 1 3

0 2 1 3 2 0 3 1

2 0 3 1 0 2 1 3

2 0 3 1 0 2 1 3

0 2 1 3 2 0 3 1

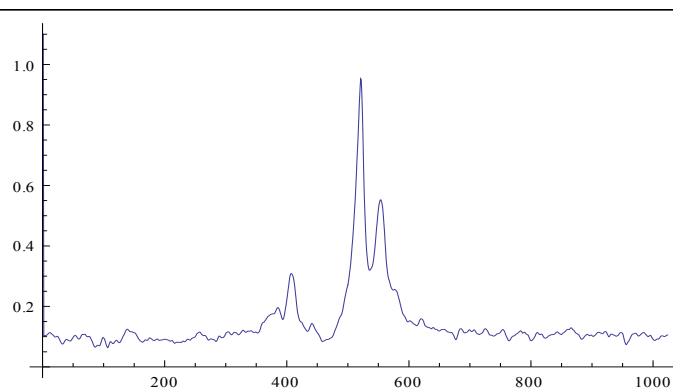
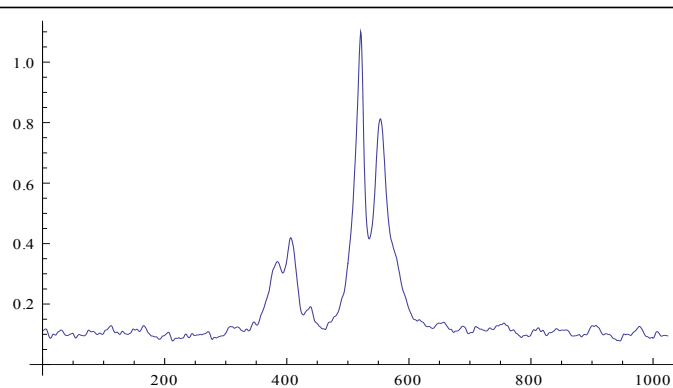
2 0 3 1 0 2 1 3

0 2 1 3 2 0 3 1

A.2 Example of Mathematica Deconvolution for Exchange Points in E(T)

```
Off[General::"spell1"];
filenameS0X: "aPP_274S0_5msX.txt";
filenameS0Y: "aPP_274S0_75msY.txt";
filenameSX: "aPP_274S0_5msX.txt";
filenameSY: "aPP_274S0_75msY.txt";
Clear[dataS0XY];
dataS0X: ReadList[filenameS0X];
dataS0Y: {Table[ReadList[filenameS0Y], {0.1}];
dataS0XY: {};
dataS0XY: Insert[dataS0XY, dataS0X, 1];
dataS0XY: Insert[dataS0XY, dataS0Y, 2];
Transpose[dataS0XY];
ListPlot[dataS0XY, Joined: True, PlotRange: All, AxesOrigin: {0, 0}];
Clear[dataSXY];
dataSX: ReadList[filenameSX];
dataSY: {Table[ReadList[filenameSY], {0.1}];
dataSXY: {};
dataSXY: Insert[dataSXY, dataSX, 1];
dataSXY: Insert[dataSXY, dataSY, 2];
Transpose[dataSXY];
ListPlot[dataSXY, Joined: True, PlotRange: All, AxesOrigin: {0, 0}]
```

Import spectral data as text files



```

A1 : 90; | 1 : 300; xc1 : 3640;
A2 : 59; | 2 : 165; xc2 : 3350;
A3 : 27; | 3 : 250; xc3 : 3020;
A4 : 211; | 4 : 350; xc4 : 2080;
A5 : 67; | 5 : 100; xc5 : 2022.7;
A6 : 123; | 6 : 190; xc6 : 1655;
A7 : 147; | 7 : 415; xc7 : 1440;

```

Input deconvolution curve data for reference spectra. A is area of each Gaussian curve, w is the width of each curve, and xc is the center of the fit curve in Hz.

$$G1 : \frac{A1}{\sqrt{2\pi}} e^{-\frac{(x-xc1)^2}{2 \cdot 300^2}}; G2 : \frac{A2}{\sqrt{2\pi}} e^{-\frac{(x-xc2)^2}{2 \cdot 165^2}}; G3 : \frac{A3}{\sqrt{2\pi}} e^{-\frac{(x-xc3)^2}{2 \cdot 250^2}}; G4 : \frac{A4}{\sqrt{2\pi}} e^{-\frac{(x-xc4)^2}{2 \cdot 350^2}};$$

$$G5 : \frac{A5}{\sqrt{2\pi}} e^{-\frac{(x-xc5)^2}{2 \cdot 100^2}}; G6 : \frac{A6}{\sqrt{2\pi}} e^{-\frac{(x-xc6)^2}{2 \cdot 190^2}};$$

$$G7 : \frac{A7}{\sqrt{2\pi}} e^{-\frac{(x-xc7)^2}{2 \cdot 415^2}}; G8 : \frac{A8}{\sqrt{2\pi}} e^{-\frac{(x-xc8)^2}{2 \cdot 18^2}}; G9 : \frac{A9}{\sqrt{2\pi}} e^{-\frac{(x-xc9)^2}{2 \cdot 9^2}}; G10 : \frac{A10}{\sqrt{2\pi}} e^{-\frac{(x-xc10)^2}{2 \cdot 10^2}};$$

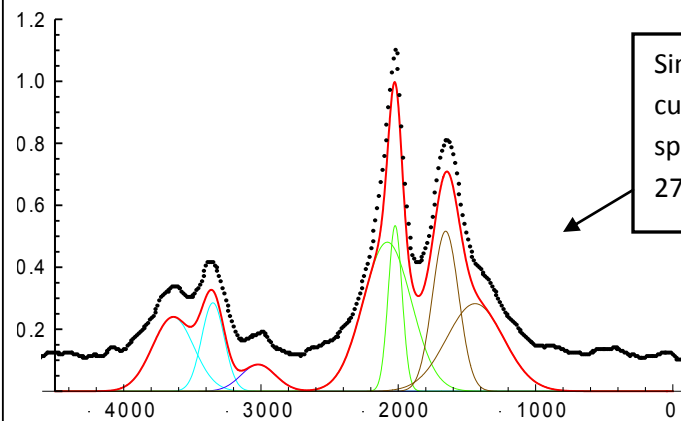
$$G11 : \frac{A11}{\sqrt{2\pi}} e^{-\frac{(x-xc11)^2}{2 \cdot 11^2}};$$

Gaussian curve equation

```

Gtot = G1 + G2 + G3 + G4 + G5 + G6 + G7;
Plot[ { G1, G2, G3, G4, G5, G6, G7, Gtot }, { x, 4500, 0 }, PlotRange -> { 0, 1.2 },
  AxesOrigin -> { 4500, 0 },
  PlotStyle -> { Hue[ 0.5 ], Hue[ 0.5 ], Hue[ 0.7 ], Hue[ 0.29 ], Hue[ 0.29 ],
    BColor[ 5, 0, 0 ], RGB[ 100, 0, 0.31 ],
    RGBColor[ 0, 0, 0 ], Thickne[ 0.003 ] },
  AxesStyle -> { GBCol[ 0, 0, 0 ], Thickness[ 0.003 ],
  BaseStyle -> { FontFamily[ "Arial", FontSize[ 12 ],
  Epilog -> Prepend[ Point[ Transpose[ dataS0XY ], PointSize[ 0.00681 ] ] ]

```



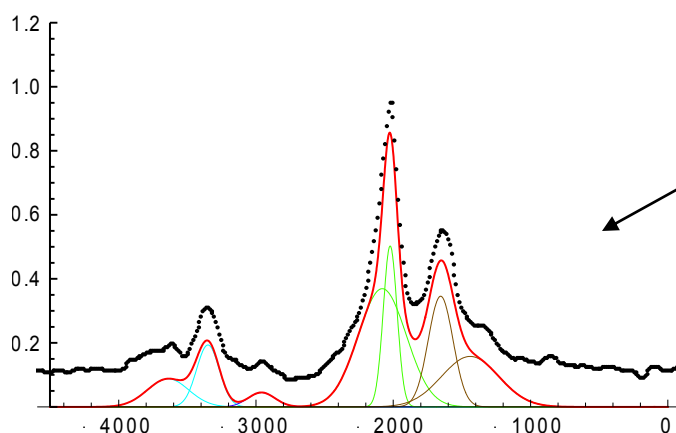
Simulated fit, individual fit curves and reference spectrum (So) for aPp at 274K

A1S : 33; | **1S** : 300; **xc1S** : 3640;
A2S : 40; | **2S** : 165; **xc2S** : 3350;
A3S : 11; | **3S** : 195; **xc3S** : 2960;
A4S : 162; | **4S** : 350; **xc4S** : 2080;
A5S : 63; | **5S** : 100; **xc5S** : 2022.7;
A6S : 78; | **6S** : 180; **xc6S** : 1655;
A7S : 82; | **7S** : 415; **xc7S** : 1440;

This the CODEX spectrum
 information and it is handled in
 the same way as for the reference
 on the previous page

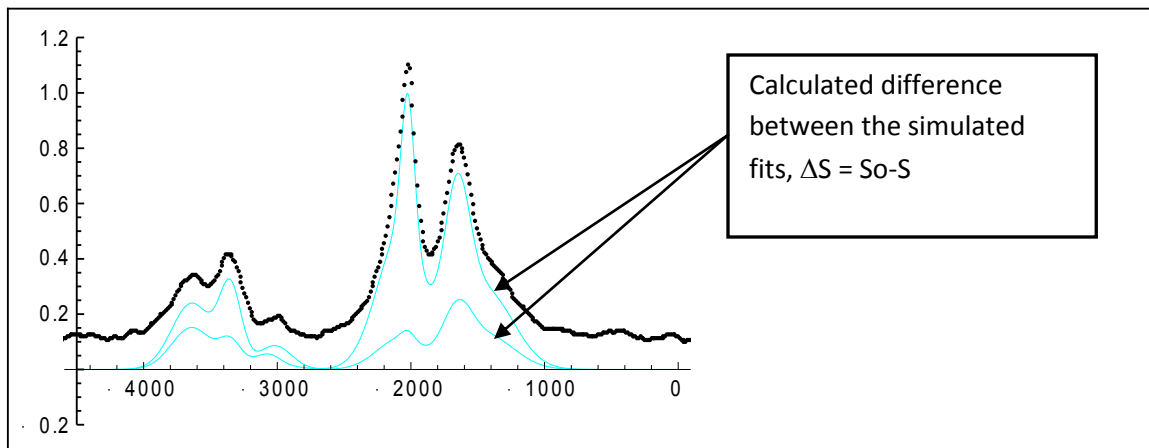
$$\begin{aligned}
 G1S &: \frac{A1S \cdot \left| \frac{x - xc1S}{1S} \right|^2}{1S \sqrt{\frac{1}{2}}} ; G2S : \frac{A2S \cdot \left| \frac{x - xc2S}{2S} \right|^2}{2S \sqrt{\frac{1}{2}}} ; G3S : \frac{A3S \cdot \left| \frac{x - xc3S}{3S} \right|^2}{3S \sqrt{\frac{1}{2}}} ; G4S : \frac{A4S \cdot \left| \frac{x - xc4S}{4S} \right|^2}{4S \sqrt{\frac{1}{2}}} ; \\
 G5S &: \frac{A5S \cdot \left| \frac{x - xc5S}{5S} \right|^2}{5S \sqrt{\frac{1}{2}}} ; G6S : \frac{A6S \cdot \left| \frac{x - xc6S}{6S} \right|^2}{6S \sqrt{\frac{1}{2}}} ; \\
 G7S &: \frac{A7S \cdot \left| \frac{x - xc7S}{7S} \right|^2}{7S \sqrt{\frac{1}{2}}} ; G8S : \frac{A8S \cdot \left| \frac{x - xc8S}{8S} \right|^2}{8S \sqrt{\frac{1}{2}}} ; G9S : \frac{A9S \cdot \left| \frac{x - xc9S}{9S} \right|^2}{9S \sqrt{\frac{1}{2}}} ; \\
 G10S &: \frac{A10S \cdot \left| \frac{x - xc10S}{10S} \right|^2}{10S \sqrt{\frac{1}{2}}} ; G11S : \frac{A11S \cdot \left| \frac{x - xc11S}{11S} \right|^2}{11S \sqrt{\frac{1}{2}}} ;
 \end{aligned}$$



Gtot : **G1S** + **G2S** + **G3S** + **G4S** + **G5S** + **G6S** + **G7S**;
Plot [**G1S**, **G2S** , **3S**, **G4S** , **G5S**, **G6S**, **G7S**, **Gtotals**] , [**x**, 4500, 0] , **PlotRange** [0, 1.2] ,
AxesOrigin 45 , 0
PlotStyle [Hue 0.5] , Hue 0.5 [Hue 0.7] , Hue 0.29 [Hue 0.29] ,
BColor 5 , 0 , 0 , **RGB** 100 0 0.31 , 0 ,
RGBColor 0, 0, 0 , **Thickne** 0.003
AxesStyle **GBColor** 0, 0, 0 , **Thickness** 0.003 ,
BaseStyle [**Fon** amily "Arial", **ntSize** 12] ,
Epilog **Prepend** **Point** [**Transpose** **dataSXY** , **PointSize** 0.00681]





Simulated fit, individual fit
 curves and CODEX
 spectrum (S) for aPP at
 274K

```
Gdiff Gtotal Gtot
Plot[ Gdiff, ta, {t, 0, 100}], t, {t, 0, 100}], a, {a, 0, 100}],
Plot[ St, e, {t, 0, 100}], {t, 0, 100}], {t, 0, 100}], {t, 0, 100}],
{Hue[ 0.2], Hue[ 0.29], RGBColor[ 0.5, 0.31, 0], RGBColor[ 0.5, 0.31, 0],
BColor[ 1, 0, 0.3], RColor[ 0.5, 0.3],
{RGBColor[ 0, 0, 0], Thickness[ 0.003]}]
AxesStyle[ RGBColor[ 0, 0, 0], Thickness[ 0.003],
BaseStyle[ FontFamily[ "Arial", FontSize[ 12],
Epilog[ Prepend[ Point[ Transpose[ dataS0XY], PointSize[ 0.00681]]]]
```



GaPPCH2 : G1 : G2 ;
 GaPPCH2S : G1S : G2S ; (: methylene group of aPP)
 AREAaPPCH2 :  GaPPCH2 ; AREAaPPCH2S :  GaPPCH2S ;
 x1 : 4500 x2 : 4500
 EaPPCH2 :
$$\frac{\text{AREAaPPCH2} \cdot \text{AREAaPPCH2S}}{\text{AREAaPPCH2}} ;$$

 N | |
 GaPPCH3 : G6 : G7 ; GaPPCH3S : G6S : G7S ; (: methyl group of aPP)
 AREAaPPCH3 :  GaPPCH3 ; AREAaPPCH3S :  GaPPCH3S ;
 x1 : 4500 x2 : 4500
 EaPPCH3 :
$$\frac{\text{AREAaPPCH3} \cdot \text{AREAaPPCH3S}}{\text{AREAaPPCH3}} ;$$

 N | |
 Null

Calculation for the
normalized exchange,
 $E(T) = S_o - S / S_o$

0.510067

0.407407

A.3 Example Mathematica Notebook (Arrhenius/log-Gaussian Distribution).

```

Nee | "LinearAlgebr MatrixManipulation`|
Off G al::spell1|;
Clear| ;

```

"Starting parameters"

```

filename "PI_CH3only_9_omega_distr_temp_T.txt";

```

```

number "1"; number "2"; number "3"; number 4 " "; number 5 : 5 number 6 : " "; number 7 : "7";
number "8"; number 9 " "; number 10 " "; number 11 " "; number 12 " "; number 13 " ";
number 4 "14"; number 15 : "15"; number 16 : "16"; number 17 : "17"; number 18 : "18"; number 19 : "19";
number 20 : "20";

```

```

R: 4000.2; powder:  $\frac{1}{8}$ ;
L: 75.47 106 2;

```

```

R: 8.314; KWW: 1; TC: 194.0; Ea: 301335; 0: 5.49 10-76; d: 0 Exp $\left(-\frac{a}{R \cdot 214}\right)$ 

```

```

T: 2; factor: 1.0;
n: 20; pi:  $\frac{180 \text{ Degree}}{n}$ ; p:  $\frac{\pi}{n}$ ; tm: 0.2; tz: 0.001; CSA: 0.0017778; t: 0.33333333 CSA;
m1: {1 1 1 1 1 1 1 1 1 1 1 1 1 1 1 1 1 1 1 1}; m1T: Transpose m1;

```

```

d1: 0.002155; d2: 0.004644; d3: 0.01; d4: 0.021552; d5: 0.04643; d6: 0.10002; d7: 0.21547; d8: 0.46419;
d9: 1; d10: 2.154269; d11: 4.64087; d12: 9.99769; d13: 21.53772; d14: 43.39804; d15: 99.95386;
d16: 215.3275;
d17: 463.87338;

```

Starting parameters

0.0196887

This notebook creates an export of the fit curve that has no σ applied to the distribution. This text file can then be imported into A.4 for applying a slope to the distribution.

Activation Energy (Ea) changes in this value increase the height of the fit curve

Changes in the τ_0 value move the fit curve left or right

Mixing time (t_m) and reference time (t_z) in sec

More description of this part of the notebook is necessary on the next page.

```

Nee | "LinearAlgebr MatrixManipulation`|
Off G al::spell1|;
Clear| ;

```

"Starting parameters"

filename: "PI_CH3only_9_omega_distr_temp_T.txt"; | FILE to EXPORT |

number "1"; number "2"; number "3"; number 4 " "; number 5 : 5 number 6 : " "; number 7 : "7";
number "8"; number 9 " "; number 10 " "; number 11 " "; number 12 " "; number 13 " ";
number 4 "14"; number 15 : "15"; number 16 : "16"; number 17 : "17"; number 18 : "18"; number 19 : "19";
number 20 : "20";

R: 4000 2; powder: $\frac{1}{8}$;
L: 75.47 10⁶ 2;

R: 8.314; KWW: 1; TC: 194.0; Pa: 301335; 0: 5.49 10⁻⁷⁶; d: 0 Exp $\left(\frac{a}{R \cdot 214}\right)$
T: 2; factor: 1.0;
n: 20; pi: $\frac{180 \text{ Degree}}{\pi}$; p: —; tm: 0.2; tz: 0.001; CSA: 0.0017778; t
m1: 1 1 1 Recoupling period (τ_{CSA}) in sec Transpose m1;

d1: 0.002155; d2: 0.004644; d3: 0.01; d4: 0.021552; d5: 0.04643; d6: 0.10002; d7: 0.21547; d8: 0.46419;
d9: 1; d10: 2.154269; d11: 4.64087; d12: 9.99769; d13: 21.53772; d14: 43.39804; d15: 99.95386;
d16: 215.3275;
d17: 463.87338;

Starting parameters

0.0196887

Number of temperature points (n) and the temperature interval (ΔT) for applying the distribution curves. The combination here will span 40°C starting at TC (194K here).

Temperature of experimental exchange maximum (214K) for PI

Points for the distribution d1-d17 applied to τ_d in the distribution dependent Arrhenius equation.

Anything not described here in the first portion of the Arrhenius distribution notebook is a fixed value that feeds into the powder averaging portion.

```

tau[p_] := (
  d1 := 0 d1 Exp[-(Ea/(R TC + p T))]; d2 := 0 d2 Exp[-(Ea/(R TC + p T))]; d3 := 0 d3 Exp[-(Ea/(R TC + p T))];
  d4 := 0 d4 Exp[-(Ea/(R TC + p T))]; d5 := 0 d5 Exp[-(Ea/(R TC + p T))]; d6 := 0 d6 Exp[-(Ea/(R TC + p T))];
  d7 := 0 d7 Exp[-(Ea/(R TC + p T))]; d8 := 0 d8 Exp[-(Ea/(R TC + p T))]; d9 := 0 d9 Exp[-(Ea/(R TC + p T))];
  d10 := 0 d10 Exp[-(Ea/(R TC + p T))]; d11 := 0 d11 Exp[-(Ea/(R TC + p T))]; d12 := 0 d12 Exp[-(Ea/(R TC + p T))];
  d13 := 0 d13 Exp[-(Ea/(R TC + p T))]; d14 := 0 d14 Exp[-(Ea/(R TC + p T))]; d15 := 0 d15 Exp[-(Ea/(R TC + p T))];
  d16 := 0 d16 Exp[-(Ea/(R TC + p T))]; d17 := 0 d17 Exp[-(Ea/(R TC + p T))];
)

```

```

Exchanged1d17 := (
  max1 = 20;
  For[m = 1, m = maxm, m++, begin of "m loop"
    difd1[m, m] := (1/(p^2 3 d1)) Cos[1/2] ; difd1[m, m - 1] := (1/(p^2 6 d1)) Sin[1/2] ;
    difd1[m - 1, m] := (1/(p^2 6 d1)) Sin[1/2] ;
    difd2[m, m] := (1/(p^2 3 d2)) Cos[1/2] ; difd2[m, m - 1] := (1/(p^2 6 d2)) Sin[1/2] ;
    difd2[m - 1, m] := (1/(p^2 6 d2)) Sin[1/2] ;
    difd3[m, m] := (1/(p^2 3 d3)) Cos[1/2] ; difd3[m, m - 1] := (1/(p^2 6 d3)) Sin[1/2] ;
    difd3[m - 1, m] := (1/(p^2 6 d3)) Sin[1/2] ;
    difd4[m, m] := (1/(p^2 3 d4)) Cos[1/2] ; difd4[m, m - 1] := (1/(p^2 6 d4)) Sin[1/2] ;
    difd4[m - 1, m] := (1/(p^2 6 d4)) Sin[1/2] ;
    difd5[m, m] := (1/(p^2 3 d5)) Cos[1/2] ; difd5[m, m - 1] := (1/(p^2 6 d5)) Sin[1/2] ;
    difd5[m - 1, m] := (1/(p^2 6 d5)) Sin[1/2] ;
    difd6[m, m] := (1/(p^2 3 d6)) Cos[1/2] ; difd6[m, m - 1] := (1/(p^2 6 d6)) Sin[1/2] ;
  ]
)

```

This is the incomplete input of the second portion of the Mathematica directly following the previous page. Here maxm is typically equal to 20. Continued on the next page from the last distribution point (d6).

The continuation of the previous page and starting with the m+1 of d6.

```

| difd6| m, 1, m| :  $\frac{1}{|p^2_6| d6} \frac{\cos\left(\frac{|m|}{2}\right)}{\sin\left(\frac{|m|}{0.5}\right)} ;$ 
| difd7| m, m| :  $\left(\frac{1}{|p^2_3| d7}\right) \cos\left(\frac{|m|}{2}\right) ;$  | difd7| m, m, 1| :  $\frac{1}{|p^2_6| d7} \frac{\cos\left(\frac{|m|}{2}\right)}{\sin\left(\frac{|m|}{0.5}\right)} ;$ 
| difd7| m, 1, m| :  $\frac{1}{|p^2_6| d7} \frac{\cos\left(\frac{|m|}{2}\right)}{\sin\left(\frac{|m|}{0.5}\right)} ;$ 
| difd8| m, m| :  $\left(\frac{1}{|p^2_3| d8}\right) \cos\left(\frac{|m|}{2}\right) ;$  | difd8| m, m, 1| :  $\frac{1}{|p^2_6| d8} \frac{\cos\left(\frac{|m|}{2}\right)}{\sin\left(\frac{|m|}{0.5}\right)} ;$ 
| difd8| m, 1, m| :  $\frac{1}{|p^2_6| d8} \frac{\cos\left(\frac{|m|}{2}\right)}{\sin\left(\frac{|m|}{0.5}\right)} ;$ 
| difd9| m, m| :  $\left(\frac{1}{|p^2_3| d9}\right) \cos\left(\frac{|m|}{2}\right) ;$  | difd9| m, m, 1| :  $\frac{1}{|p^2_6| d9} \frac{\cos\left(\frac{|m|}{2}\right)}{\sin\left(\frac{|m|}{0.5}\right)} ;$ 
| difd9| m, 1, m| :  $\frac{1}{|p^2_6| d9} \frac{\cos\left(\frac{|m|}{2}\right)}{\sin\left(\frac{|m|}{0.5}\right)} ;$ 
| difd10| m, m| :  $\left(\frac{1}{|p^2_3| d10}\right) \cos\left(\frac{|m|}{2}\right) ;$  | difd10| m, m, 1| :  $\frac{1}{|p^2_6| d10} \frac{\cos\left(\frac{|m|}{2}\right)}{\sin\left(\frac{|m|}{0.5}\right)} ;$ 
| difd10| m, 1, m| :  $\frac{1}{|p^2_6| d10} \frac{\cos\left(\frac{|m|}{2}\right)}{\sin\left(\frac{|m|}{0.5}\right)} ;$ 
| difd11| m, m| :  $\left(\frac{1}{|p^2_3| d11}\right) \cos\left(\frac{|m|}{2}\right) ;$  | difd11| m, m, 1| :  $\frac{1}{|p^2_6| d11} \frac{\cos\left(\frac{|m|}{2}\right)}{\sin\left(\frac{|m|}{0.5}\right)} ;$ 
| difd11| m, 1, m| :  $\frac{1}{|p^2_6| d11} \frac{\cos\left(\frac{|m|}{2}\right)}{\sin\left(\frac{|m|}{0.5}\right)} ;$ 
| difd12| m, m| :  $\left(\frac{1}{|p^2_3| d12}\right) \cos\left(\frac{|m|}{2}\right) ;$  | difd12| m, m, 1| :  $\frac{1}{|p^2_6| d12} \frac{\cos\left(\frac{|m|}{2}\right)}{\sin\left(\frac{|m|}{0.5}\right)} ;$ 
| difd12| m, 1, m| :  $\frac{1}{|p^2_6| d12} \frac{\cos\left(\frac{|m|}{2}\right)}{\sin\left(\frac{|m|}{0.5}\right)} ;$ 
| difd13| m, m| :  $\left(\frac{1}{|p^2_3| d13}\right) \cos\left(\frac{|m|}{2}\right) ;$  | difd13| m, m, 1| :  $\frac{1}{|p^2_6| d13} \frac{\cos\left(\frac{|m|}{2}\right)}{\sin\left(\frac{|m|}{0.5}\right)} ;$ 
| difd13| m, 1, m| :  $\frac{1}{|p^2_6| d13} \frac{\cos\left(\frac{|m|}{2}\right)}{\sin\left(\frac{|m|}{0.5}\right)} ;$ 
| difd14| m, m| :  $\left(\frac{1}{|p^2_3| d14}\right) \cos\left(\frac{|m|}{2}\right) ;$  | difd14| m, m, 1| :  $\frac{1}{|p^2_6| d14} \frac{\cos\left(\frac{|m|}{2}\right)}{\sin\left(\frac{|m|}{0.5}\right)} ;$ 
| difd14| m, 1, m| :  $\frac{1}{|p^2_6| d14} \frac{\cos\left(\frac{|m|}{2}\right)}{\sin\left(\frac{|m|}{0.5}\right)} ;$ 
| difd15| m, m| :  $\left(\frac{1}{|p^2_3| d15}\right) \cos\left(\frac{|m|}{2}\right) ;$  | difd15| m, m, 1| :  $\frac{1}{|p^2_6| d15} \frac{\cos\left(\frac{|m|}{2}\right)}{\sin\left(\frac{|m|}{0.5}\right)} ;$ 
| difd15| m, 1, m| :  $\frac{1}{|p^2_6| d15} \frac{\cos\left(\frac{|m|}{2}\right)}{\sin\left(\frac{|m|}{0.5}\right)} ;$ 
| difd16| m, m| :  $\left(\frac{1}{|p^2_3| d16}\right) \cos\left(\frac{|m|}{2}\right) ;$  | difd16| m, m, 1| :  $\frac{1}{|p^2_6| d16} \frac{\cos\left(\frac{|m|}{2}\right)}{\sin\left(\frac{|m|}{0.5}\right)} ;$ 
| difd16| m, 1, m| :  $\frac{1}{|p^2_6| d16} \frac{\cos\left(\frac{|m|}{2}\right)}{\sin\left(\frac{|m|}{0.5}\right)} ;$ 
| difd17| m, m| :  $\left(\frac{1}{|p^2_3| d17}\right) \cos\left(\frac{|m|}{2}\right) ;$  | difd17| m, m, 1| :  $\frac{1}{|p^2_6| d17} \frac{\cos\left(\frac{|m|}{2}\right)}{\sin\left(\frac{|m|}{0.5}\right)} ;$ 
| difd17| m, 1, m| :  $\frac{1}{|p^2_6| d17} \frac{\cos\left(\frac{|m|}{2}\right)}{\sin\left(\frac{|m|}{0.5}\right)} ;$ 
| end of "m loop" ;

Print| "Exchange matrix elements ready" ;
)

```

This marks the end of the exchange matrix loop for isotropic rotational diffusion. The powder average input begins.

The beginning of the powder averaging and point assignment for the distribution curves.

```
POWDERaverage| dstart_ :: |
| min: 18 Degree; | max: 342 Degree; | : 36 Degree;
| min: 18 Degree; | max: 342 Degree; | : 36 Degree;
| min: 9 Degree; | max: 171 Degree; | : 18 Degree;

| TridiagonalMatrix difd1, 20 | TridiagonalMatrix difd2, 20 | TridiagonalMatrix difd3, 20
| TridiagonalMatrix difd4, 20 | TridiagonalMatrix difd5, 20 | TridiagonalMatrix difd6, 20
| TridiagonalMatrix difd7, 20 | 8 | diagonalMatrix | d d8, 20 | ; | 0 | diagonalMatrix | difd8, 20 | ;
| 0 | TridiagonalMatrix difd10, 20 | .1 | TridiagonalMatrix difd11, 20 | .2 | TridiagonalMatrix difd12, 20
| 3 | TridiagonalMatrix difd13, 20 | .1 | TridiagonalMatrix difd14, 20 | .15 | TridiagonalMatrix difd15, 20
| 16 | TridiagonalMatrix difd16, 20 | ; | 17 | TridiagonalMatrix difd17, 20 ;

For | d | dstart, d | 17, d | , | begin of "d loop" |
Print "Powder averaging REFERENCE_", d ;
REFERENCE | d | :
powd
Sum
Sin | | | Sum | | Sum | | MatrixExp | | d |  $\frac{1}{2} \frac{CSA}{2}$  | |  $\frac{1}{2} \frac{CSA}{2}$  | .MatrixExp | | d | tz | .MatrixExp | | d |  $\frac{1}{2} \frac{CSA}{2}$  | |  $\frac{1}{2} \frac{CSA}{2}$  | .L,
| | , | min, | max, | | | , | | , | min, | max, | | | , | | , | min, | max, | | | ;

Print "Powder averaging CODEX_", d ;

CODEX | d | :
powd
Sum
Sin | | | Sum | | Sum | | MatrixExp | | d |  $\frac{1}{2} \frac{CSA}{2}$  | |  $\frac{1}{2} \frac{CSA}{2}$  | .MatrixExp | | d | tm | .MatrixExp | | d |  $\frac{1}{2} \frac{CSA}{2}$  | |  $\frac{1}{2} \frac{CSA}{2}$  | .L,
| | , | min, | max, | | | , | | , | min, | max, | | | , | | , | min, | max, | | | ;
| d | : Re | m1 . REFERENCE | d | . m1T | ; Gtm | d | : Re | m1 . CODEX | d | . m1T | ;
| | end of "d loop" |

pointassignm JLL :: |
Gtzd1: Gtz Gtmd1: Gtm | it will be assigned out the loop |
Gtzd2: Gtz Gtmd2: Gtm Gtzd3: Gtz Gtmd3: Gtm Gtzd4: Gtz Gtmd4: Gtm Gtzd5: Gtz
Gtmd5: Gtm Gtzd6: Gtz Gtmd6: Gtm ; Gtzd7: Gtz | 7 | ; | 17: Gtm | 7 | ; | 18: Gtz | 8 | ; Gtr | } | Gtm | 8 | ;
Gtzd9: Gtz ; Gtmd9: Gtm | 9 | ; | 10: Gtz | 10 | ; | 10: Gtm | 10 | ; | 11: Gtz | 11 | ; | 11: Gtm | 11 |
Gtzd12: Gtz | 2 | Gtmd12: Gtm | 2 | Gtzd13: Gtz | 3 | Gtmd13: Gtm | 3 | Gtzd14: Gtz | 4 | Gtmd14: Gtm | 4 |
Gtzd15: Gtz | 15 | ; Gtmd15: Gtm | 15 | ; Gtzd16: Gtz | 16 | ; Gtmd16: Gtm | 16 | ; Gtzd17: Gtz | 17 | ; Gtmd17: Gtm | 17 | ;
```

Fixed angle jumps for the powder averaging over the surface of a sphere

The next will continue the point assignments for the distribution

Continuation of the point assignments for distribution

```

point| 1| Gtzd1| 1| | points needed for EXPORT |
point , 1 Gtzd2 , 1
point , 1 Gtzd3 , 1
point , 1 Gtzd4 , 1
point , 1 Gtzd5 , 1
point , 1 Gtzd6 , 1
point , 1 Gtzd7 , 1
point , 1 Gtzd8 , 1
point , 1| Gtzd9| | | |
point 0, 1 Gtzd10 , 1
point 1, 1 Gtzd11 , 1
point 2, 1 Gtzd12 , 1
point 3, 1 Gtzd13 , 1
point 4, 1 Gtzd14 , 1
point 5, 1 Gtzd15 , 1
point 6, 1 Gtzd16 , 1
point 7, 1 Gtzd17| 1, 1| ;
point 8, 1 TT;
point 9, 1 TT;
point 0, 1 TT;
point 1, 1 Gtmd1 , 1
point 2, 1 Gtmd2 , 1
point 3, 1 Gtmd3 , 1
point 4, 1 Gtmd4 , 1
point 5, 1 Gtmd5 , 1
point 6, 1 Gtmd6 , 1
point 7, 1 Gtmd7 , 1
point 8, 1 Gtmd8 , 1
point 9, 1 Gtmd9| 1|
point 0, 1 Gtmd10 , 1
point 1, 1 Gtmd11 , 1
point 2, 1 Gtmd12 , 1
point 3, 1 Gtmd13 , 1
point 4, 1 Gtmd14 , 1
point 5, 1 Gtmd15 , 1
point 6, 1 Gtmd16 , 1
int| 37, 1| : Gtmd17| 1, 1| | ;
|

po tassignmentMINUS1 :|
| number 1 't calculat
Gtzd2 : Gtz| Gtmd2 : Gtm Gtzd3 : Gtz| Gtmd3 : Gtm Gtzd4 : Gtz| Gtmd4 : Gtm Gtzd5 : Gtz|
Gtmd5 : Gtm Gtzd6 : Gtz Gtmd6 : Gtm ; Gtzd7 : Gtz| 7| ;| 17 : Gtm| 7| ;| 8 : Gtz| 8| ; Gtz 3 Gtm| 8| ;
Gtzd9 : Gtz| ; Gmd9 : Gtm| 9| ;| 110 : Gtz| 10| ;| 110 : Gtm| 10| ;| 111 : Gtz| 11| ;| 111 : Gtm| 11|
Gtzd12 : Gtz 2 Gtmd12 : Gtm 2 Gtzd13 : Gtz 3 Gtmd13 : Gtm 3 Gtzd14 : Gtz 4 Gtmd14 : Gtm 4
Gtzd15 : Gtz| 15| ; Gtmd15 : Gtm| 15| ; Gtzd16 : Gtz| 16| ; Gtmd16 : Gtm| 16| ; Gtzd17 : Gtz| 17| ; Gtmd17 : Gtm| 17| ;

point , 1 0.000 ;| most zero contribution from point : 1|
point , 1 Gtzd2 , 1
point , 1 Gtzd3 , 1
point , 1 Gtzd4 , 1
point , 1 Gtzd5 , 1
point , 1 Gtzd6 , 1
point , 1 Gtzd7 , 1
point , 1 Gtzd8 , 1
point , 1| Gtzd9| | | |
point 0, 1 Gtzd10 , 1
point 1, 1 Gtzd11 , 1
point 2, 1 Gtzd12 , 1
point 3, 1 Gtzd13 , 1
point 4, 1 Gtzd14 , 1
point 5, 1 Gtzd15 , 1
point 6, 1 Gtzd16 , 1
point 7, 1 Gtzd17| 1, 1| | ;
point 8, 1 TT;
point 9, 1 TT;
point 0, 1 TT;
point 1, 1 0.000 ;| most zero contribution from point : 1|
point 2, 1 Gtmd2 , 1
point 3, 1 Gtmd3 , 1
point 4, 1 Gtmd4 , 1
point 5, 1 Gtmd5 , 1
point 6, 1 Gtmd6 , 1
point 7, 1 Gtmd7 , 1
point 8, 1 Gtmd8 , 1
point 9, 1 Gtmd9| 1|
point 0, 1 Gtmd10 , 1
point 1, 1 Gtmd11 , 1
point 2, 1 Gtmd12 , 1
point 3, 1 Gtmd13 , 1
point 4, 1 Gtmd14 , 1
point 5, 1 Gtmd15 , 1
point 6, 1 Gtmd16 , 1
oint| 37, 1| : Gtmd17| 1, 1| | ;
|

```

more on the next page.....

Continuation of point assignments for distribution

```

po tassignmentMINUS2 :
| numbers aren't calc ed |
Gtzd3 : Gtz Gtmd3 : Gtm Gtzd4 : Gtz Gtmd4 : Gtm Gtzd5 : Gtz Gtmd5 : Gtm Gtzd6 : Gtz
Gtmd6 : Gtm / zsd7 : Gtz 7 / zsd8 : Gtz 8 / Gtz 3 / Gtm 8 / Gtmd9 : Gtz 9 / Gtmd9 : Gtm 9 /
Gtzd10 : Gtz 0 Gtmd10 : Gtm 0 Gtzd11 : Gtz 1 Gtmd11 : Gtm 1
Gtzd12 : Gtz 2 Gtmd12 : Gtm 2 Gtzd13 : Gtz 3 Gtmd13 : Gtm 3 Gtzd14 : Gtz 4 Gtmd14 : Gtm 4
Gtzd15 : Gtz 15 / Gtmd15 : Gtm 15 / Gtzd16 : Gtz 16 / Gtmd16 : Gtm 16 / Gtzd17 : Gtz 17 / Gtmd17 : Gtm 17 /

point , 1 0.000001; almost zero contribution from point : 1
point , 1 0.000 /; most zero contribution from point : 2
point , 1 Gtzd3 , 1
point , 1 Gtzd4 , 1
point , 1 Gtzd5 , 1
point , 1 Gtzd6 , 1
point , 1 Gtzd7 , 1
point , 1 Gtzd8 , 1
point , 1 Gtzd9 / / /
point 0, 1 Gtzd10 , 1
point 1, 1 Gtzd11 , 1
point 2, 1 Gtzd12 , 1
point 3, 1 Gtzd13 , 1
point 4, 1 Gtzd14 , 1
point 5, 1 Gtzd15 , 1
point 6, 1 Gtzd16 , 1
point 7, 1 Gtzd17 / / 1, 1 /
point 8, 1 TT;
point 9, 1 TT;
point 0, 1 TT;
point 1, 1 0.000001; almost zero contribution from point : 1
point 2, 1 0.000 /; most zero contribution from point : 2
point 3, 1 Gtmd3 , 1
point 4, 1 Gtmd4 , 1
point 5, 1 Gtmd5 , 1
point 6, 1 Gtmd6 , 1
point 7, 1 Gtmd7 , 1
point 8, 1 Gtmd8 , 1
point 9, 1 Gtmd9 / / 1
point 0, 1 Gtmd10 , 1
point 1, 1 Gtmd11 , 1
point 2, 1 Gtmd12 , 1
point 3, 1 Gtmd13 , 1
point 4, 1 Gtmd14 , 1
point 5, 1 Gtmd15 , 1
point 6, 1 Gtmd16 , 1
oint 37, 1 / Gtmd17 / / 1, 1 /

po tassignmentMINUS3 :
| numbers aren't calc ed |
Gtzd4 : Gtz Gtmd4 : Gtm Gtzd5 : Gtz Gtmd5 : Gtm Gtzd6 : Gtz Gtmd6 : Gtm / zsd7 : Gtz 7
Gtmd7 : Gtm / zsd8 : Gtz 8 / zsd9 : Gtz 9 / Gtmd9 : Gtm 9 / Gtmd10 : Gtz 10 / Gtmd10 : Gtm 10 /
Gtzd11 : Gtz 1 Gtmd11 : Gtm 1
Gtzd12 : Gtz 2 Gtmd12 : Gtm 2 Gtzd13 : Gtz 3 Gtmd13 : Gtm 3 Gtzd14 : Gtz 4 Gtmd14 : Gtm 4
Gtzd15 : Gtz 15 / Gtmd15 : Gtm 15 / Gtzd16 : Gtz 16 / Gtmd16 : Gtm 16 / Gtzd17 : Gtz 17 / Gtmd17 : Gtm 17 /

point , 1 0.000001; almost zero contribution from point : 1
point , 1 0.000001; almost zero contribution from point : 2
point , 1 0.000 /; most zero contribution from point : 3
point , 1 Gtzd4 , 1
point , 1 Gtzd5 , 1
point , 1 Gtzd6 , 1
point , 1 Gtzd7 , 1
point , 1 Gtzd8 , 1
point , 1 Gtzd9 / / /
point 0, 1 Gtzd10 , 1
point 1, 1 Gtzd11 , 1
point 2, 1 Gtzd12 , 1
point 3, 1 Gtzd13 , 1
point 4, 1 Gtzd14 , 1
point 5, 1 Gtzd15 , 1
point 6, 1 Gtzd16 , 1
point 7, 1 Gtzd17 / / 1, 1 /
point 8, 1 TT;
point 9, 1 TT;
point 0, 1 TT;
point 1, 1 0.000001; almost zero contribution from point : 1
point 2, 1 0.000001; almost zero contribution from point : 2
point 3, 1 0.000 /; most zero contribution from point : 3
point 4, 1 Gtmd4 , 1
point 5, 1 Gtmd5 , 1
point 6, 1 Gtmd6 , 1
point 7, 1 Gtmd7 , 1
point 8, 1 Gtmd8 , 1
point 9, 1 Gtmd9 / / 1
point 0, 1 Gtmd10 , 1
point 1, 1 Gtmd11 , 1
point 2, 1 Gtmd12 , 1
point 3, 1 Gtmd13 , 1
point 4, 1 Gtmd14 , 1
point 5, 1 Gtmd15 , 1
point 6, 1 Gtmd16 , 1
oint 37, 1 / Gtmd17 / / 1, 1 /

```

More on the next page.....

Continuation of point assignments for distribution, observe many points were determined to yield very small values and were negated to conserve time as these calculations can take several hours.

```

po  tassignmentMINUS4 :: |
|, numbers      aren't calc    ed |
Gtzd5: Gtz|      Gtmd5: Gtm      Gtzd6: Gtz|      Gtmd6: Gtm|      ; Gtzd7: Gtz| 7|      H 17: Gtm| 7| ; ( sc : Gtz| 8| ;
Gtmd8: Gtm|      ; Gtzd9: Gtz| 9|      H 19: Gtm| 9| ; ( zc ) : Gtz| 10| ; ( ac ) : Gtm| 10| ; ( sc 1 : Gtz| 11| ; ( ac 1 : Gtm| 11| ;
Gtzd12: Gtz| 2      Gtmd12: Gtm| 2      Gtzd13: Gtz| 3      Gtmd13: Gtm| 3      Gtzd14: Gtz| 4      Gtmd14: Gtm| 4
Gtzd15: Gtz| 15| ; Gtmd15: Gtm| 15| ; Gtzd16: Gtz| 16| ; Gtmd16: Gtm| 16| ; Gtzd17: Gtz| 17| ; Gtmd17: Gtm| 17| ;

point  , 1      0.000001;  almost zero contribution from point : 1
point  , 1      0.000001;  almost zero contribution from point : 2
point  , 1      0.000001;  almost zero contribution from point : 3
point  , 1      0.000      ;|  most zero contribution from point : 4
point  , 1      Gtzd5      , 1
point  , 1      Gtzd6      , 1
point  , 1      Gtzd7      , 1
point  , 1      Gtzd8      , 1
point  , 1|      Gtzd9|      .| |
point  0, 1      Gtzd10      , 1
point  1, 1      Gtzd11      , 1
point  2, 1      Gtzd12      , 1
point  3, 1      Gtzd13      , 1
point  4, 1      Gtzd14      , 1
point  5, 1      Gtzd15      , 1
point  6, 1      Gtzd16      , 1
point  7, 1      Gtzd17| | 1, 1| | ;
point  8, 1      TT;
point  9, 1      TT;
point  0, 1      TT;
point  1, 1      0.000001;  almost zero contribution from point : 1
point  2, 1      0.000001;  almost zero contribution from point : 2
point  3, 1      0.000001;  almost zero contribution from point : 3
point  4, 1      0.000      ;|  most zero contribution from point : 4
point  5, 1      Gtmd5      , 1
point  6, 1      Gtmd6      , 1
point  7, 1      Gtmd7      , 1
point  8, 1      Gtmd8      , 1
point  9, 1      Gtmd9|      1|
point  0, 1      Gtmd10      , 1
point  1, 1      Gtmd11      , 1
point  2, 1      Gtmd12      , 1
point  3, 1      Gtmd13      , 1
point  4, 1      Gtmd14      , 1
point  5, 1      Gtmd15      , 1
point  6, 1      Gtmd16      , 1
oint| 37, 1| : Gtmd17| | 1, 1| | ;
|

```

More on the next page.....

Continuation of point assignments for distribution

```

po tassignmentMINUS5 :: |
| | numbers      aren't calc    ed |
Gtzd6: Gtz|      Gtmd6: Gtm|      ; Gtzd7: Gtz| 7|      ; Gtmd7: Gtm| 7| ; Gtzd8: Gtz| 8| ; Gtmd8: Gtm| 8| ; Gtzd9: Gtz| 9| ;
Gtmd9: Gtm|      ; Gtzd10: Gtz| 1|      ; Gtmd10: Gtm| 1|      ; Gtzd11: Gtz| 1|      ; Gtmd11: Gtm| 1|      ;
Gtzd12: Gtz| 2|      Gtmd12: Gtm| 2|      Gtzd13: Gtz| 3|      Gtmd13: Gtm| 3|      Gtzd14: Gtz| 4|      Gtmd14: Gtm| 4|
Gtzd15: Gtz| 15| ; Gtmd15: Gtm| 15| ; Gtzd16: Gtz| 16| ; Gtmd16: Gtm| 16| ; Gtzd17: Gtz| 17| ; Gtmd17: Gtm| 17| ;

point  , 1  0.000001;  almost zero contribution from point : 1
point  , 1  0.000001;  almost zero contribution from point : 2
point  , 1  0.000001;  almost zero contribution from point : 3
point  , 1  0.000001;  almost zero contribution from point : 4
point  , 1  0.000      ;  most zero contribution from point : 5
point  , 1  Gtzd6      , 1
point  , 1  Gtzd7      , 1
point  , 1  Gtzd8      , 1
point  , 1|  Gtzd9|      |
point  0, 1  Gtzd10     , 1
point  1, 1  Gtzd11     , 1
point  2, 1  Gtzd12     , 1
point  3, 1  Gtzd13     , 1
point  4, 1  Gtzd14     , 1
point  5, 1  Gtzd15     , 1
point  6, 1  Gtzd16     , 1
point  7, 1  Gtzd17| | 1, 1| | ;
point  8, 1  TT;
point  9, 1  TT;
point  0, 1  TT;
point  1, 1  0.000001;  almost zero contribution from point : 1
point  2, 1  0.000001;  almost zero contribution from point : 2
point  3, 1  0.000001;  almost zero contribution from point : 3
point  4, 1  0.000001;  almost zero contribution from point : 4
point  5, 1  0.000      ;  most zero contribution from point : 5
point  6, 1  Gtmd6      , 1
point  7, 1  Gtmd7      , 1
point  8, 1  Gtmd8      , 1
point  9, 1  Gtmd9|      |
point  0, 1  Gtmd10     , 1
point  1, 1  Gtmd11     , 1
point  2, 1  Gtmd12     , 1
point  3, 1  Gtmd13     , 1
point  4, 1  Gtmd14     , 1
point  5, 1  Gtmd15     , 1
point  6, 1  Gtmd16     , 1
oint| 37, 1| : Gtmd17| | 1, 1| | ;
|

```

This marks the end of this input box for the distribution calculation. The next page begins the next input box for calculating the equilibrium population of site ‘j’ in the isotropic rotational diffusion model

```

CellPrint[Cell["Populations", "Section", CellDingbat["|"], Background->GrayLevel[.9], CellTags->{"cell.populations"}];

max= 20;
For[k=1, k<=max, k++, |begin of "k loop"|

  pop[k, k]=Sin[k*0.5]*Sin[ $\frac{k}{2}$ ]; pop[k+1, k]=0; pop[k, k+1]=0;

  |end of "k loop"|

"Site populations"
population=Array[pop, {20, 2}]; MatrixForm[population];
L=TridiagonalMatrix[pop, 20]; MatrixForm[L];

Null

```

The next box calculates the matrix of NMR frequencies and contains the CSA tensor components specific to a particular species. Designated $\delta\text{component}[1,1]$, $\delta\text{component}[2,2]$, $\delta\text{component}[3,3]$ from the diagonal of the 3X3 CSA matrix, this example is for PI. The entire input box is on the next page, and this is excerpt from that box showing the parameters that need to be changed for a particular samples CSA tensor value.

```

|component[1,1]=28.5; |component[2,2]=00.0; |component[3,3]=0.0;
|component[1,2]=00.0; |component[2,1]=26.3; |component[2,3]=0.0;
|component[3,1]=00.0; |component[3,2]=0.0; |component[3,3]=8;
PAS1=106Array[|component[3,3]|]; MatrixForm[PAS1]

```

Full input box on next page.....

Full input box including the portion that calculates the matrix of NMR frequencies following the maxf loop.

```
CellPrint[Cell["Frequency", "Section", CellDingbat -> " ", Background -> GrayLevel[.9], CellTags -> "cell.frequency"]];

| component , 1 28.5; | component , 2 00.0; | component , 3 0.0;
| component , 1 00.0; | component , 2 26.3; | component , 3 0.0;
| component , 3, 1 00.0; | component , 2 0.0; | component , 3, 3 8;
PAS1 = 10^6 Array[component, {3, 3}]; MatrixForm PAS1

max = 20;
For[f = 1, f = max, f++, | begin of "f loop" |
Clear[|, |, |];
a = 0 Degree; b = | f - 0.5 |; c = 0 Degree;

Relement , 1 Cos[| s |] Cos[| c |] Sin[| s |] Sin[| c |]; | element , 2 | | n | a | | b | | | c | Cos[| a |] Sin[| c |];
Relement , 3 | Sin[| s |] Cos[| c |] Sin[| s |] Sin[| c |]; | a | Cos[| b |] Sin[| c |] Sin[| c |];
Relement , 2 | Sin[| c |] Cos[| s |] Cos[| c |] Sin[| c |]; | 2, 3 | | | b | Sin[| c |];
Relement[3, 1] | Cos[| a |] Sin[| c |]; | element[3, 2] | Sin[| a |] Sin[| b |]; Relement[3, 3] | Cos[| b |];
rotation = Array[Relement, {3, 3}];
MF = rotation.PAS1.Transpose[rotation];
C2 =
1/3 (3 (MF[3, 3] - 1/3 Tr[MF]) Sin[| |] Sin[| |] - 1/2 (1/2 MF[2, 2] - MF[1, 1] | Cos[2 |] - MF[1, 2] Sin[2 |]) Cos[2 |] + 3 |
| MF[1, 3] Cos[| |] + MF[2, 3] Sin[| |] Sin[2 |]);
S2 = 2/3 ((1/2 MF[2, 2] - MF[1, 1] | Sin[2 |] + MF[1, 2] Cos[2 |]) Cos[| |] + MF[1, 3] Sin[| |] + MF[2, 3] Cos[| |] Sin[| |]);
C1 =
sqrt(2)/3 (3/2 (MF[3, 3] - 1/3 Tr[MF]) Sin[2 |] - (1/2 MF[2, 2] - MF[1, 1] | Cos[2 |] - MF[1, 2] Sin[2 |]) Sin[2 |] +
2 | MF[1, 3] Cos[| |] + MF[2, 3] Sin[| |] Cos[2 |]);
S1 = 2 sqrt(2)/3 ((1/2 MF[2, 2] - MF[1, 1] | Sin[2 |] + MF[1, 2] Cos[2 |]) Sin[| |] + MF[1, 3] Sin[| |] + MF[2, 3] Cos[| |] Cos[| |]);
| LF = sqrt(2) Cos[2 |] R t | | S2 Sin[2 |] R t | | C Cos[2 |] R t | | S1 Sin[2 |] R t | |;
freq[f, f] = L 1/3 Tr[MF] + L LF; freq[f, 1, f] = 0; freq[f, f, 1] = 0;
| end of "f loop" |

"Site frequency:
Frequency = Array[freq, {20, 20}]; MatrixForm Frequency;
| Tridiag Matrix[freq, 20];
MatrixForm |]
```

The next page is an example of the frequency matrix

Frequency matrix output

FREQUENCY

CSA matrix output

$$\begin{pmatrix} 0.0000285 & 0. & 0. \\ 0. & 0.0000263 & 0. \\ 0. & 0. & \frac{1}{125\,000} \end{pmatrix}$$

Site frequencies

The site frequency matrix is too large to paste here, but the first few characters are provided below

$$9926.42 \cdot 4.74192 \cdot 10^8 \left(\frac{1}{3} \cos[29.7873 \cdot 2] \cdot \left(\frac{1}{2} \cdot 3 \cdot \cos[2] \right) \cdot \left(1.0369 \cdot 10^{-6} \cos[2] + 0. \sin[2] \right) \cdot 0.0000192107 \sin[2]^2 \cdot 1.60345 \right)$$

The following page contains the initiation of the applied distributions and export string for the text output of G_ etc....

The input cell for the first 1-11 points of the 20 point distribution (p).

```

cellName: "cell.temperature.";
cellDisplay: "temperature : T";

maxj 11;
For p: 1, 11, r: tp, p, begin of "p loop"
  CellPrint Cell StringInse: cellDisplay, number: p, "Section", CellDingbat: " ", Background: GrayLevel .9,
    CellTags: StringInsert cellName, number: p, . 1 || ;

  TT: p: T;
  tau: p;
  ExchangedId17;

  POWDERaverage 1;
  pointassignmentFULL;

  GzGmvectorT: Array point 37, 1; MatrixForm Transpose GzGmvectorT
  Export StringInsert filename, number: p, . 5, GzGmvectorT, "TSV"

```

Automatic export command for
the distribution data

The following is an example of the output from the above input cell

| temperature = T1 | |
|--------------------------------|--|
| Exchange matrix elements ready | |
| Powder averaging REFERENCE_1 | |
| Powder averaging CODEX_1 | |
| Powder averaging REFERENCE_2 | |
| Powder averaging CODEX_2 | |
| Powder averaging REFERENCE_3 | |
| Powder averaging CODEX_3 | |

To finalize the distribution of the 20 temperature points set earlier in the distribution notebook the following cells must be initialized.

The following cell initiates calculation of the distribution points 12-15 of 20

```
For| p: 12 | p| , | k in of "p loop" |
CellPrint| Cell| StringInse: | ceLLdisplay, n: | p | | , "Section", CellDingbat: " | ", Background: GrayLevel| .9| ,
CellTags: | StringInsert| ceLLname, number| p| , . 1| | | ;

TT: | p| T;
tau| p| ;
ExchangedId17;

dstart: 2; | | number d1 isn't calculated |

POWDERaverage| dstart| ;
pointassignmentMINUS1;

GzGmvectorT: Array| point, | 37, 1| | ; MatrixForm| Transpose| GzGmvectorT| |

Export| StringInsert| filename, number| p| , . 5| , GzGmvectorT, "TSV"|
|
```

The following cell initiates calculation of the distribution points final points 16-20 of 20

```
For| p: 16 | p| , | k in of "p loop" |
CellPrint| Cell| StringInse: | ceLLdisplay, n: | p | | , "Section", CellDingbat: " | ", Background: GrayLevel| .9| ,
CellTags: | StringInsert| ceLLname, number| p| , . 1| | | ;

TT: | p| T;
tau| p| ;
ExchangedId17;

dstart: 4; | | numbers d1 d3 aren't calculated |

POWDERaverage| dstart| ;
pointassignmentMINUS3;

GzGmvectorT: Array| point, | 37, 1| | ; MatrixForm| Transpose| GzGmvectorT| |

Export| StringInsert| filename, number| p| , . 5| , GzGmvectorT, "TSV"|
|
```

This is the final part of the distribution notebook (not all output is shown).

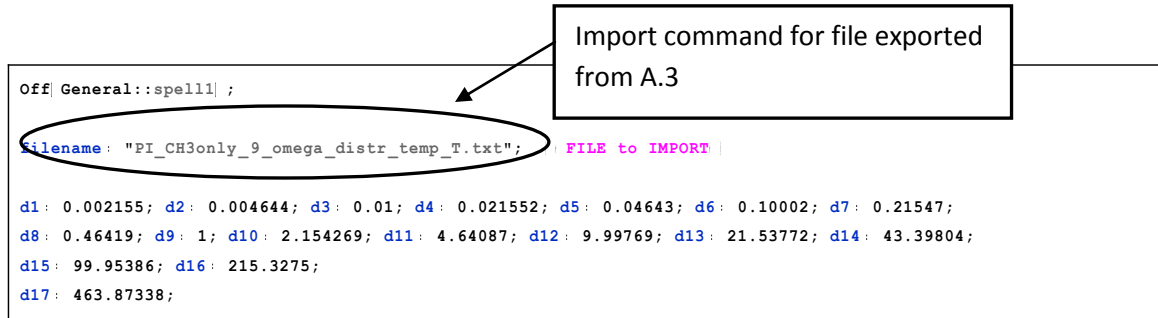
A.4 Applying the Temperature Dependent Weighting Factor (σT) to the Log-Gaussian Distribution

The weighting factor $g(\tau, T)$ was calculated according to:

$$g(\tau, T)_{\log-Gauss} = \frac{1}{\sigma(T)\sqrt{2\pi}} \exp\left[-\frac{(\ln(\tau) - \ln(\tau_c(T)))^2}{2\sigma^2(T)}\right]$$

where the width of the distribution decreases with temperature, $\sigma(T) = a k_B T + \sigma_0$, with k_B being the Boltzmann constant, and the mean correlation time, $\tau_c(T)$, follows Arrhenius behavior.

The Mathematica notebook is provided over the next few pages



The next input cell is on the next page

This cell imports the distribution from A.3

```
AssignG[p_, n_] := |
  "G_ : : m : d hroug : ?";
  Gzd1 = n, 1 Gmd1 = n 1, 1 Gzd2 = n, 1 Gmd2 = n 2, 1
  Gzd3 = n, 1 Gmd3 = n 3, 1 Gzd4 = n, 1 Gmd4 = n 4, 1
  Gzd5 = n, 1 Gmd5 = n 5, 1 Gzd6 = n, 1 Gmd6 = n 6, 1
  Gzd7 = n, 1 Gmd7 = n 7, 1 Gzd8 = n 1 1 md8 p 2 1 1 ;
  Gzd9 = n 1 1 md9 p 2 1 1 ; d10 p 1 1 1 ; d10 p 3 1 1 ;
  Gzd11 = n 1, 1 Gmd11 = n 1, 1 Gzd12 = n 2, 1 Gmd12 = n 2, 1
  Gzd13 = n 3, 1 Gmd13 = n 3, 1 Gzd14 = n 4, 1 Gmd14 = n 4, 1
  Gzd15 = n 5, 1 Gmd15 = n 5, 1 Gzd16 = n 16 1 ; Gmd16 p n 36, 1 1 ;
  z 7 p n 17, 1 1 ; Gmd17 p n 37, 1 1 ; TTT p n 20, 1 1 ;
  | | end of function |

ReadGdataTlTpmax[maxp_] := |
  For[p = 1, maxp, p, | begin of "p loop"|
    GdataT p :=
      Transpose[
        ToExpression[St eplace ReadList[StringInsert filename, ToString p, - 5, "String"],
          "e" -> "10^"]];
      MatrixForm[GdataT p];
      SignG[p, GdataT p];
  | | e of "p loop"| ;
  nt["Imported Gdata for temperatures from T1 to T", maxp];
  | | end of function |

Calculate[S[p_, A_, a_, b_, n_] := (
  Clear[ ];
  | : a TC p T : b;

  For[s = 1, s = 17, s, | begin "s loop"|
    d[s] := ToExpression[StringInsert "d", ToString s, - 1];
    f[s] :=  $\frac{1}{\sqrt{2} t_i^2} \text{Exp} \left[ \left( \frac{\text{Log}[d[s]]}{\sqrt{2} t_i} \right)^2 \right]$ ;
  | | end "s loop"| ;

  Gtz = 1 G : p 2 G : p 3 G : p f Gzd : + 5 Gzd5 f G : 16 p
  f : d7 p 8 G : p G : 15 p f G : 1 p f G : 11 Gzd12 p
  f 13 13 f : Gzd1 : Gz : p 16 : : f 17 : 11 ;
  Gtm = 1 G : p 2 G : p 3 G : p f Gmd : + 5 Gmd5 f G : 16 p
  f : d7 p 8 G : p G : 15 p f G : 1 p f G : 11 Gmd12 p
  f 13 Gmd13 p f 14 Gmd14 p f 15 Gmd15 p f 16 Gmd16 p f 17 Gmd17 p ;

  | S = A  $\frac{\text{Gtz} - \text{Gtm}}{\text{Gtz}}$  ; Print[S];

  points1, p : TTT p ; points2, p : S ;

  ) | | end of function |
```

The next input cell is on the next page...

The next few boxes conclude the input cells for applying the weighting factors to the distribution.

```

maxp: 20;
ReadGdataT1[ max, maxp] | Read the Gdata and assign Gzd[ p] Gmd
2,...,pmax"|

A: 1.60`; | a: 0.070`; | b: 21.35`;
pi: 3.141592`; TC: 244; | T: 2;

For[ p: 1, p: maxp, p: Calculate[ S] | A, | a, | GdataT[ p] | ];
Pointsof[ S: Transpose[ Array[ pointS, | 2, maxp] | ]; Pointsof[ S

Distribution_ready

Experimental: | | | 0.057971|, | | 0.0175953|, | | 0.0650888| | 04, 0.192308| | 8, 0.418605|,
| 10, 0.5 | 93|, | 214, 0.842657|, | 218, 0.488372|, | 222, 0.12963|, | 226, 0.0989583|, | 230, 0.0515464|,
| 234, 0.0|

calculating_Plot

ListPlot[ Pointsof[ S, PlotRange: | 0.0 |, 1|, PlotStyle: | Point: | e 0. | |, Thickness| 0.007`| |,
Joined: Tru | Epilog: Prepend[ Point| | Experimental, P
BaseStyle: | FontFamily: "A | |, | tSiz |, AxesS
AxesLabel: TraditionalForm| | "T| K| ", "E| T| " |

```

Note: **A**, **σa** , and **σb** are adjusted to get the distribution to fit the experimental data more closely. Don't forget the **TC** and **ΔT** values need to match those in **A.3**.

The Experimental must be entered and is the exactly from the CODEX experiment as determined from **A.2**

```

Export[ "PI_CH3_L1_6_200ms_rotational_9_distr_T1_20.txt", Pointsof[ S, "TSV" |

```

Arrhenius fit to the experimental data

Export command for text file of Arrhenius fit

This is the end of the notebook for applying the weighting factor to the distribution and finalizes the Arrhenius/log-Gaussian fitting of the E(T) data.

A.5 Direct Excitation version of CODEX Pulse Program

```
;hpdec.rel

;simple onepuls acquisition using the DDS phase shifter

;with CW proton decoupling, standard method in solids NMR

;read through include files to understand what they mean

#include <preamp.incl>

                                ;protects HP preamps during pulse

#include <powswi.incl>

                                ;enables HP transmitter gain switching

                                ;if new style 400V boards are available

#include <trigg.incl>

                                ;this provides a trigger output from

                                ;HP router BNC NMR5-13

#include <observe.incl>

                                ;this is only necessary for 3 channel

                                ;SE-451 and uxnmr versions before

                                ;vs. xwin-nmr.a.9

define delay cd15mp1

define delay cd15m1h

define delay cd15mp2

"d15=0.25s/l31-2u"

"cd15mp1=0.25s/l31-p1-2u"
```

"cd15m1h=0.25s/l31-p1-p1/2-2u"

"cd15mp2=0.25s/l31-p2-2u"

"d30=p3+3u-p1-2u" ;rotor synch.delay in tm

"l3=ns/l0"

;-----

1 ze ;set RCU to replace mode

2 10m rf #0 ;reset the file pointer to the beginning of the ser file

3 d1 do:f2 ;recycle delay, turn the decoupler off

10u pl1:f1 ;preselect pl1 drive power level for F1

10u pl2:f2 ;preselect pl2 drive power for F2

1u:f2 ph1

1u:f1 ph2

rpp5 ;reset phase lists for xy-8

1u trigpe1 ;record rotor phase

7u

(p3 ph2):f1 ;transmitter pulse on F1 with power level pl1

```

1u cw:f2          ;turn on F2 decoupling
1u pl12:f2        ;set decoupling drive power level

cd15mp1 pl11:f1   ;tr/4
d15:f1 ph5        ;tr/4
2u pl22:f2        ;high 1H power during 13C pulse
p2:f1 ph5^        ;13C 180 deg. pulse
2u pl12:f2
d15
4 cd15mp2:f1 ph5
2u pl22:f2        ;high 1H power during 13C pulse
p2:f1 ph5^        ;13C 180 deg. pulse
2u pl12:f2
d15
lo to 4 times l1  ;an even number

cd15m1h pl1:f1    ;tr/4
2u pl22:f2        ;high 1H power during 13C pulse

p1:f1 ph8         ;first mixing time
d6 do:f2
1u trigpe1        ;same phase as above
d30:f1 ph9
2u cw:f2 pl22:f2
p1:f1 ph9

```

2u pl12:f2 ;remember to remove it
 cd15m1h pl11:f1 ;tr/4
 5 d15:f1 ph5
 2u pl22:f2 ;high 1H power during 13C pulse
 p2:f1 ph5^ ;13C 180 deg. pulse
 2u pl12:f2
 cd15mp2
 lo to 5 times l1 ;an even number

d15:f1 ph5 ;tr/4
 2u pl22:f2 ;high 1H power during 13C pulse
 p2:f1 ph5^ ;13C 180 deg. pulse
 2u pl12:f2
 d15
 cd15mp1 pl1:f1 ;tr/4
 2u pl22:f2

p1:f1 ph3 ;second z-filter
 d16 do:f2
 1u trigpe1 ;same phase as above
 d30:f1 ph4
 2u cw:f2 pl12:f2
 p1:f1 ph4

```

2u:f1 ph0      ;dead time delay, reset RF phase to detect
gosc ph31      ;do NS scans, (gosc does not loop !!!)
10u do:f2      ;turn decoupler off
10m id18
lo to 3 times l0    ;loop to 3
30m wr #0 if #0    ;(wr= transfer acquisition data to file fid/ser. Start writing at current
position of file pointer). (if= advance file pointer for ser files)

```

```

=====
;
=====

```

```

13 d1 do:f2      ;recycle delay, turn the decoupler off
10u pl1:f1      ;preselect pl1 drive power level for F1
10u pl2:f2      ;preselect pl2 drive power for F2
1u:f2 ph1
1u:f1 ph2

rpp5            ;reset phase lists for xy-8
1u trigpe1      ;record rotor phase
7u

(p3 ph2):f1      ;transmitter pulse on F1 with power level pl1
1u cw:f2        ;turn on F2 decoupling
1u pl12:f2      ;set decoupling drive power level

cd15mp1 pl11:f1  ;tr/4
d15:f1 ph5      ;tr/4

```

2u pl22:f2 ;high 1H power during 13C pulse

p2:f1 ph5^ ;13C 180 deg. pulse

2u pl12:f2

d15

14 cd15mp2:f1 ph5

2u pl22:f2 ;high 1H power during 13C pulse

p2:f1 ph5^ ;13C 180 deg. pulse

2u pl12:f2

d15

lo to 14 times l1 ;an even number

cd15m1h pl1:f1 ;tr/4

2u pl22:f2 ;high 1H power during 13C pulse

p1:f1 ph8 ;first mixing time

d7 do:f2

1u trigpe1 ;same phase as above

d30:f1 ph9

2u cw:f2 pl22:f2

p1:f1 ph9

2u pl12:f2 ;remember to remove it

cd15m1h pl11:f1 ;tr/4

15 d15:f1 ph5

2u pl22:f2 ;high 1H power during 13C pulse

p2:f1 ph5^ ;13C 180 deg. pulse

2u pl12:f2

cd15mp2

lo to 15 times l1 ;an even number

d15:f1 ph5 ;tr/4

2u pl22:f2 ;high 1H power during 13C pulse

p2:f1 ph5^ ;13C 180 deg. pulse

2u pl12:f2

d15

cd15mp1 pl1:f1 ;tr/4

2u pl22:f2

p1:f1 ph3 ;second z-filter

d17 do:f2

1u trigpe1 ;same phase as above

d30:f1 ph4

2u cw:f2 pl12:f2

p1:f1 ph4

2u:f1 ph0 ;dead time delay, reset RF phase to detect

gosc ph31 ;do NS scans

10u do:f2 ;turn decoupler off

10m id18

lo to 13 times l0 ;to speed up tests I replaced l0 with 4.

30m wr #0 rf #0 zd

10m

lo to 2 times l3

exit

exit

ph0= 0 ;constant phase for acquisition

ph1= 0 ;1H 90 excitation. not used

ph2= 1 1 2 2 3 3 0 0 ;initial 13C pi/2 pulse

ph3= 3 3 0 0 1 1 2 2

ph4= 1 1 2 2 3 3 0 0 ;readout after 2nd z period

ph5= 0 1 0 1 1 0 1 0 ;xy-8

ph8= 3 3 0 0 1 1 2 2

3 3 0 0 1 1 2 2

2 2 3 3 0 0 1 1

2 2 3 3 0 0 1 1

1 1 2 2 3 3 0 0

1 1 2 2 3 3 0 0

0 0 1 1 2 2 3 3

0 0 1 1 2 2 3 3

ph9= 1 1 2 2 3 3 0 0

3 3 0 0 1 1 2 2

0 0 1 1 2 2 3 3

2 2 3 3 0 0 1 1

ph31=3 3 0 0 1 1 2 2 ;signal routing corresponds to pulse phase list

1 1 2 2 3 3 0 0

3 3 0 0 1 1 2 2

1 1 2 2 3 3 0 0

1 1 2 2 3 3 0 0

3 3 0 0 1 1 2 2

1 1 2 2 3 3 0 0

3 3 0 0 1 1 2 2

VITA

Lance Wayne Gill

Candidate for the Degree of

Doctor of Philosophy

Thesis: POLYOLEFIN BLEND MISCIBILITY: QUANTITATIVE
INVESTIGATIONS OF DYNAMIC HETEROGENEITY

Major Field: Chemistry

Biographical:

Education:

Completed the requirements for the Doctor of Philosophy in Chemistry at Oklahoma State University, Stillwater, Oklahoma in December, 2012.

Completed the requirements for the Bachelor of Arts in Chemistry at Southwestern Oklahoma State University, Weatherford, Oklahoma in 2006.

Experience: Worked as a graduate student at Oklahoma State University from July 2006 to present. Employed as an undergraduate researcher under Dr. William Kelly at Southwestern Oklahoma State University in summer of 2004, 2005, and 2006. Also, worked as organic and general chemistry lab assistant at Southwestern Oklahoma University from spring 2003 to spring 2006.

Professional Memberships: American Chemical Society, Polymer Science Division, Physical Chemistry Division

Name: Lance Wayne Gill

Date of Degree: December, 2012

Institution: Oklahoma State University

Location: Stillwater, Oklahoma

Title of Study: POLYOLEFIN BLEND MISCIBILITY: QUANTITATIVE
INVESTIGATIONS OF DYNAMIC HETEROGENEITY

Pages in Study: 126

Candidate for the Degree of Doctor of Philosophy

Major Field: Chemistry

Scope and Method of Study: Using advanced solid-state NMR to study the microscopic interactions of amorphous polymer blends and the influences of each component to the dynamic heterogeneity of those miscible blends.

Findings and Conclusions: The chain-specific information gained through this experimental approach based on solid-state CODEX NMR experiments reveals that the effective glass transition for each component in a miscible blend may not occur at a common temperature. The slow chain dynamics associated with conformational changes at the chain level have unique central correlation times and correlation time distributions. The quantitative analysis of the CODEX data and methods used in this study produce results that are in good agreement with those produced by other documented methods. Results from the temperature dependent models show a clear sensitivity to the changes that occur upon blend formation when compared to the pure components. Entropy increases that occur upon mixing are detected using the CODEX experimental data. The unique advantage to this approach is that such quantitative data can be obtained without isotopic labeling, electric dipole moment constraints, or introduction of probe molecules. This demonstrates the particular capabilities of the experimental strategy that applies to a wide range of more complex macromolecular systems including polymer nanocomposites, organic/inorganic hybrid materials, biological macromolecules, and block copolymers.

ADVISER'S APPROVAL: Dr. Jeffery White
